The Dissertation Committee for Timothy Ashworth Meckel Certifies that this is the approved version of the following dissertation:

Tectonics of the Hjort region of the Macquarie Ridge Complex, southernmost Australian-Pacific Plate Boundary, southwest Pacific Ocean

Committee:

Sharon Mosher, Co-Supervisor

Millard F. Coffin, Co-Supervisor

Paul Mann

Philip A. Symonds

James N. Connelly

Ian W. D. Dalziel

Tectonics of the Hjort region of the Macquarie Ridge Complex, southernmost Australian-Pacific Plate Boundary, southwest Pacific Ocean

by

Timothy Ashworth Meckel, B.A, M.S.

Dissertation

Presented to the Faculty of the Graduate School of

The University of Texas at Austin

in Partial Fulfillment

of the Requirements

for the Degree of

Doctor of Philosophy

The University of Texas at Austin

May, 2003

Dedication

To the little one, soon to come.

Acknowledgements

I am particularly indebted to my committee members for seeing this work to completion. I earnestly thank Sharon and Mike for allowing me to freely pursue my ideas and for providing outstanding critiques of my work. Paul deserves momentous recognition for his involvement and guidance. Much appreciation goes to Ian and Jim for their advice along the way. Without the involvement of Phil, the opportunity to pursue this research would not have been available.

My sincerest thanks to Geoscience Australia for making the marine geophysical data available for my dissertation research, and the Department of Geological Sciences and the Institute for Geophysics of the Jackson School of Geosciences, The University of Texas at Austin for continual financial, scientific, and academic support. I thank S. Saustrup, M. Weiderspan, and K. Johnson for superb technical assistance, and W. Keller for providing additional data resources. Many thanks to N. Daczko, D. Cathro, S. Nordfjord, C. Massell, L. Schuur, I Ahmed, and D. Goodwin, for keeping morale up.

I will never be able to express my appreciation adequately for the support extended to me by my family. You inspired confidence when I lost mine, and

reminded me what was important at all stages of my academic career. I cannot imagine any success without your involvement. And, above all, to my loving wife Amanda, for all your sacrifices along the way, I am eternally in debt.

Tectonics of the Hjort region of the Macquarie Ridge Complex, southernmost Australian-Pacific Plate Boundary, southwest Pacific Ocean

Publication No._____

Timothy Ashworth Meckel, Ph.D.

The University of Texas at Austin, 2003

Supervisors: Sharon Mosher and Millard F. Coffin

The Hjort Ridge, Trench, and Plateau comprise the southernmost portion of the Macquarie Ridge Complex (MRC), the Australian-Pacific plate boundary south of New Zealand. The MRC is an ideal location to study deformation and structural development at an obliquely convergent plate boundary involving oceanic lithosphere. This dissertation documents structures and processes in the Hjort region associated with incipient subduction, an outstanding problem in plate tectonics.

I investigated the evolution of the plate boundary from ~33 Ma to the present day, concentrating on the active and recent structural development. Interpretations are based on analyses of recently collected geophysical data in the Hjort region, including swath bathymetry, reflectivity, seismic reflection, gravity,

magnetics, and seismicity. The Australian plate is actively underthrusting the Pacific plate along the Hjort Trench, but self-sustaining subduction does not appear to have commenced.

Transpression along the length of the plate boundary has been accomodated by lithospheric flexure, strike slip faulting, and geographically limited underthrusting. A consistent relationship exists between the convergence angle and the amount of dynamically supported topography; up to 50 km of convergence has been accomodated by flexure forming ridges and troughs. A continuous, strike slip fault accomodates oblique convergence along the length of the boundary. Where angles of convergence are highest ($>20^{o}$), underthrusting is observed in addition. Gravity modeling and seismicity suggest ~50 km of underthrusting in the southern Hjort Trench, but only define an eastwardly dipping Australian slab to about 20 km depth. Lithosphere underthrust in the southern trench is translated subparallel to the ~N-trending boundary, limiting the eastward extent of underthrust slab.

Reconstructions of the plate boundary since 33.3 Ma show that the Antarctic-Australian-Pacific triple junction migrated southward with respect to the Australian plate resulting in the present day curved plate boundary. Migration resulted in lengthening of the dextral transform fault connecting the Macquarie Ridge and Southeast Indian Ridge spreading centers and shortening of the easternmost ridge-segment of latter spreading center. The MRC in the Hjort region changed from a dextral transform into an obliquely convergent zone of incipient subduction.

Table of Contents

List of Tables xii

List of Figures xiii

Chapter 1: Introduction to the Regional Tectonic Setting of the Australian-Pacific Plate Boundary south of New Zealand since the Oligocene 1

1.1 Introduction 1

1.2 Reconstructions 3

1.3 Overview of dissertation 11

Chapter 2: Underthrusting at the Hjort Trench, Australian-Pacific Plate Boundary: Incipient Subduction? 18

2.1 Abstract 18

2.2 Introduction 19

2.3 Geodynamic Setting 22

2.4 Analysis of Upper Crustal Structure 25

2.4.1 Bathymetry, Reflectivity, and Seismic Reflection Data 25

2.4.2 Methods 28

2.4.3 Upper Crustal Structure by Region 31

West of the Hjort Trench 31

Hjort Trench 32

Hjort Ridge 38

Hjort Plateau 39

2.4.4 Upper Crustal Discussion 40

2.5 Analysis of Active Lithospheric Deformation 47

2.5.1 International Seismological Center catalog (ISC) 49

2.5.2 Engdahl, van der Hilst, and Buland (1998) relocations (EHB) .. 49

2.5.3 Harvard Centroid Moment Tensor Catalog (CMT) 50

2.5.4 Active Lithospheric Deformation Discussion 50

2.6 Gravity Modeling of Integrated Crustal Structure 54
2.6.1 Data and Methods 54
2.6.2 Integrated Crustal Structure Results 56
2.6.3 Integrated Crustal Structure Discussion 58
2.7 Concluding Discussion 62
Strain Partitioning 63
Fracture Zone Reactivation 65
Incipient Subduction 67

Chapter 3: Tectonic geomorphology of an active, obliquely-convergent submarine plate boundary: Influence of convergence angles on topography and fault development in oceanic crust 70
3.1 Abstract 70
3.2 Introduction 72
3.3 Data 76
3.4 Tectonic setting 78
3.5 Location of the main australian-pacific plate boundary faults and associated topography 79
3.6 Constraints on seafloor age adjacent to the mrc from magnetic anomaliy interpretations 86
3.7 Timing of uplift at the plate boundary 87
3.8 Stage Rotations and estimates of convergence 90
3.8.1 Methods 90
3.8.2 Analysis: Influence of variable convergence angles on observed faults 98
3.9 Convergence and deformation of crust 101
3.9.1 Methods 102
3.9.2 Analysis - Relationship between convergence and crustal deformation 106
3.10 Discussion 115
3.10.1 Implications for individual segments of the MRC 116
3.10.2 Regional implications 121

3.10.3 Global Implications 123
3.11 Conclusions 126

Chapter 4: Evolution of the Macquarie Triple Junction since the Oligocene and Implications for Tectonics of the Southern Macquarie Ridge Complex 128
4.1 Introduction 128
4.2 Methods 131
4.2.1 Reconstructions 131
4.2.2 Determining instantaneous relative motion and estimates of error 132
4.2.3 Construction of vector diagrams 134
4.2.4 Determination of previous triple junction locations 135
4.2.5 Simulated magnetic anomaly locations 137
Results 138
Discussion 150
Conclusions 159

Summary 162

Appendices 165
Appendix A: Un-interpreted output from the PLATES program for each of the reconstructions 166
Appendix B: volume Calculations 174

References 177

Vita 192

List of Tables

Table 1. Finite rotation poles used in this study from Cande and Stock [in review]..... 93

Table 2. Stage poles calculated from finite poles [Le Pichon, 1973]..... 95

Table 3. Amount of shortening perpendicular to the plate boundary orientation for the various models..... 97

List of Figures

(some figures require 11” X 17” paper for printing)

Figure 1.1. Geographic setting of the Australian-Pacific plate boundary and Macquarie Ridge Complex (MRC) south of New Zealand. 2

Figure 1.2. Paleogeographic reconstruction of the Australian-Antarctic-Pacific three plate system at 33.3 Ma. 4

Figure 1.3. Paleogeographic reconstruction for 26.6 Ma. 6

Figure 1.4. Paleogeographic reconstruction for 20.1 Ma. 7

Figure 1.5. Paleogeographic reconstruction for 10.9 Ma. 9

Figure 1.6. Paleogeographic reconstruction for 5.9 Ma. 10

Figure 1.7. Paleogeographic reconstruction for 2.6 Ma. 12

Figure 1.8. Map for the present day. 13

Figure 2.1. Geographic setting of the Hjort Trench at the southern end of the Macquarie Ridge Complex. 20

Figure 2.2. Regional magnetic isochron map. 24

Figure 2.3. Regional satellite-derived, free-air gravity anomaly map. 26

Figure 2.4. Structural interpretation of the Hjort region of the MRC. 29

Figure 2.5. Close-up views of the northern part of the Hjort Trench. 33

Figure 2.6. *L’Atalante* seismic reflection profile 48a, oriented obliquely to the trench axis. 34

Figure 2.7. *L’Atalante* seismic reflection profile 48b, oriented normal to the trench axis. 36

Figure 2.8. Rig Seismic seismic reflection profiles oriented normal to the trench axis. 37
Figure 2.9. Seismicity in the Hjort region. 48
Figure 2.10. Modeled gravity transects across the Macquarie and Hjort segments of the MRC. 55
Figure 2.11. Cross sections of the plate boundary zone and relative plate convergence. 64
Figure 3.1. Geographic setting of the Australian-Pacific plate boundary and Macquarie Ridge Complex (MRC) south of New Zealand. 74
Figure 3.2. Physiography of the Macquarie Ridge Complex. 77
Figure 3.3. Contoured bathymetry for each of the various ridge segments along the length of the marine expression of the Australian-Pacific plate boundary south of New Zealand. 80
Figure 3.4. Bathymetric profiles perpendicular to the plate boundary orientation. 81
Figure 3.5. Comparison of angles of convergence with respect to the plate boundary orientation and boundary-normal convergence predicted by stage rotations 92
Figure 3.6. Plots of stage pole locations used in assessing variability in amount of convergence at the plate boundary. 96
Figure 3.7. Method for calculating volumes of crust deformed during convergence adjacent to the plate boundary zone. 104

Figure 3.8. Plot of cumulative plate boundary-normal convergence since anomaly 3Ay (5.9 Ma). 107
Figure 3.9. Plot of cumulative plate boundary-normal convergence since anomaly 5o (10.9 Ma). 109
Figure 3.10. Plots of cumulative plate boundary-normal convergence for Macquarie and McDougall segments from stage rotations since anomaly 3Ay (5.9 Ma) vs. displaced crust adjacent to plate boundary. 111
Figure 3.11. Comparison of calculated plate boundary-normal convergence with boundary-normal convergence estimates from cumulative stage rotations since 5.9 Ma. 112
Figure 4.1. Geographic setting of the Australian-Pacific plate boundary, Macquarie Ridge Complex (MRC), and Macquarie Triple Junction (MTJ) south of New Zealand. 129
Figure 4.2. Reconstruction of the Macquarie Triple Junction region at 33.3 Ma. 139
Figure 4.3. Reconstruction of the Macquarie Triple Junction region at 26.6 Ma. 141
Figure 4.4. Reconstruction of the Macquarie Triple Junction region at 20.1 Ma. 143
Figure 4.5. Reconstruction of the Macquarie Triple Junction region at 10.9 Ma. 144
Figure 4.6. Reconstruction of the Macquarie Triple Junction region at 5.9 Ma . 146

Figure 4.7. Reconstruction of the Macquarie Triple Junction region at 2.6 Ma. 148
Figure 4.8. Present day map of the Macquarie Triple Junction region. 149

Chapter 1: Introduction to the Regional Tectonic Setting of the Australian-Pacific Plate Boundary south of New Zealand since the Oligocene

1.1 INTRODUCTION

The southern Australian-Pacific plate boundary exists between the South Island of New Zealand and the Australian-Antarctic-Pacific triple junction (MTJ) (Figure 1.1). Since the Oligocene (33.3 Ma), the poles of rotation for describing the relative motion of the Australian Plate with respect to the Pacific Plate have been located within 2000 km to the east of the plate boundary (Figure 1.1). The close proximity of these poles to the curvilinear Australian-Pacific Plate boundary has resulted in a complex progression during the Late Tertiary from divergent seafloor spreading between the Campbell Plateau and Resolution Ridge (Figure 1.1) to strike-slip deformation at the Macquarie Ridge Complex (MRC) (Figure 1.1), and most recently to oblique convergence at the plate boundary.

Research of the Australian-Pacific plate boundary south of New Zealand has focused on its notable seismicity (including the largest strike-slip earthquake ever recorded, a magnitude 8.2 event in 1989 located at 52.37ºS and 160.64ºE; Figure 1.1) [*Ruff et al.*, 1989; *Das*, 1993; *Frohlich et al.*, 1997], exposure of oceanic crust at Macquarie Island (considered a pristine ophiolite; Figure 1.1) [*Goscombe and Everard*, 2001; *Wertz et al.*, in review], and the potential to document processes involved in subduction initiation [*Collot et al.*, 1995; *Meckel et al.*, in review].

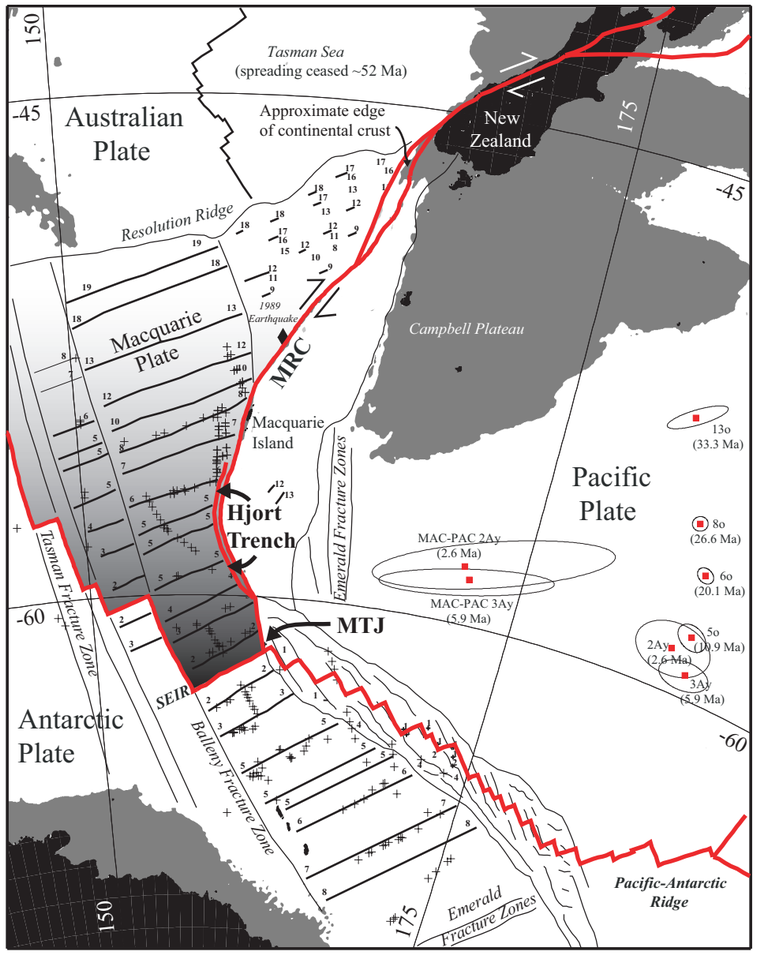

Figure 1.1. Geographic setting of the Australian-Pacific plate boundary and Macquarie Ridge Complex (MRC) south of New Zealand. Solid gray shading represents regions shallower than 2000 m. Magnitude 8.2 strike-slip earthquake in 1989 indicated with solid black diamond symbol at 52.3ºS and 160.6ºE. Sinistral offset of the Emerald Fracture Zones (indicated) has occurred across the Antarctic-Pacific boundary. Euler pole locations (red squares) and error ellipses for the rotation of Australian Plate with respect to the Pacific Plate (AUS-PAC) are from Cande and Stock [in review]. Two westernmost pole locations are for rotation of the Macquarie Plate with respect to the Pacific Plate (MAC-PAC). The hypothesized Macquarie Plate (transitional shading) extends east of ~145°E and south of 52°S, bound to the east by the MRC and to the south by the SEIR [Cande and Stock, in review]. Interpreted schematic magnetic isochrons are numbered from Weissel et al. [1977], Wood et al. [1996], Cande et al., 2000, and the PLATES database [Lawver et al., 2001]. Weissel et al. [1977] and Ruff et al. [1989] interpreted ~200 km of underthrusting at the Hjort Trench based on the observed truncation of magnetic anomalies 5 through 8 (~10 to 25 Ma) [Cande and Kent, 1995] as compared to their conjugate anomalies on the Antarctic plate to the south of the easternmost segment of the Southeast Indian Ridge (SEIR).

To understand the dynamic interactions at the Australian-Pacific plate boundary over time, I generated seven reconstructions from 33.3 Ma to the present. The reconstructions presented here represent the most accurate yet compiled for illustrating the evolution of the southern MRC, development of the Hjort Trench (Figure 1.1), and migration of the MTJ. These regional maps serve to introduce the general tectonic setting of the Australian-Pacific plate boundary south of New Zealand.

Important observations from the reconstructions include: (i) oceanic crust generated at the easternmost segment of the Southeast Indian Ridge (SEIR) from 26.6 Ma to 10.9 Ma that is observed on the Antarctic plate is currently unaccounted for on the Australian plate west of the Hjort Trench today, (ii) oblique convergence began for the Hjort region ~10.9 Ma, while spreading was still occurring on the plate boundary to the north, and (iii) the MTJ continually migrated southeastward with respect to the Australian plate since 33.3 Ma.

1.2 RECONSTRUCTIONS

Paleogeographic reconstructions were created using the PLATES software at The University of Texas at Austin Institute for Geophysics. These maps illustrate the interaction of the Australia, Pacific, and Antarctic Plates at seven times from 33.3 Ma to the present. Data and methods used to create these reconstructions are presented in Chapter Three. Reconstructions use the finite rotation poles of *Cande and Stock* [in review]. At anomaly 13o (33.3 Ma), the MRC spreading ridge is essentially continuous with the SEIR (Figure 1.2). Spreading on the MRC accommodated divergence between the Campbell Plateau

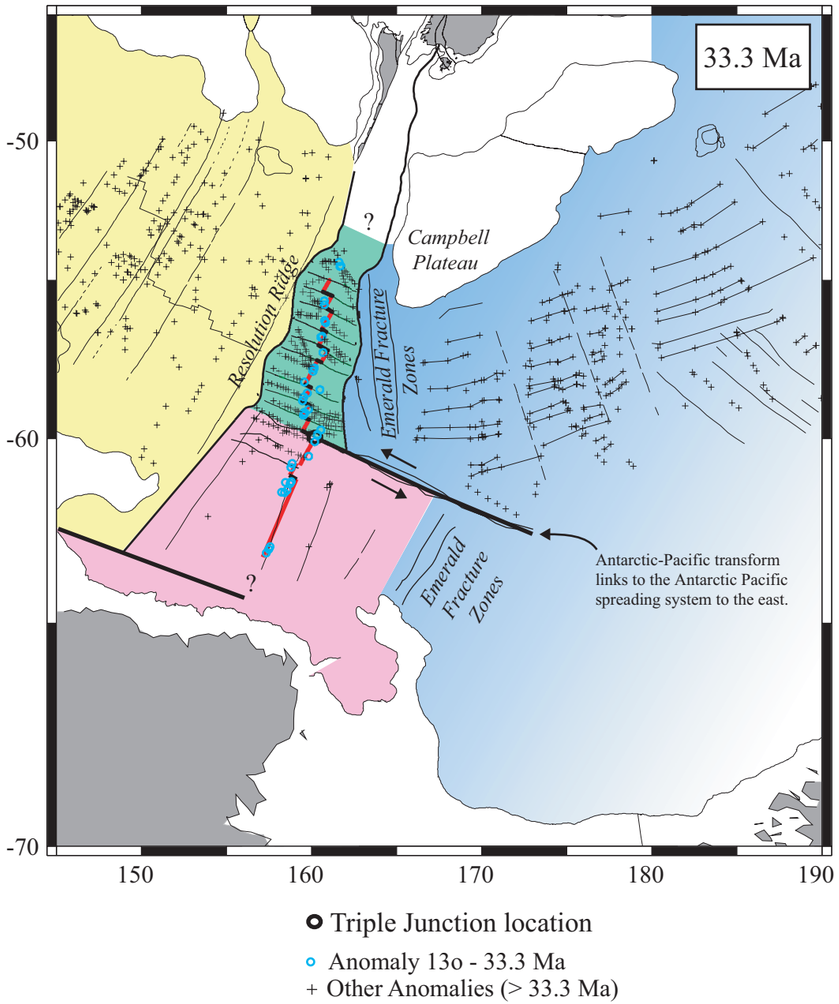

Figure 1.2. Paleogeographic reconstruction of the Australia-Antarctic-Pacific three plate system at 33.3 Ma. Pale yellow color indicates the extinct spreading in the Tasman Sea at ~52 Ma. Blue shading represents crust that was formed by continual spreading processes at the Antarctic-Pacific spreading ridge. Pink shading indicates crust that was formed by spreading ridges at the Southeast Indian Ridge that are still active today. Green shading indicates crust that was formed by spreading processes at the Macquarie Ridge. The distinction between pink and green shading is that crust colored green was formed at spreading ridges that are no longer active whereas crust shaded pink was formed at ridge segments that are still active today. Magnetic anomaly locations with assigned ages of 33.3 Ma are indicated with blue circles. Cross symbols denote older anomaly positions. Open black circle denotes interpreted triple junction location. Black arrows indicate approximate relative plate motion on the Antarctic-Pacific boundary. Emerald Fracture Zones are sinistrally offset across the Antarctic-Pacific plate boundary. This boundary is assumed to connect with Antarctic-Pacific spreading ridges to the east, although magnetic anomaly data used for the reconstructions do not permit that intersection to be constrained beyond the interpretation shown.

and the Resolution Ridge (Figure 1.2). Based on the amount of crust formed north and south of ~60ºS (Figure 1.2), the southern spreading on the SEIR occurred at a faster rate than on the MRC segments to the north. At 33.3 Ma the Antarctic-Pacific boundary was a transform fault hundreds of kilometers long (Figure 1.2). This transform fault had sinistral strike-slip displacement, as evidenced by the offset of the Emerald Fracture Zones (Figure 1.2).

Since anomaly 13o (33.3 Ma), spreading continued in a generally NW/SE direction for both the MRC and SEIR. By 26.6 Ma, differences in the rates of spreading on the SEIR and MRC spreading ridges resulted in the left step of the trends of the two spreading ridges along a dextral transform fault that increased in length since 33.3 Ma (Figure 1.3). The Antarctic-Pacific plate boundary remained a dominantly sinistral strike-slip boundary, but may have accommodated a transtensional component at this time, as indicated by the separation of the lineaments defining the boundary (Figure 1.3).

By 20.1 Ma spreading became more oblique at the MRC due to changes in relative motion between the Australian and Pacific Plates. This resulted in the formation of curved fracture zones adjacent to the MRC as the orientation of spreading centers adjusted to the change in direction of relative motion (Figure 1.4) [*Lamarche et al*., 1997; *Massell et al*., 2000]. The SEIR and MRC spreading ridges were separated by approximately 300 km due to different rates of spreading on the two ridge systems (Figure 1.4). Australian-Antarctic relative motion rotated slightly to the east, but remained generally oriented NW/SE. The

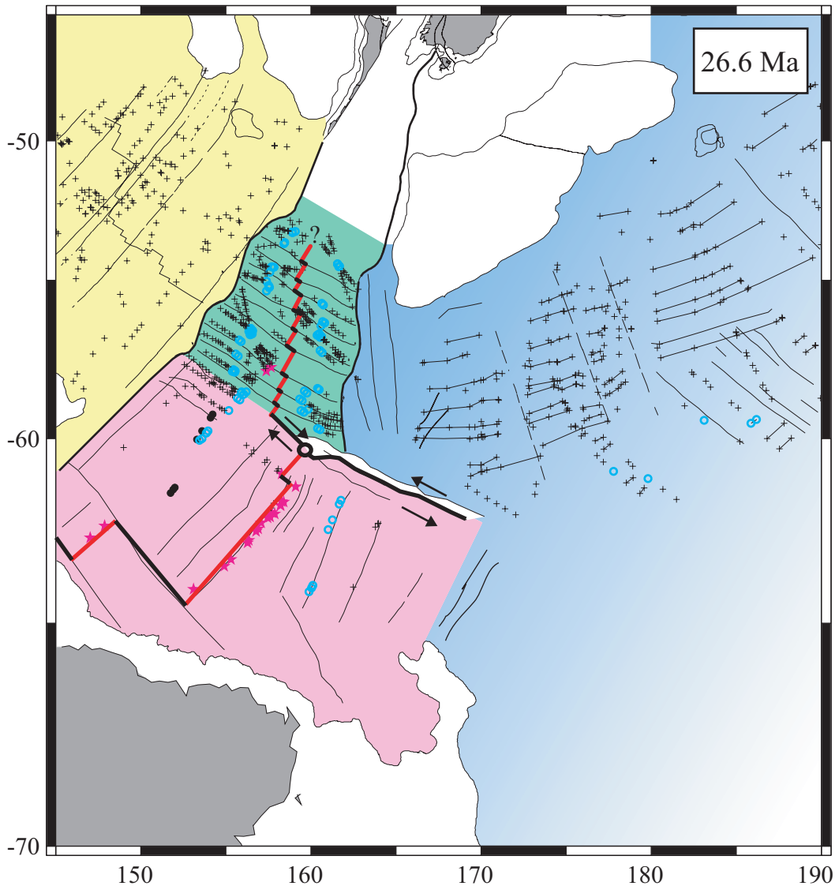

Figure 1.3. Paleogeographic reconstruction for 26.6 Ma. Solid black symbols denote magnetic anomalies identified on the Antarctic crust south of the easternmost SEIR that have been duplicated and rotated with the Australian plate. Magnetic anomaly locations with assigned ages of 26.6 Ma are indicated with pink stars. Black arrows indicate approximate relative plate motion for the Australian-Pacific and Antarctic-Pacific plate boundaries. White area on Antarctic-Pacific plate boundary represents minor divergence may have occurred at this time.

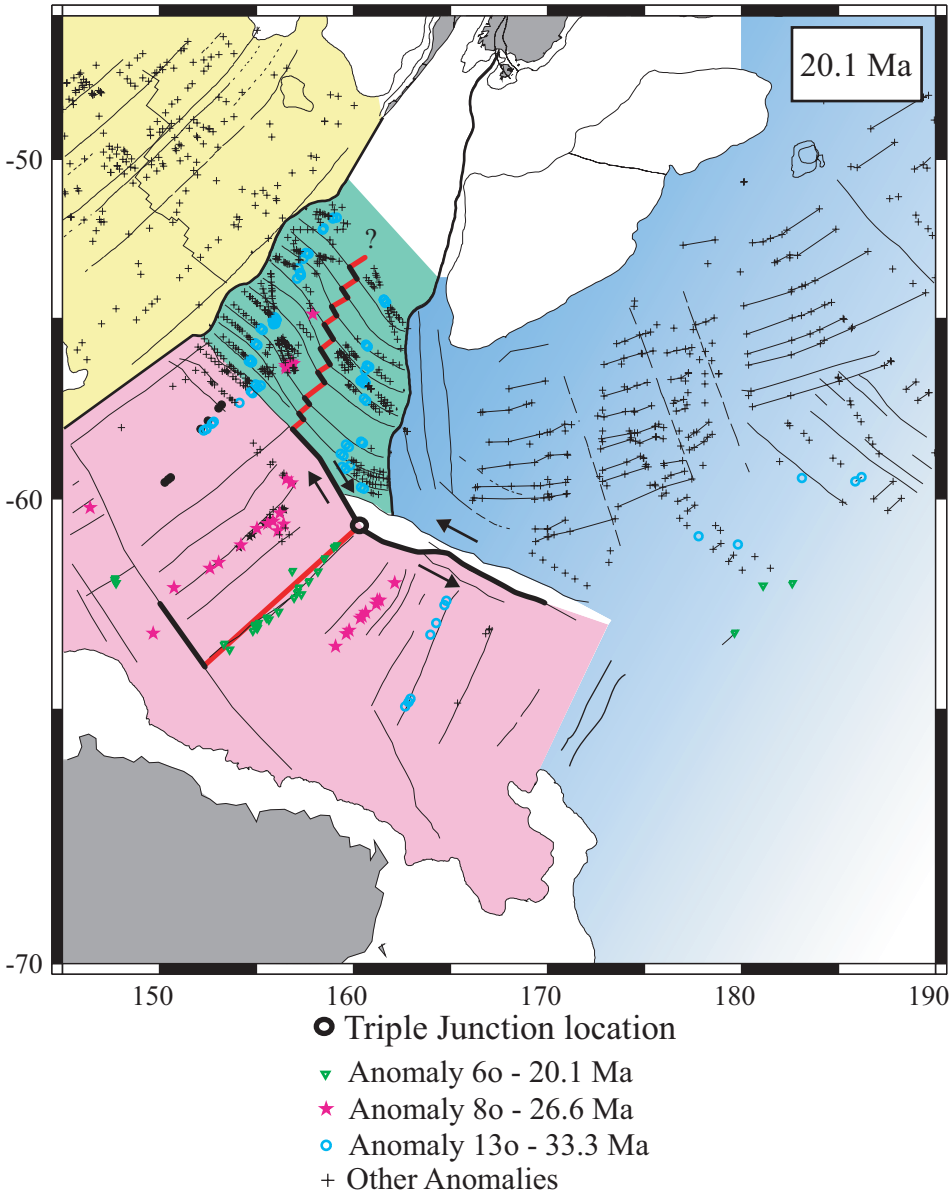

Figure 1.4. Paleogeographic reconstruction for 20.1 Ma. Magnetic anomaly locations with assigned ages of 20.1 Ma are indicated with green triangles. Black arrows indicate approximate relative plate motion for the Australian-Pacific and Antarctic-Pacific plate boundaries.

Antarctic-Pacific boundary remained a dominantly sinistral strike-slip boundary, although it may be best characterized as a leaky transform due to the minor divergence that is indicated by the white region at the plate boundary in Figure 1.4.

Between 20.1 and 10.9 Ma relative motion between the Australia and Pacific plates became extremely oblique, resulting in the lengthening of transforms between the MRC spreading centers and a decrease in the width of spreading segments (Figure 1.5). The active SEIR length was significantly shorter than it was at 33.3 Ma (Figure 1.5). However, spreading remained oriented generally NW/SE on the SEIR. The Antarctic-Pacific boundary remained a dominantly sinistral strike-slip boundary, or leaky transform.

By 5.9 Ma relative motions of the Australian and Pacific plates became so oblique that spreading ceased everywhere along the MRC, and dextral strike-slip displacement and oblique convergence (transpression) dominated the boundary at this time (Figure 1.6). At this time, the MRC became an extensive transform fault boundary connecting the SEIR and the Alpine fault system in the South Island of New Zealand (Figure 1.6). Spreading continued on the SEIR with an orientation similar to 10.9 Ma. The easternmost SEIR ridge segment continued to shorten, as a result of triple junction migration along the southern Australian-Pacific boundary at this time. Convergence is indicated by the overlap of the (rotated Antarctic) anomaly 6o locations at ~58ºS (solid black triangles in Figure 1.6). A change in Antarctic-Pacific plate motion around anomaly 3Ay (5.9 Ma) caused

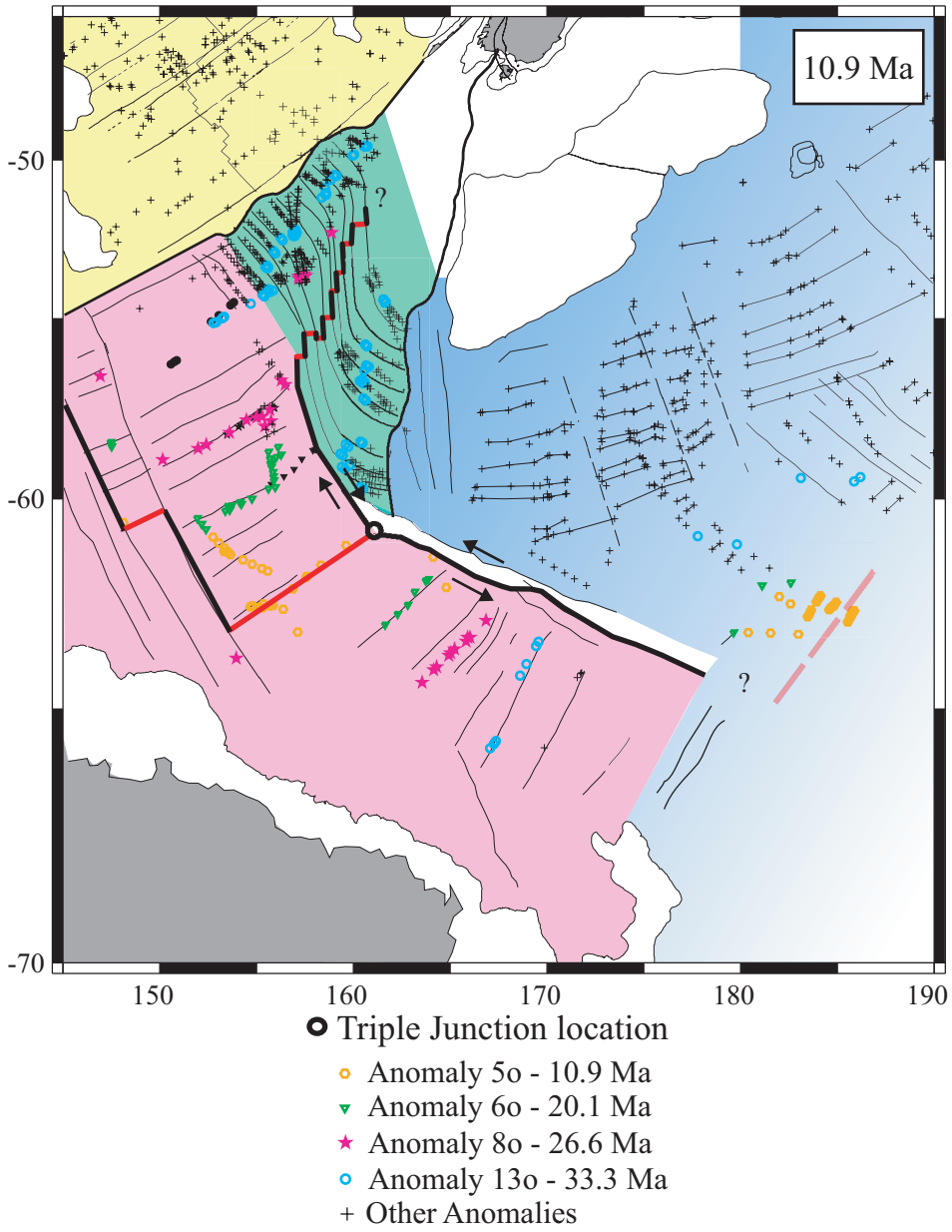

Figure 1.5. Paleogeographic reconstruction for 10.9 Ma. Magnetic anomaly locations with assigned ages of 10.9 Ma are indicated with orange hexagons. Black arrows indicate approximate relative plate motion for the Australian-Pacific and Antarctic Pacific plate boundaries.

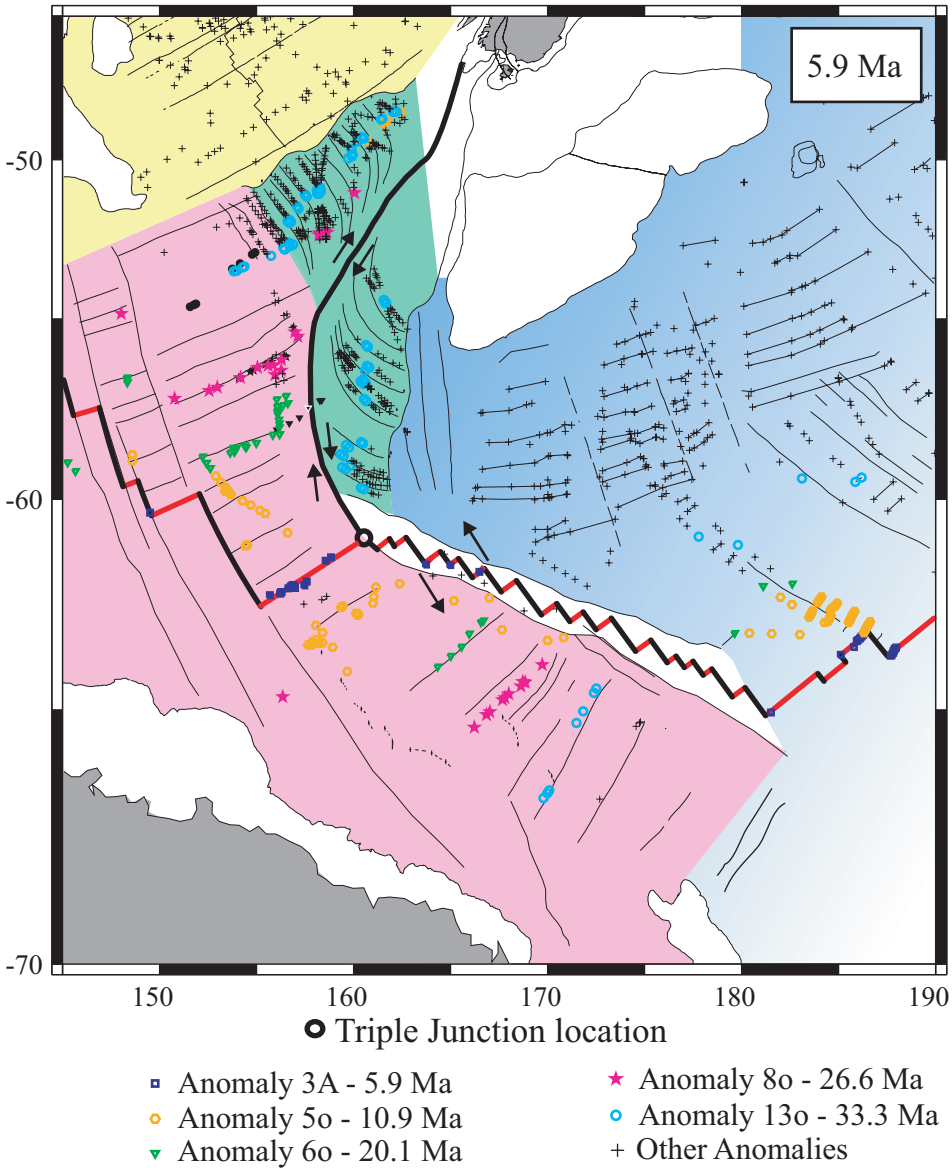

Figure 1.6. Paleogeographic reconstruction for 5.9 Ma. Magnetic anomaly locations with assigned ages of 10.9 Ma are indicated with blue squares. Black arrows indicate approximate relative plate motion for the Australian-Pacific and Antarctic Pacific plate boundaries.

the transform between the Pacific and Antarctic plates to evolve into an oblique spreading center (Figure 1.6).

At 2.6 Ma convergence at the southern Australian-Pacific boundary is indicated by the increased overlap of (rotated Antarctic) anomaly 6o locations at approximately 57ºS (black triangles in Figure 1.7), and (rotated Antarctic) anomaly 5o locations at approximately 60ºS (black hexagons in Figure 1.7). The SEIR spreading direction rotated clockwise, and the easternmost segment of the SEIR continued to shorten to the minimum amount observed for the reconstructions. The Antarctic-Pacific boundary continued to accommodate oblique divergence.

The present day map differs only slightly from the map at 2.6 Ma. Additional convergence on the southern Australian-Pacific boundary is indicated by increased overlap of (rotated Antarctic) anomaly 6o (solid black triangles) and 5o (solid black hexagons) locations (Figure 1.8). The Australian-Pacific boundary lengthened slightly to the south with migration of the triple junction. Oblique spreading at a relatively constant rate continued to accommodate oblique divergence at the Antarctic-Pacific boundary.

1.3 OVERVIEW OF DISSERTATION

Paleogeographic reconstructions emphasize the critical observations of the southern MRC that require tectonic explanations. Outstanding problems related to the evolution of the Hjort Region include:

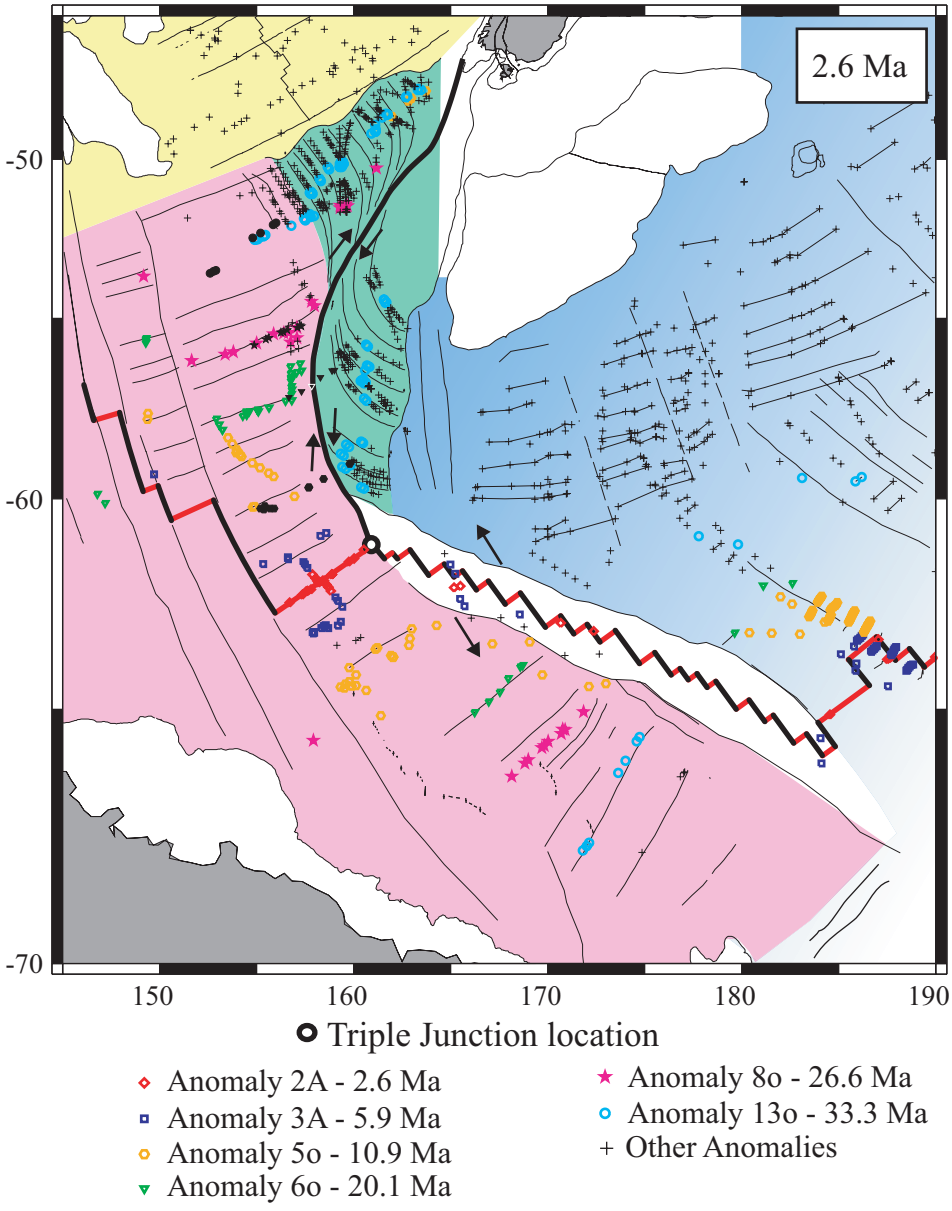

Figure 1.7. Paleogeographic reconstruction for 2.6 Ma. Magnetic anomaly locations with assigned ages of 2.6 Ma are indicated with red diamonds. Black arrows indicate approximate relative plate motion.

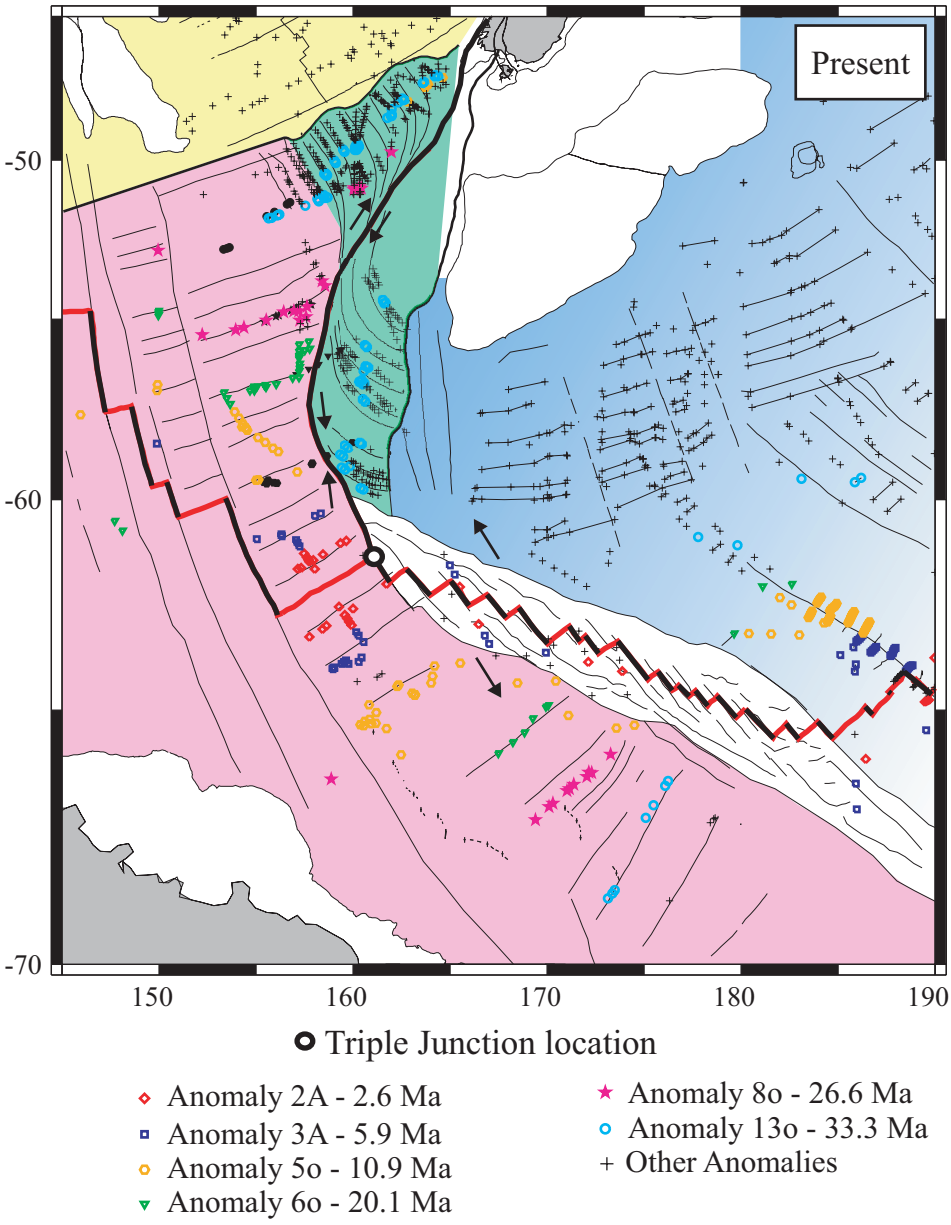

Figure 1.8. Map for the present day. Black arrows indicate approximate relative plate motion.

1) What was the fate of the crust that previously existed west of the Hjort Trench? This crust has either been deformed at the plate boundary, translated laterally along the boundary, underthrust in a young (<10.9 Ma) subduction zone, or some combination of these three.
2) How has the convergence history influenced the anomalous morphology (ridge and trough features) of the southern MRC? The variable orientation of the plate boundary has resulted in significantly different convergence histories along the length of the boundary. Is there a consistent relationship between the morphology, convergence history, and structural development along the boundary?
3) What processes resulted in the curved shape of the plate boundary in the Hjort region? How did the complex interaction of convergence and the migration of the triple junction generate the presently observed shape of the boundary?

Until recently, insufficient data have been available to accurately characterize the tectonic development of the Australian-Pacific plate boundary south of 56ºS. These problems are addressed in the following chapters.

Chapter Two uses marine geophysical data acquired during a January 2000 survey over the Hjort region to investigate the structural, geophysical, and seismogenic characteristics of the Hjort Trench. Various faults are interpreted from lineaments in the swath bathymetry and reflectivity data. The offset on the faults is interpreted where multi-channel seismic profiles traverse those structures, and is used to infer kinematics. Two major plate boundary faults are identified in

the Hjort region: an interpreted strike-slip fault in the crest of the MRC and an interpreted thrust fault in the trench. Seismicity data from three catalogs are evaluated for the Hjort region and the most reliable events are used to interpret the distribution of events and to characterize focal mechanisms. The distribution of events is confined to the plate boundary zone, with the deepest event occurring at 64 km. Seismicity data do not define a Wadati-Benioff zone east of the trench. Both thrust and strike slip mechanisms occur, suggesting oblique convergence has been partitioned at the plate boundary between the major interpreted thrust and strike-slip faults. Gravity profiles across the Hjort region are used to infer crustal structure. Models suggest ~50 km of underthrusting of the Australian plate beneath the Pacific plate, and favor dynamic support rather than Airy compensation for topography of the MRC. These datasets are integrated to arrive at a consistent interpretation of active tectonics at the Hjort Trench, concluding that the Hjort Trench represents an incipient subduction zone.

Chapter Three considers the anomalously deep and shallow topography adjacent to the plate boundary and seeks to constrain the amount of convergence that may have been accommodated by the generation such topography. For 17 locations on the boundary south of 51ºS, the volumes of crust displaced from the average seafloor depth are determined for 50 km by 140 km swaths of gridded bathymetry data. The amount of convergence perpendicular and parallel to the plate boundary at each point is determined using stage rotation poles since 10.9 Ma. A consistent relationship is established between the volumes of crust displaced from the average seafloor depth and the boundary-normal component of

convergence that has occurred at the plate boundary, suggesting that up to 50 km of boundary-normal convergence has been accommodated by deformation at the plate boundary. Convergence in the Hjort Trench that is not accounted for by the observed topography has been partitioned into strike-slip translation of crust northward on the boundary and limited underthrusting.

Chapter Four considers the details of the migration history of the MTJ and the influence migration had on the curved shape of the southern Australian-Pacific plate boundary in the Hjort region. Detailed reconstructions of the triple junction region are presented for seven times since 33.3 Ma. Directions and rates of relative motion of the Australian, Antarctic, and Pacific plates are determined using stage rotation poles for the reconstructed positions of the triple junction. Vector diagrams illustrating relative motion of the Australian, Antarctic, and Pacific plates at the triple junction for each reconstruction are used to infer tectonic processes occurring at the different boundaries over time. In addition, previous triple junction locations are inferred from relative motion information in the vector diagrams. Results indicate that the Hjort region of the MRC never experienced divergence, but evolved as a dextral transform fault connecting the SEIR and MRC. Oblique convergence across the transform fault since 10.9 Ma caused incipient subduction at the Hjort Trench. The migration history of the triple junction is used to constrain ~220 km of convergence at the southern MRC. Southeastern migration of the triple junction since 33.3 Ma caused the length of the Australian-Pacific transform boundary to increase by ~1100 km and resulted in a decrease of ~300 km in the length of the easternmost SEIR from 26.6 Ma to

5.9 Ma. Migration of the triple junction resulted in the presently observed curved shape of the Australian-Pacific plate boundary in the Hjort region.

Chapter 2: Underthrusting at the Hjort Trench, Australian-Pacific Plate Boundary: Incipient Subduction?

2.1 ABSTRACT

The Hjort Ridge, Trench, and Plateau comprise the southernmost portion of the Macquarie Ridge Complex (MRC), the Australian-Pacific plate boundary south of New Zealand. On the basis of marine geophysical (swath bathymetry/reflectivity, seismic reflection, gravity, magnetic) data, teleseismic data, and gravity modeling, we argue that the Australian plate is actively underthrusting the Pacific plate along the Hjort Trench, but self-sustaining subduction does not yet appear to have commenced. We interpret a crustal discontinuity in the Trench as a fracture zone separating oceanic crust generated at the Southeast Indian Ridge (SEIR crust), located to the south, from oceanic crust generated at the extinct Australian-Pacific spreading center located to the north (MRC crust). This fracture zone has been reactivated as a significant plate boundary decollement in the Hjort Trench, but our estimate of ~50 km of underthrusting does not support the existence of an eastwardly dipping Australian slab below ~20 km depth. For the length of the Hjort Ridge and Trench system, oblique convergence is partitioned between a decollement in the Trench and a strike-slip fault system in the ridge complex. South of 57.5ºS, the Trench decollement accommodates thrusting. North of 57.5ºS, the boundary-parallel component of convergence becomes dominant, the Trench gradually shallows, and the trench decollement evolves into a low-angle, strike-slip fault. The trench

decollement and strike-slip system in the ridge complex are structural boundaries that contain tectonic slivers of inferred MRC crust east of the Trench that currently belong to neither the Australian nor the Pacific plates.

2.2 INTRODUCTION

Despite the critical importance of subduction zones in plate tectonic theory, the tectonic setting and dynamics of their origin are poorly known. Many observations suggest that subduction has initiated along transform faults or fracture zones. Using plate reconstructions, *Uyeda and Ben-Avraham* [1972], *Hilde et al.* [1977], and *Stern and Bloomer* [1992] suggested that subduction zones in the western Pacific may have formed at active or relict strike-slip plate boundaries. *Dewey* [1975] used geometric plate models to demonstrate how changes in relative plate motion and migration of triple junctions can cause fracture zones to evolve into subduction zones. In the Fiordland region of southernmost New Zealand and the contiguous Puysegur region offshore, *Christoffel and van der Linden* [1972] proposed that a transform fault evolves northward into a subduction zone, which is shaped like an inverted plowshare. In their example, the subduction zone strikes obliquely to the direction of relative plate motion. In the same region, *Collot et al.* [1995] also concluded that fracture zone reactivation plays a significant role in subduction initiation. Much farther south of New Zealand, the Hjort Trench lies along the southernmost portion of the Macquarie Ridge Complex (MRC), the active, submarine portion of the Australian-Pacific plate boundary that extends to the Australian-Pacific-Antarctic triple junction [*Falconer, 1972; Lodolo and Coren, 1994 & 1997;* Figure 2.1].

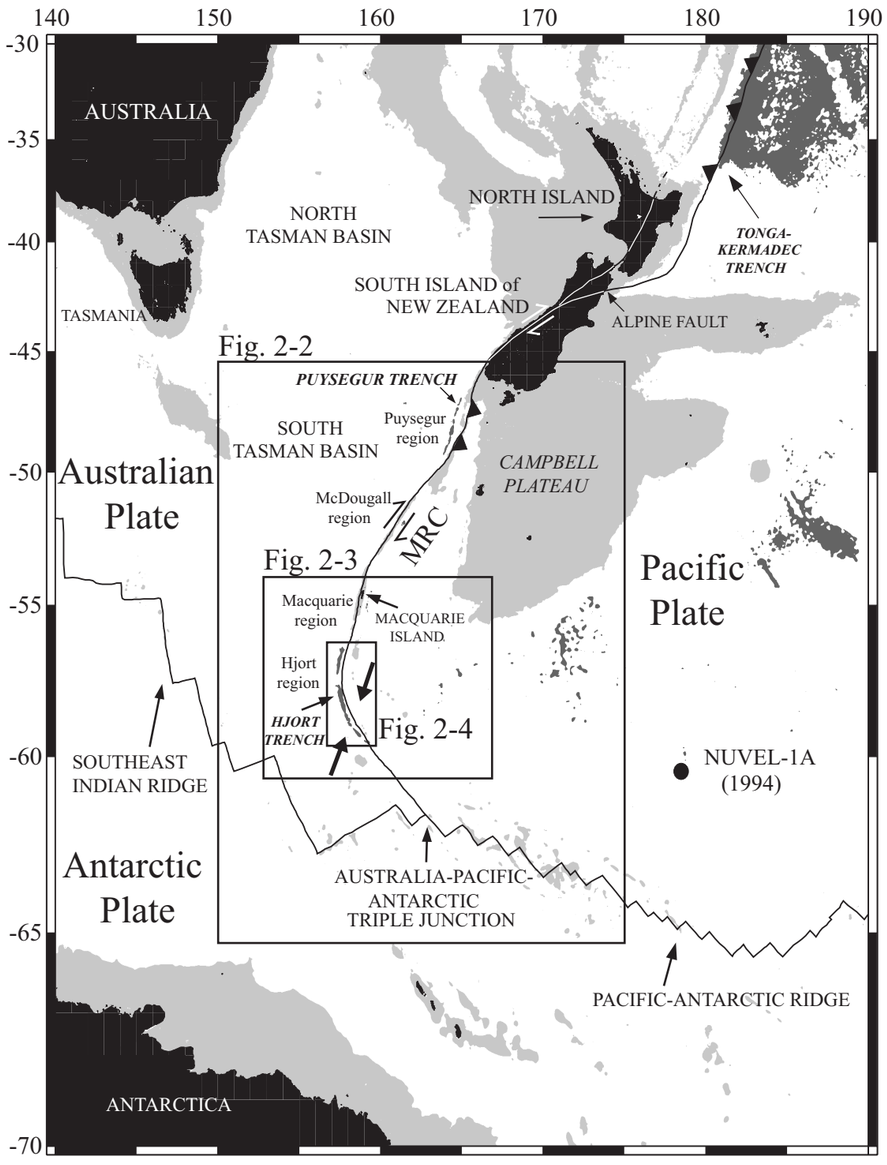

Figure 2.1. Geographic setting of the Hjort Trench at the southern end of the Macquarie Ridge Complex (MRC). Light shading represents regions shallower than 2000 m and darker shading represents regions deeper than 5500 m. Location of NUVEL-1A [DeMets et al., 1994] pole of rotation for relative motion between the Australian and Pacific plates is shown as dark circle. Small arrows along the MRC plate boundary indicate predicted relative motion using NUVEL-1A pole. The close proximity of the NUVEL-1A pole to the curvilinear Australian-Pacific plate boundary results in dramatic along-strike variability in the orientation and magnitude of relative motion across the boundary. Whereas the current tectonic regime for the McDougall and Macquarie regions is dominantly strike-slip [Frohlich et al., 1997; Massell et al., 2000], the NUVEL-1A model predicts that the Hjort region is experiencing oblique NNE-SSW convergence (bold arrows). The locations of Figures 2.2, 2.3 and 2.4 are shown with labeled boxes.

The Hjort Trench provides a unique opportunity for documenting the tectonic setting, geomorphology, and geophysical characteristics of incipient underthrusting. We present morphologic, structural, seismicity and gravity data indicating that underthrusting involving strain partitioning and fracture zone reactivation is occurring at this obliquely convergent setting within oceanic lithosphere.

Lithospheric scale interactions at convergent plate boundaries may be described by various terms, which are commonly inconsistent or ambiguous in the literature. To clarify our use of such terms, we provide the following definitions. 'Subduction' refers to the mature process that is associated with a bathymetric trench, a seismically active Wadati-Benioff zone defining an underthrust lithospheric slab at depth, and associated arc volcanism. Other terms describe various phases that may precede, but do not necessarily evolve into subduction. Different terms are used for different amounts of lithospheric displacement. 'Underthrusting' refers to thrust offsets that are significant at the lithospheric scale, and 'incipient underthrusting' refers to the formation of sub-lithospheric scale faults (some of which have thrust displacement) and associated diffuse seismicity within the lithosphere that characterizes the earliest stages of convergence. 'Incipient subduction' refers to an advanced stage of underthrusting in which a decollement penetrating the entire lithosphere accommodates increasing displacement of underthrust crust. 'Subduction initiation' refers to a still more mature stage in which underthrust lithosphere has descended below the overriding lithosphere, and subduction processes such as seismicity deeper than

~50 km, metamorphism of basalt/gabbro to eclogite, and volcanism have commenced. It is important to note that incipient subduction does not necessarily evolve into subduction initiation.

2.3 GEODYNAMIC SETTING

Initial reconnaissance studies of the MRC employed bathymetry, gravity, and magnetics data and established it as a location of Australian-Pacific plate interaction [*Hayes*, 1972; *Weissel and Hayes*, 1972]. The tectonic evolution of the MRC has been controlled by changing relative motions between the Australian and Pacific plates and ensuing southward migration of the their rotation pole since ~10 Ma [*Walcott*, 1984]. The tectonic interpretation of the MRC has been controversial. *Ewing and Heezen* [1956] proposed that the MRC is part of the mid-oceanic ridge system, which was later echoed by *Varne et al.* [1969]. *Summerhayes* [1967, 1969] and *McKenzie and Morgan* [1969] proposed that the MRC represents a Tertiary-Quaternary island arc. *Houtz et al.* [1971] suggested that the MRC was originally formed as a shear zone but may have recently developed into an island arc in the Hjort region. *Hayes and Talwani* [1972] concluded that the tectonics of the Hjort Trench are dominantly transcurrent with a secondary compressive component, and that various portions of the MRC may represent each of the previously proposed models. This recognition of the complex variability of tectonic interpretations directed subsequent, detailed research of specific portions of the MRC (e.g., Puysegur, McDougall, Macquarie, and Hjort regions; Figures 2.1 and 2.2) [*Frohlich et al.*,

1997; *Lebrun et al*., 1998; *Schuur et al*., 1998; *Melhuish et al*., 1999; *Lamarche and Lebrun*, 2000; *Massell et al*., 2000, *Bernardel and Symonds*, 2001].

In the most critical examination of seismicity of the MRC to date, *Frohlich et al*. [1997] evaluated teleseimically determined focal mechanisms and epicenters for earthquakes along the entire MRC (Figure 2.2), and concluded that all better determined focal mechanisms on the MRC in this region were strike-slip. No geophysical or seismological evidence presented by *Frohlich et al*. [1997] suggests ongoing or incipient subduction in the McDougall or Macquarie regions (Figure 2.1). For the same regions, *Massell et al.* [2000] interpreted marine bathymetry and identified curved fracture zones that become asymptotic to the MRC but maintain an orthogonal relationship with relict spreading fabric. They attributed this geometry to changes in the direction of oblique spreading on the MRC since 40 Ma. They identified a fault valley at the crest of the MRC and interpreted this as the modern transform boundary. They argue against underthrusting in the McDougall region, but suggested limited (incipient) underthrusting in the Macquarie region. The Puysegur region has been shown to involve a transition from strike-slip faulting to oblique subduction beneath Fiordland [*Lamarche and Lebrun*, 2000; *Lebrun et al.*, 2000].

Previous geophysical investigations of the Hjort Trench associated the bathymetric depression with established subduction of Australian oceanic crust to the west beneath Pacific oceanic crust to the east. *Weissel et al.* [1977] interpreted magnetic anomalies west of, and at high angle to, the Hjort Trench (Figure 2.2), and observed that the anomalies are shorter than their correlative

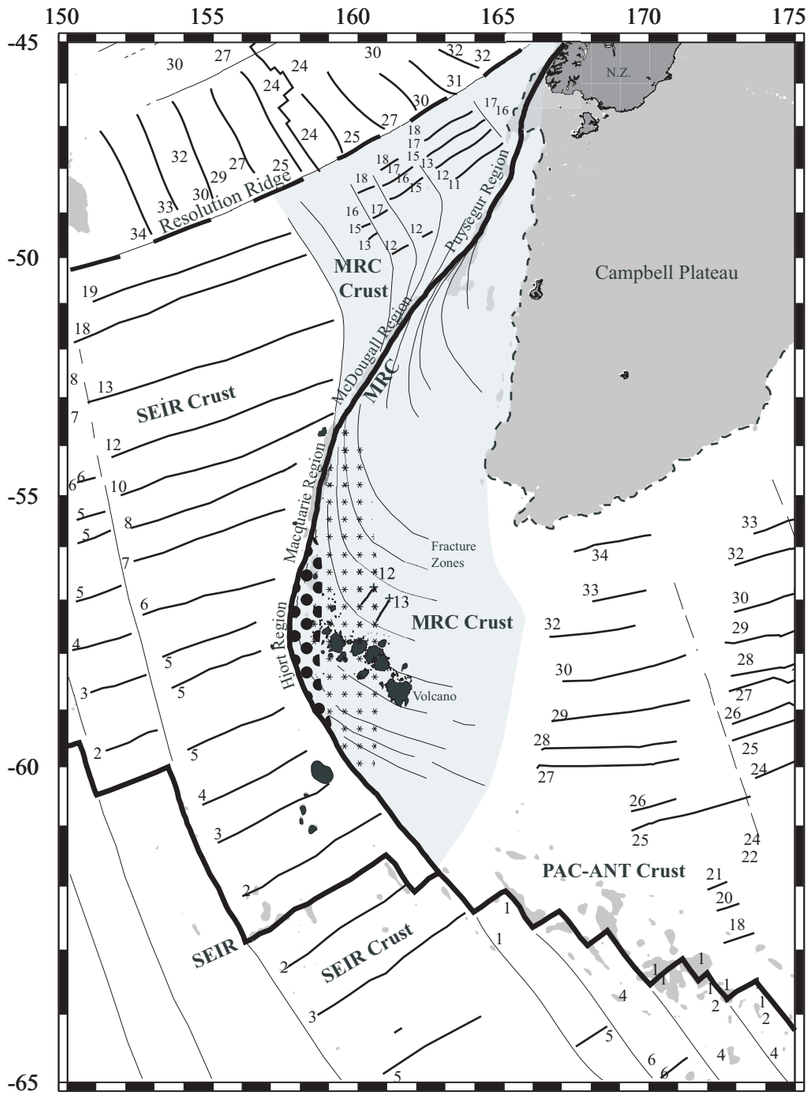

Figure 2.2. Regional magnetic isochron map. Interpreted isochrons are numbered from Weissel et al. [1977], Wood et al. [1996], and the PLATES database [Lawver et al., 2001]. Continental crust of the Campbell Plateau is outlined with a dashed black line, enclosing the grey-colored region shallower than 2000 m water depth. Light gray area is oceanic crust which formed at the extinct MRC spreading center from 40 to ~10 Ma. Thin black lines are fracture zones, and volcanoes are filled with solid black color. Asterisk pattern (*) is the predicted amount of SEIR crust (labeled) underthrust at the Hjort Trench proposed by Weissel et al. [1977] and Ruff et al. [1989] based on the observed truncation of magnetic anomalies 5 through 8 (~10 to 25 Ma) [Cande and Kent, 1995] as compared to their conjugate anomalies on the south side of the easternmost segment of the SEIR. Large gray dot pattern represents amount of underthrusting proposed in this paper.

counterparts on the southeastern side of the easternmost portion of the Southeast Indian Ridge. They assumed that the anomalies were originally of similar length to those on the southern side of the Ridge, or approximately 300 km longer than their observed length today (Figure 2.2). Two explanations were proposed for the "missing crust" implied by the shorter anomalies. Either 300 km of Australian oceanic crust has been subducted at the Hjort Trench, or was "captured" by the Pacific plate when the plate boundary moved west. *Ruff and Cazenave* [1985] proposed active subduction at the Hjort Trench based on a comparison of the geoid anomaly over the Trench with the Aleutian-Komandorski region, an oblique subduction zone, and the speculative focal mechanism of a 1924 earthquake. *Jones and McCue* [1988] investigated seismicity records for the MRC and concluded that the mechanisms in the Hjort Trench are consistent with right-lateral strike-slip motion, with an element of east-west thrusting south of 51?S. A later study by *Ruff et al.* [1989] concluded that subduction is initiating aseismically at the Hjort Trench, although their most compelling evidence for subduction was derived from considerations of the Australian-Pacific-Antarctic triple junction. Thus, the tectonics of the Hjort Trench have remained controversial.

2.4 Analysis of Upper Crustal Structure

2.4.1 Bathymetry, Reflectivity, and Seismic Reflection Data

Our study focuses on the Hjort region of the MRC (Figure 2.3; box in Figure 2.1), utilizing geophysical data from R/V *L'Atalante* AUSTREA-2 and R/V *Rig Seismic* 124 surveys. Geoscience Australia's R/V *L'Atalante*

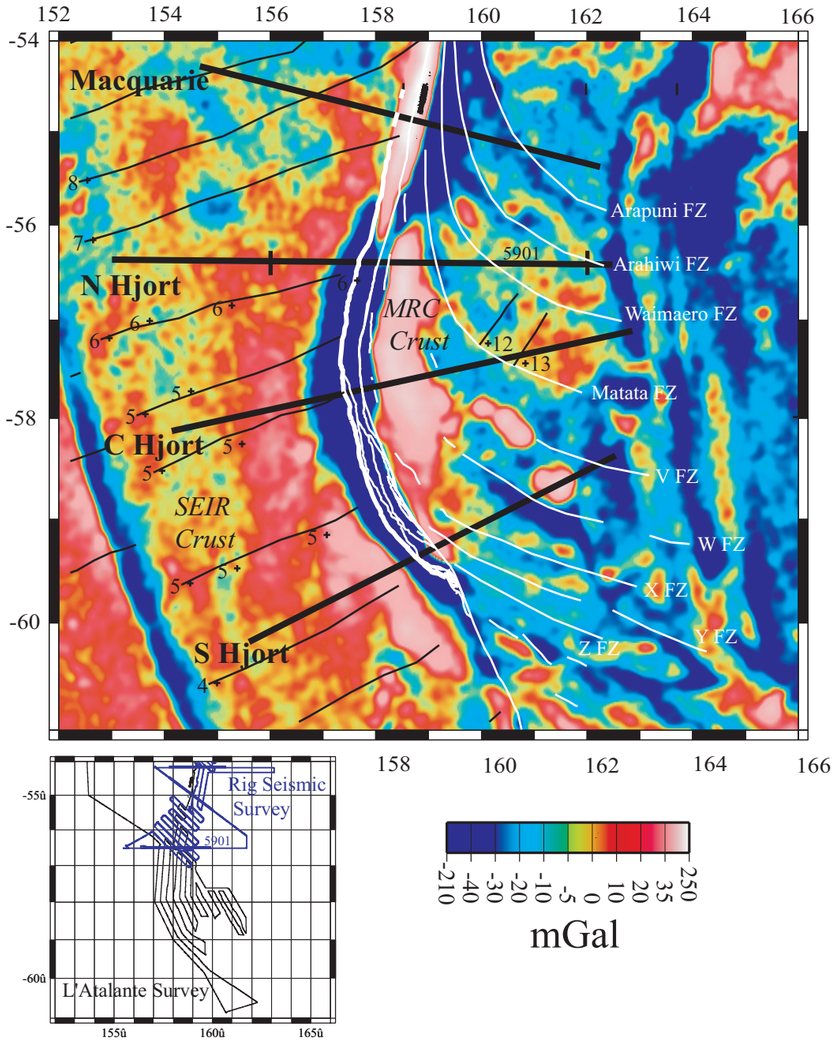

Figure 2.3. Satellite-derived, free-air gravity anomaly map. Numbered cross symbols are magnetic anomalies from Weissel et al. [1977] and the PLATES database [Lawver et al., 2001], and thin black lines represent interpreted magnetic isochrons. White lines represent fracture zones and active plate boundary faults and bold black lines are gravity model transects. Vertical bars on northern Hjort transect indicate extent of shipboard gravity and bathymetry data (not shown on map) from line 5901 of the 1994 Rig Seismic 124 cruise. Ship track coverage of the L'Atalante and Rig Seismic 124 surveys are shown below (Note location of line 5901 for Rig Seismic survey).

AUSTREA-2 [*Bernardel, et al*., 2000, *Bernardel and Symonds*, 2001] survey examined the southern segment of the MRC (Figure 2.3). Data acquired include ~60,000 km^2 of Simrad EM12D multi-beam swath bathymetry and backscatter data, and ~4,300 line-km of 6-channel seismic reflection (6-CS), gravity, and magnetic data (Figure 2.3, inset). The EM12D is a 162-beam deep-water swath mapping system, and output consists of both an interpolated bathymetric model and a spatially-referenced backscatter intensity image (reflectivity). Vertical bathymetric resolution is 0.2% of water depth (i.e. 10 m at 5000 m). For the range of water depths encountered during the survey, individual beam footprints ranged from 120 m^2 to 160 m^2. Total swath width varied between ~8 to 20 km. Bathymetry and reflectivity data were processed with 0.0025 degree lateral spatial resolution. A 2-D spline surface was fit to the bathymetry data using cell resolution of 0.001 degree. The 6-CS data were acquired using a 300 m digital streamer and two generator-injector (GI) air guns operating in harmonic mode (each at 45/105 in^3 capacity) at a pressure of 2000 psi. Data were recorded as 8 s records sampled every 2 ms using a fixed shot rate of 10 s (11 s in deep water). The dominant frequency in the shallowest 1 s of two-way travel time is 50 Hz. Using a velocity of ~1600 m/s, the Rayleigh resolution limit of the seismic reflection data is ~8 m for the shallowest portions of the profiles. Gravity data were collected with a shipboard gravity meter, with a nominal accuracy of 1 mGal. At the start and conclusion of the survey, gravity ties were established in the respective ports. Magnetic data were collected using a proton precession magnetometer with an accuracy of 1 nT.

The 1994 cruise of R/V *Rig Seismic 124* [*Coffin et al.*, 1994] surveyed a 170,000 km^2 area along an 800 km long northern segment of the MRC from the southern Puysegur region to the northern Hjort region. We utilize the portion of this data set south of 54?S (Figure 2.3, inset). Data include HAWAII-HMR1 swath backscatter and bathymetry, and ~7,300 line-km of 8- and 96-channel seismic reflection data (8-CS and 96-CS, respectively) (*Frohlich et al.*, 1997; *Schuur et al.*, 1998; *Massell et al.*, 2000). Acquisition parameters are described in *Massell et al*. [2000]. We utilize the *Rig Seismic* data to provide continuity of swath coverage north of the *L'Atalante* survey, and additional shipboard gravity and seismic reflection data. The *L'Atalante* and *Rig Seismic* bathymetric surveys have been integrated [*Bernardel and Symonds*, 2001] with predicted bathymetry from satellite altimetry data [*Smith and Sandwell*, 1997] (Figure 2.4). *Bernardel and Symonds* [2001] used the L'Atalante data to initially describe seafloor morphology and characteristics in the Hjort region.

2.4.2 Methods

Seafloor morphology was investigated using various scales of images of shaded bathymetric relief, reflectivity amplitudes, and 2-D profiles. In interpreting shaded bathymetry and reflectivity grids, we utilized the highest possible resolution afforded by the EM12D data. The primary features we identified from the bathymetric and reflectivity data are faults, fracture zones, volcanoes, and seafloor sediment distribution. Seismic reflection data image stratigraphy and structure at and beneath the seafloor. We interpret faults on seismic reflection data, and the data allow some of these faults, which were also

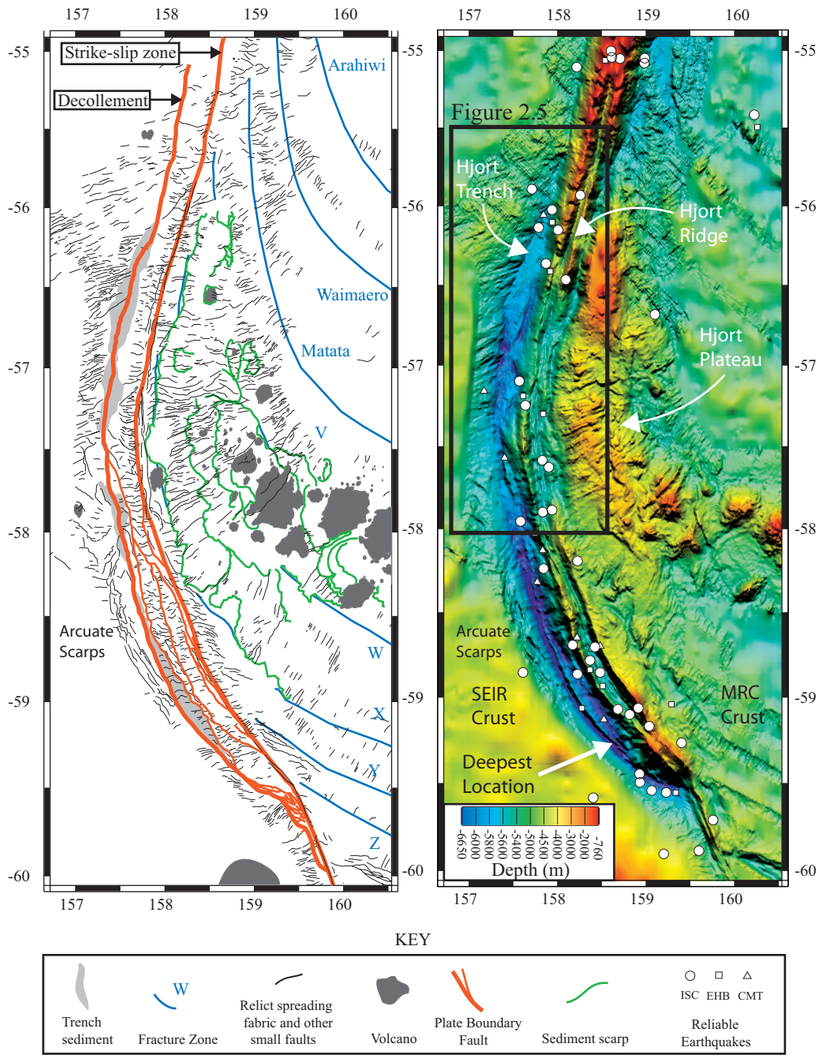

Figure 2.4. Interpreted structures (left) and combined L'Atalante, Rig Seismic, and predicted [Smith and Sandwell, 1997; Bernardel and Symonds, 2001] bathymetry shaded from the north (top) in the Hjort region. Left: Red lines indicate major faults within the plate boundary zone. Bold red lines are the decollement (left) and strike-slip (right) zone that together accommodate oblique convergence. The westernmost red fault in the Trench represents the boundary between SEIR and MRC oceanic crust that has been reactivated as a thrust fault. Right: White arrows point to bathymetric features described in the text. Earthquake locations of more reliable events from the ISC, EHB, and CMT catalogs (see text for discussion). Note location of Figure 2.5.

mapped as seafloor lineaments in bathymetry data, to be extended as much as 2.5 s two-way travel time (TWTT) beneath the seafloor.

Faults generally have linear trends with bathymetric relief of tens to hundreds of meters, and typically have relatively high reflectivity values, indicating a general lack of sediment on the fault scarps. Fault scarp slopes in the study area are typically shallower than 20?. Faults of this scale are poorly expressed in the gravity data. We identified fracture zones using bathymetry, gravity, and seismic reflection data. Because fracture zones have significant expression in the free-air gravity anomaly field, satellite-derived free-air anomaly maps (*Smith and Sandwell*, 1997; Figure 2.3) were most useful for confirming fracture zone locations. Fracture zones are orders of magnitude longer along trend than the faults described above. Fracture zones commonly have short-wavelength bathymetric expressions on the seafloor that reflect uncompensated subsurface crustal offsets [*Mueller and Roest*, 1992]. The seafloor expressions of fracture zones are typically accompanied by gradients in the gravity anomaly, and fracture zones typically coincide with negative free-air gravity anomalies [*Vogt et al.*, 1984]. In the Hjort region, we mapped fracture zones using a combination of the bathymetric offset, where shipboard bathymetric data were available, and their expression in satellite-derived regional free-air gravity anomaly field. East of the Trench, sediment cover commonly obscures seafloor expression of fracture zones, and bathymetry and reflectivity data typically record characteristics of various sedimentary processes, volcanoes, and faults smaller than fracture zones. Where apparent, we mapped fracture zones at the base of bathymetric scarps. Relief

across the fracture zones varies from tens to hundreds of meters. Fracture zones are generally observed at the base of the anomaly gradient in the free-air gravity field. Values change by up to 30 mGal across interpreted fracture zones. Sedimentary deposits are generally sparse in the study area [*Schuur* et al., 1998]. Sediment distribution on the seafloor was mapped as regions of low reflectivity, and was confirmed with seismic reflection data. The Trench contains the most significant accumulation of sediment. Sediment also occurs on the eastern side of the Trench, where it is characterized by low reflectivity values.

2.4.3 Upper Crustal Structure by Region

West of the Hjort Trench

The oceanic crust west of, and descending into, the Hjort Trench belongs to the Australian plate and was generated at the Southeast Indian spreading ridge (SEIR) [*Weissel et al.*, 1977; Figure 2.2]. We refer to this crust as SEIR crust. We identify prominent WSW-ENE oriented scarps that characterize this crust (Figure 2.4). Normal displacements are observed across these scarps on bathymetric and seismic reflection profiles, and reflectivity values are high, indicating lack of sediment cover. These scarps trend oblique to the Trench, but do not continue onto the Hjort Ridge (see below) east of the Trench. The southern portion of the western flank of the Trench (58.5?S, 157.5?E) contains a family of generally N-S to NW-SE oriented scarps that are arcuate, and concave toward the Trench (labeled in Figure 2.4). These scarps truncate the WSW-ENE oriented scarps. Reflectivity values are generally high for the SEIR crust west of

the northern portion of the Trench, whereas reflectivity values on SEIR crust south of ~57.5º are noticeably lower (Figure 2.5C).

Hjort Trench

The Hjort Trench is arcuate, and convex to the west. The western boundary of the Trench is the point of maximum flexure of the SEIR crust. The Trench deepens toward the east, reaching maximum depth (6650 m) at its southern end (Figure 2.4). The eastern margin of the Trench is bounded by the steep western scarp of the Hjort Ridge (see below). The Trench terminates to the north by a relatively gradual narrowing and shallowing in bathymetry, in contrast to the sharp termination to the south, where the plate boundary changes orientation abruptly (Figure 2.4). Sedimentary deposits in the Trench are shaded in light gray in Figure 2.4. We mapped a bathymetric low in the medial portion of the Trench that is continuous and parallel to the Trench (Figure 2.4).

The Trench contains up to 2.2 s (TWTT) of sediment in the northern portion, but significantly less (1.2 s TWTT) in the south (Figure 2.4). In the northern Trench, sediment has been deposited on SEIR crust in the western portion of the Trench, and to the east on oceanic crust of the Hjort Ridge (Figure 2.6; note strike orientation, Figure 2.5A). In one location (B, Figure 2.6), continuous reflections within the trench sediment truncate against less reflective sediment that overlies crust of the Hjort Ridge. Trench sediment (Figures 2.5D and 2.6; dark gray shading) has stronger and more continuous internal reflections than the sediment it onlaps (Figure 2.6).

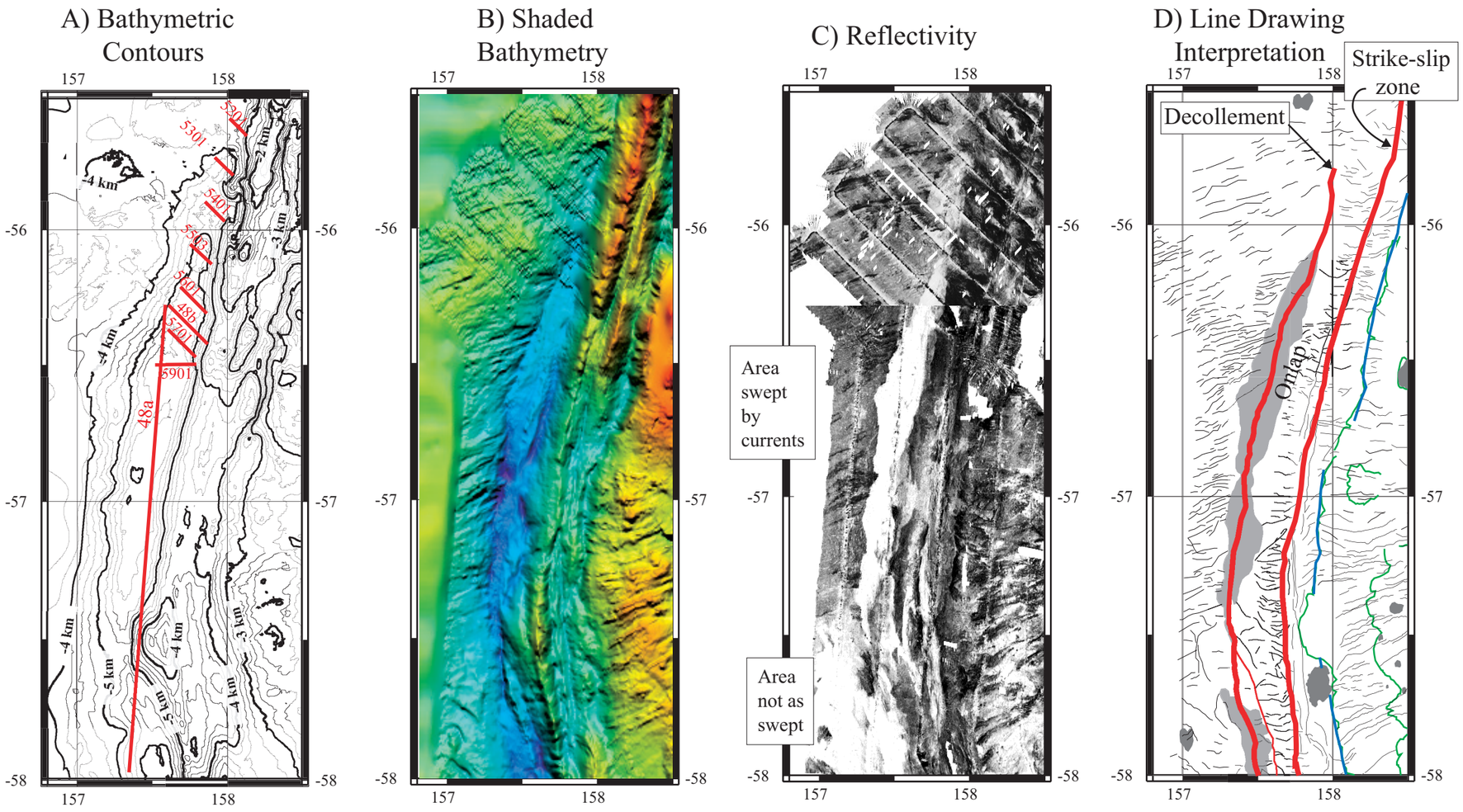

Figure 2.5. Close-up views of the northern part of the Hjort Trench. (See Figure 2.4 for location). A) Contoured bathymetry with locations of interpreted seismic reflection lines (red). B) Bathymetric map shaded from the north. C) Reflectivity map. White colors are low reflectivity values that are interpreted to be sediment and black areas are high reflectivity values interpreted as exposed igneous crust. D) Line drawing of structures from bathymetry, reflectivity, and seismic reflection data. Red lines are major plate boundary faults. See Figures 2.6 and 2.7 for seismic reflection profiles illustrating the nature of the decollement and evidence for onlap by trench sediments.

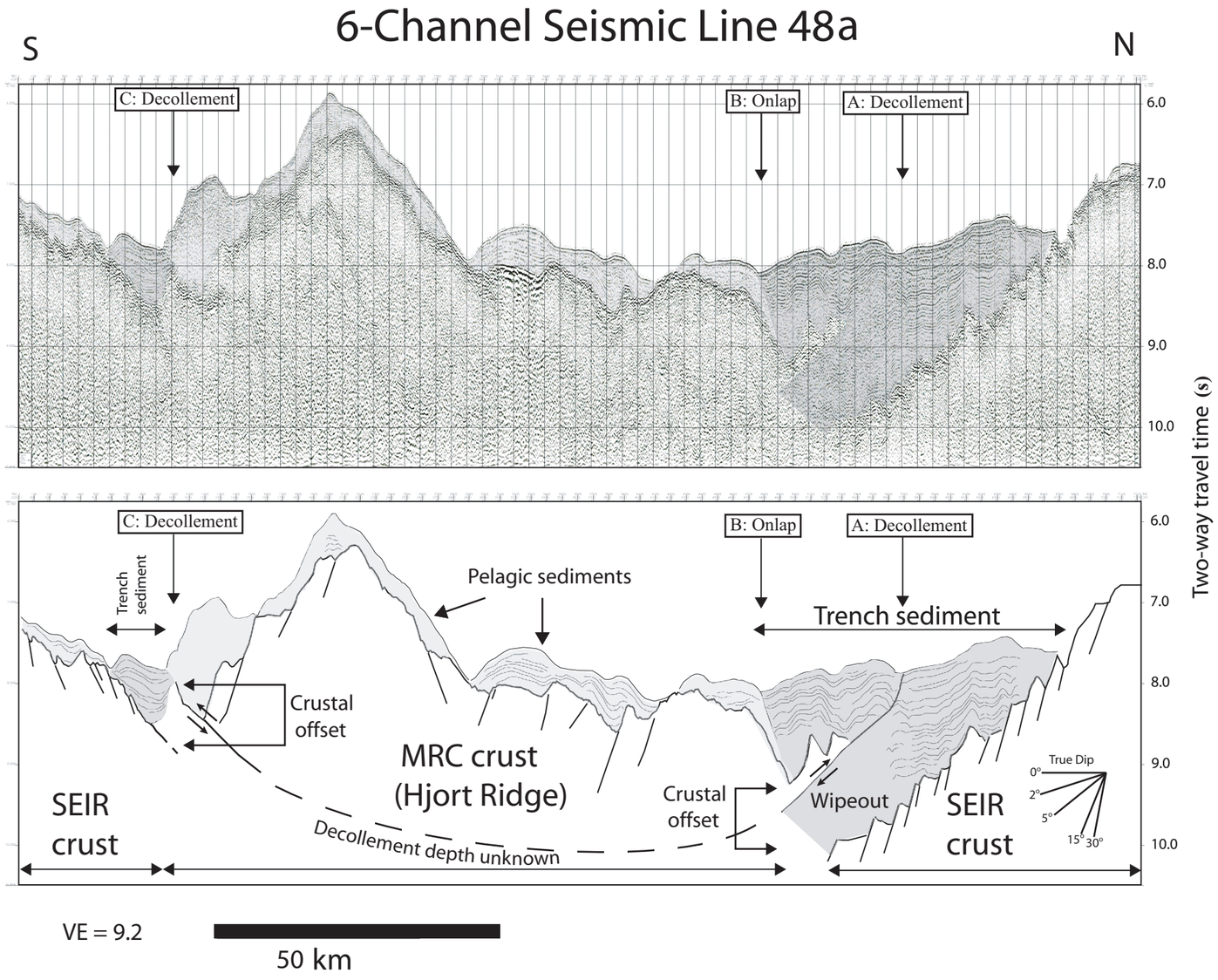

Figure 2.6. L'Atalante seismic reflection profile 48a, oriented obliquely to trench axis (see Figure 2.5A for location and Figure 2.5D for the extent of the decollement trace and onlap). The decollement is the major crustal boundary between SEIR and MRC oceanic crust, seen as a ~1 s offset in the contact between sediment (gray) and igneous basement (white) to the north. The decollement accommodates underthrusting of SEIR crust beneath MRC crust (~5º dip; note arrows showing inferred relative displacement). The area labeled 'wipeout' highlights the lack of continuous reflections within the trench sediment (gray) below the interpreted thrust fault, which may be attributed to dewatering due to compression. Onlap of trench sediment on pelagic sediment overlying MRC crust is indicated. Onlap may signify the creation of accommodation space during trench formation. To the south, the line crosses the same decollement, again accommodating underthrusting, where trench sediment onlaps MRC crust. True dips determined using a seismic velocity of 1500 m/s.

Fault density and average fault displacement in the igneous basement change abruptly across the Trench. North and west of the Trench, fault density is much higher than on the Hjort Ridge to the south and east of the Trench (Figure 2.6). Higher fault density is generally accompanied by smaller offsets across the faults. These changes in fault density and offest occur where there is a ~1 s offset of igneous basement (Figure 2.6). Farther south, in the central portion of the Trench, the 6-CS profile shows the same extensively faulted SEIR crust south of less faulted crust of the Hjort Ridge, as well as onlapping of trench sediment onto Hjort Ridge crust, and an approximately 500 ms offset of the igneous basement (Figure 2.6). A less oblique seismic reflection transect of the Trench (Figure 2.7) shows strong reflections in the trench sediment overlying SEIR crust dipping toward the MRC crust. In the central part of the Trench, east of location D (Figure 2.7), the sediment-igneous basement contact is offset by 750 ms.

Limited basement offsets in the northernmost portion of the Hjort Trench have been observed on Rig Seismic 124 6- and 96-CS data (Figure 2.8; *Schuur et al*., 1998), although L'Atalante 6-CS data are perhaps more convincing. The contact between sediment and igneous crust is offset vertically in the three southernmost Rig Seismic profiles. The northernmost four profiles do not exhibit any substantial crustal offset, bathymetric expression at the seafloor in the Trench disappears, and the Trench shallows and lacks the sedimentary fill seen to the south (Figure 2.8). Again, SEIR crust is characterized by a higher fault density than MRC crust.

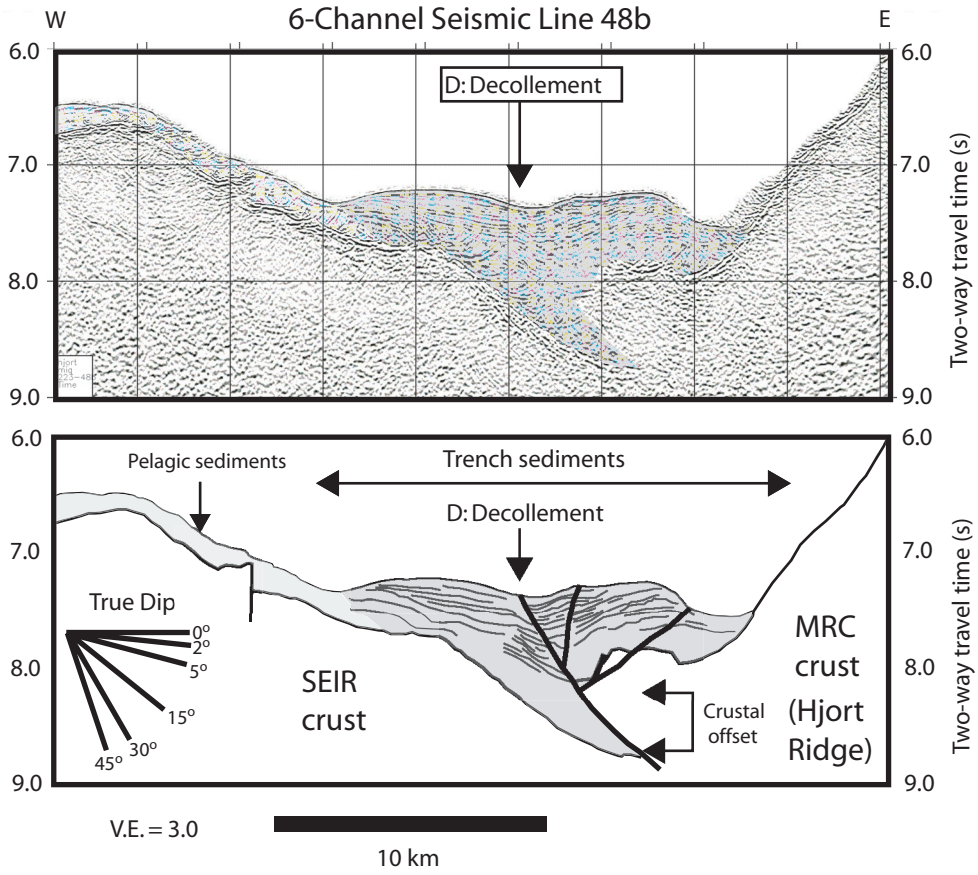

Figure 2.7. L'Atalante seismic reflection profile 48b, perpendicular to the trench axis (see Figure 2.5A for location). Arrow labeled 'decollement' indicates the surface expression of underthrusting of SEIR crust beneath MRC crust (see Figure 2.6, and Figure 2.5D for surface trace of decollement). The contact between sediment (gray) and igneous basement (white) is offset ~750 ms across the decollement. True dips determined using a seismic velocity of 1500 m/s.

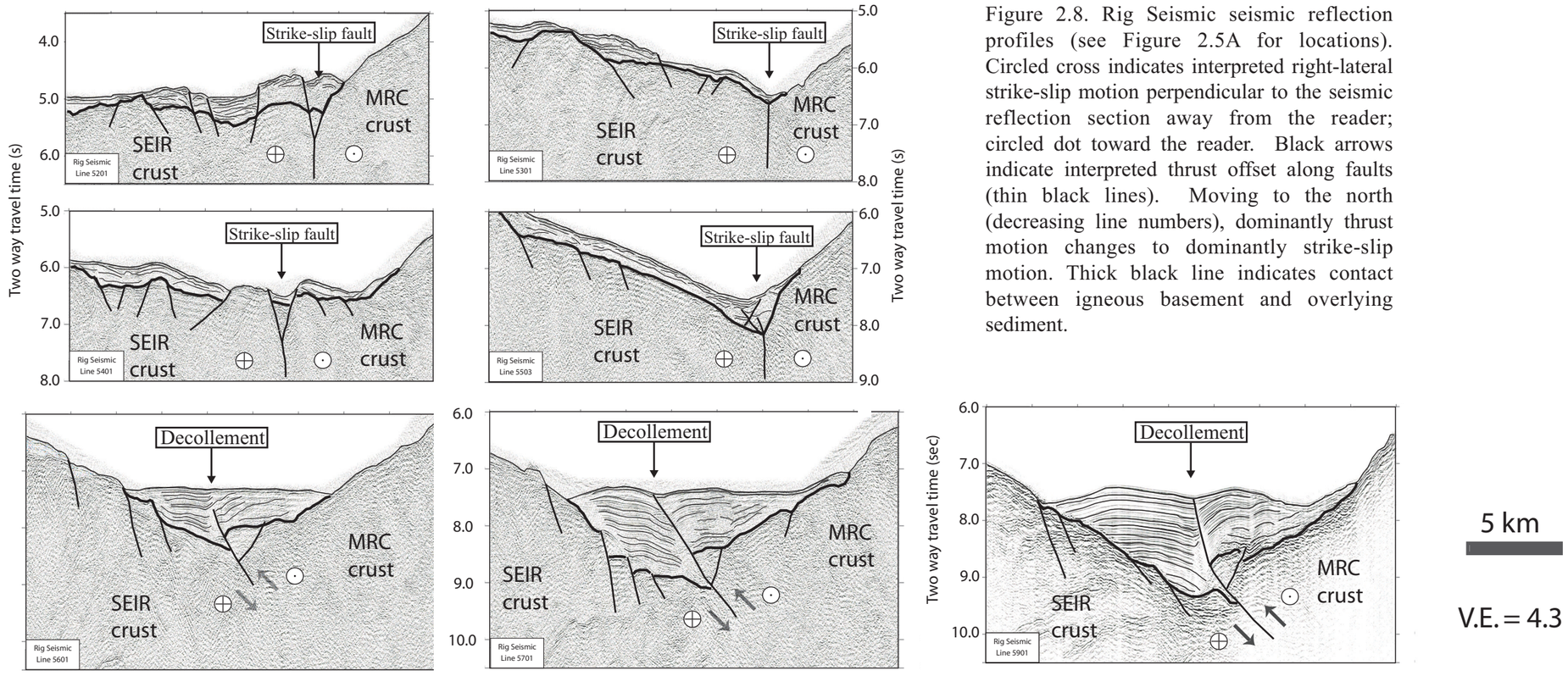

Figure 2.8. Rig Seismic seismic reflection profiles (see Figure 2.5A for locations). Circled cross indicates interpreted right-lateral strike-slip motion perpendicular to the seismic reflection section away from the reader; circled dot toward the reader. Black arrows indicate interpreted thrust offset along faults (thin black lines). Moving to the north (decreasing line numbers), dominantly thrust motion changes to dominantly strike-slip motion. Thick black line indicates contact between igneous basement and overlying sediment.

Hjort Ridge

In the Hjort segment of the MRC, a paired ridge (Hjort Ridge) separates the trench sub-region from a volcanic plateau (Hjort Plateau; see below) to the east (Figure 2.4). Previous studies [*Massell et al.*, 2000; *Bernardel and Symonds*, 2001] used the term 'Hjort Ridge' to refer to the entire elevated region of seafloor east of the Hjort Trench. The L'*Atalante* AUSTREA-2 data allow the identification of two distinct physiographic provinces within the original one. The Hjort Ridge described here has a continuous valley at its crest, and is a continuation of the paired ridge system identified in Macquarie region to the north [*Massell et al.*, 2000]. Due to the physical continuity with the Macquarie Ridge to the north, the terminology of Hjort Ridge used here is preferred. The only exposure of this ridge system is at Macquarie Island (Figure 2.1), north of the Hjort Ridge. The island is composed of the entire section of oceanic crust as well as upper mantle rocks (*Varne and Rubenach*, 1972). For the Hjort Ridge, relief across the valley between the paired ridges can be as much as 2000 m, but is typically less than half that amount. The crest of the Hjort Ridge typically lies between 1000 and 3000 m deep, and extends to the base of the flanks of the MRC. The crest of the central section of the Hjort Ridge (~57ºS; Figure 2.4) is deeper than its continuation to the south and north, and relief decreases to approximately half of what is observed to the north. Structurally, the Hjort Ridge is dominated by ridge-parallel lineaments, with a subsidiary set of ridge-perpendicular lineaments (Figure 2.4). Ridge-perpendicular lineaments generally terminate against ridge-parallel lineaments.

Hjort Plateau

A submarine plateau (Hjort Plateau) encompassing at least 20,000 km^2 lies east of the base of the eastern flank of the Hjort Ridge (Figure 2.4). Depths range from 1000 to 3500 m, and are shallower than the adjacent Hjort Ridge to the west between 56.5ºS and 58ºS (Figure 2.4). Between these latitudes, relief on the Hjort Plateau is over two times that observed for the Hjort Ridge. The Plateau is characterized by linear, generally NE-SW-oriented, small-scale scarps, and volcanic edifices (Figure 2.4).

Five newly identified arcuate lineaments in the Hjort Plateau region asymptotically approach the Hjort Ridge from the southeast (lineaments V-Z, Figure 2.4). The smaller-scale NE-SW oriented scarps are consistently oriented sub-perpendicular to the arcuate lineaments. Massell et al. [*2000*] also observed this relationship north of the Hjort region. At some locations on the Hjort Plateau, the bathymetric expressions of the curved lineaments are obscured by volcanic edifices (Figure 2.4).

Dozens of volcanic edifices characterize the Hjort Plateau, rising from 200 to 3500 m above ambient seafloor (Figure 2.4). Most are conical and vary between circular and stellate at mid-height circumference. Smaller volcanoes tend to have more rounded perimeters. To date, no ages or compositions are available for any of the volcanic edifices.

Scarps associated with the erosion of thick deposits of sediment are common in the Plateau region. The boundaries of these scarps are most apparent in maps of the slope of the seafloor [*Bernardel and Symonds*, 2001]. Steep slopes

at the margins of these sedimentary deposits (up to 20º) are sinuous and lobate (Figure 2.4). Relief across the scarps reaches 500 meters and individual sedimentary deposits cover up to 5000 km^2.

2.4.4 Upper Crustal Discussion

We interpret the WSW-ENE oriented scarps in the SEIR crust to the west of the Hjort Trench to be relict spreading fabric formed at the easternmost portion of the Southeast Indian Ridge to the south. Spreading fabric faults form at spreading ridges through interaction of extensional tectonics and volcanism [*Macdonald et al.*, 1996], and typically face both toward and away from the spreading center. The trend of these faults is consistent with the available magnetic anomaly data west of the Trench (Figure 2.2). Seismic reflection data do not allow these faults to be extended across the Trench and onto the Hjort Ridge. In addition, the data show no evidence indicating reactivation of these faults in the vicinity of the Trench. Rather, the N-S to NW-SE oriented, arcuate scarps at ~58.5ºS (Figure 2.4) are interpreted as normal faults that formed due to bending of the Australian crust as it approaches the Trench. Similar features have been described in the outer rise region of subduction zones [e.g., *Jones et al*., 1978; *Masson* 1991; *Kobayashi et al.*, 1998].

We interpret the NE-SW to E-W oriented scarps in the Hjort Ridge and Plateau regions (Figure 2.4) to be relict spreading fabric, as did *Bernardel and Symonds* [2001], and we propose that these faults formed during spreading processes at the MRC to the north. Limited magnetic anomaly data east of the Trench are consistent with this interpretation (Figure 2.2). The strikes of these

faults rotate to a more easterly orientation approaching the plate boundary. This reflects the changing orientation of the spreading segments at which the faults formed, as divergence at the Macquarie ridge evolved from a normal to oblique direction with respect to the plate boundary in response to changes in the relative motion of the Pacific and Australian plates [*Massell et al.*, 2000]. We interpret the NW-SE curving lineaments that become sub-parallel to the Hjort Ridge to be fracture zones that record offsets of spreading segments along the extinct Macquarie spreading ridge. The changes in strike of these fracture zones also record changes in relative motion between the Australian and Pacific plates, and hence the direction of spreading at the extinct Macquarie spreading ridge. Fracture zones and spreading fabric can be traced onto the MRC in the Hjort, Macquarie, and McDougall regions. Spreading fabric faults are perpendicular to fracture zones, suggesting that shearing has not led to fracture zone re-orientation. *Massell et al.* [2000] previously identified a similar orthogonal relationship between fracture zones (Matata, Waimaero and Arahiwi fracture zones, Figure 2.4) and relict spreading fabric on the Pacific plate to the north of the Hjort region from *Rig Seismic 124* data and the satellite-derived free-air gravity field. Thus, the genesis of the crust east of the Trench associated with the Hjort Ridge and Plateau is similar to that proposed for the crust east of the Macquarie, McDougall, and Puysegur regions, and is definitely not genetically related to SEIR crust west of the Hjort Trench. The crust formed at the MRC paleo-spreading ridge has been previously referred to as STOC, or southeast Tasman oceanic crust [*Wood et al.*, 1996], and is hereafter referred to as MRC crust.

Magnetic anomaly identifications (Figure 2.2) imply a boundary between SEIR and MRC crust in the vicinity of the Hjort Trench. In addition, the lack of fracture zones associated with SEIR spreading west of the Hjort Trench is also strong evidence for such a boundary. We interpret the boundary between SEIR and MRC crust to lie at a change in the style of basement faulting in the Trench (between A and B, Figure 2.6). The SEIR crust (north and west of A, Figure 2.6) is pervasively faulted, whereas the MRC crust (south and east of B, Figure 2.6) is significantly less faulted and has a different structural style. One possible explanation for the observed variability in fault density is that the SEIR and MRC crust that is juxtaposed at the Hjort Trench formed at different spreading rates. Abyssal hill morphology has been directly related to spreading rates [*Carbotte and Macdonald*, 1994; *Goff*, 1991 & 1992], with higher spreading rates generally producing faults with closer spacing [*Macario et al.*, 1994]. Although factors other than spreading rate (volcanism, crustal thickness, heat flux, etc.) can significantly influence abyssal hill morphology [*Goff et al.*, 1995], a simple correlation between estimated spreading rate and observed fault density can be attempted here with the available data.

Lodolo et al. [1996] determined instantaneous spreading velocities for the easternmost SEIR. For the crust north of the SEIR and immediately west of the Hjort Trench, full spreading rates for anomalies 5 through 8 vary from 4 to 9 cm/yr, with the lowest rate occurring for anomaly 6 (~29 Ma; Figure 2.2). No magnetic anomalies have been identified on the Hjort Ridge east of the Trench. *Wood et al.* [1996] estimated MRC spreading velocities from magnetic anomaly

data in the southeast Tasman Sea (Figures 2.1 and 2.2). Between anomalies 18 and 11 (40-30 Ma), full spreading rates were 3.0 cm/yr. At least at ~30 Ma, it appears that MRC spreading rates were less than those on the SEIR. If this qualitative relationship continued after 30 Ma, the variability in fault density observed in the seismic reflection profiles may be attributed to differences in spreading rate.

If the change in fault density in igneous basement observed on seismic reflection profiles across the Trench represents a boundary between crust formed at two distinct spreading ridges (SEIR and MRC), then that boundary was a transform fault when spreading was active on both the SEIR and MRC spreading ridges. When spreading ceased on the MRC, that boundary became a fracture zone boundary with dextral sense offset. This interpreted fracture zone has vertical displacement across it presently, suggesting it has been reactivated during the change from oblique spreading to transpression that has been documented for the Macquarie and McDougall segments [*Massell et al.*, 2000]. The eastward dip of the reactivated fracture zone (Figures 2.6, 2.7, and 2.8) suggests that compression accounts for part of its orientation and displacement. Although bathymetric offset may have existed when transpression began, the current offset across the fault cannot be attributed solely to isostatic adjustment across a vertical fracture zone. The amount of bathymetric offset prior to compression is unknown, but seismic reflection lines north of the Trench (Figure 2.8) suggest that there was little offset prior to the onset of transpression.

The observed vertical offsets in reflections from the sediment-igneous basement interface for both seismic reflection data sets (Rig Seismic and L'Atalante) argue convincingly for underthrusting of the SEIR crust beneath the MRC crust at this fracture zone boundary. We interpret a decollement separating SEIR and MRC crust that is expressed as a continuous bathymetric low (A, Figure 2.6; Figure 2.5). Beneath the decollement (A, Figure 2.6), reflections are discontinuous, perhaps the result of compression and dewatering related to underthrusting. Sediment on the hanging wall of the thrust is deformed in low amplitude, open folds, but retains continuous reflections typical of the trench sediments. The decollement in the Trench extends along the western base of the ridge complex as far north as 55ºS (Figures 2.4 and 2.5), where Massell et al. [2000] identified limited underthrusting from seismic reflection data.

Both to the north of and adjacent to the Hjort Trench, we interpret the valley at the crest of the Hjort Ridge to be the locus of strike-slip faulting associated with strike-slip focal mechanisms (see seismicity discussion below; Figure 2.4). The fault system in the Hjort Ridge is an extension of the plate boundary fault system identified in the crest of the MRC to the north [Massell et al., 2000], and is a continuous feature along the length of the MRC as far south as 59.5ºS. For the Macquarie and McDougall regions, relative plate motion is accommodated predominantly by strike-slip motion along this central fault valley in the ridge [Frohlich et al., 1997]. However, in the Hjort region, we also identify a component of underthrusting at the Australian-Pacific plate boundary. The combination of underthrusting in the Trench and strike-slip faulting at the ridge

crest is characteristic of strain partitioning at obliquely convergent margins. The fault system in the Hjort Ridge accommodates strike-slip deformation, while the fault system in the Trench accommodates the increase in boundary-normal relative convergence predicted by the NUVEL-1A plate model for the Hjort region [DeMets et al., 1994]. Thus, multiple faults characterize the active plate boundary in the Hjort region, encompassing a zone of distributed strain 20-50 km wide (from the medial-Trench to the crest of the ridge complex) that accommodates both convergent and lateral displacement associated with current oblique compression.

Interpretations of seismic reflection data (Figures 2.6, 2.7, and 2.8) indicate a transition from underthrusting in the northern part of the Trench to dominantly strike-slip faulting north of the Trench, where bathymetry indicates that the Trench gradually shallows. This transition from thrust to strike-slip behavior has been observed at the Puysegur Trench [Lamarche and Lebrun, 2000; Lebrun et al., 2000], as well as other more mature convergent settings [Doser and Lomas, 2000; Bilich et al., 2001]. In the Hjort region, this transition likely results from a gradual northward increase in obliquity of plate convergence vectors as suggested by the NUVEL-1A plate motion model [DeMets et al., 1994]. From 57.5ºS to 55ºS, underthrusting becomes less significant as plate motion is gradually transferred from partitioned faulting within the Hjort Trench and Ridge to primarily strike-slip faulting focused in the valley at the crest of the MRC. North of 55ºS, relative plate motion is accommodated dominantly within the crest of the ridge complex, as identified by Massell et al. [2000]. Seismic reflection

data illustrate the gradual decrease in thrust offset on the trench decollement to the north, concurrent with the shallowing and disappearance of trench sediment, and the dominance of interpreted strike-slip faulting. These data suggest that the decollement in the Trench may be propagating northward.

The volcanic edifices 5 to 220 km east of the Trench could represent either subduction-related magmatism or hot spot volcanism. Assuming a depth of 100 km for magma generation from a subducting plate, the required dip of the Australian crust would be >24º in an easterly direction, which is not unreasonable for crust approximately 15-20 million years old (Figure 2.2; *Vlaar and Wortel* [1976]; *Wortel and Vlaar* [1978], *Jarrard* [1986a]). Alternatively, these volcanoes may be related to hot spot volcanism, as their relatively linear trend (315º) might suggest (Figure 2.2). No hotspots have been previously identified in the area, although this does not preclude this mechanism. The generally WNW-trend of the volcanoes is consistent with WNW motion of the Pacific plate over the Hawaii and Louisville hotspots since ~43 Ma [Cande et al., 1995; Wessel and Kroenke, 1998; Norton, 2000]. The hotspot hypothesis predicts that the easternmost seamount is the youngest, which is supported by its relatively shallow depth. We will discuss the origin of these volcanic features further in a later section.

Seismic reflection data and lower reflectivity values for the SEIR crust south of ~57.5º indicate thicker sedimentary cover than to the north. The lack of sediment on SEIR crust west of the northern Trench suggests that sediment in the Trench may be pelagic cover that has been transported to the Trench from the

west by the Deep Western Boundary Current and Antarctic Circumpolar Current (Schuur et al., 1998). The southern portion of the Trench has less sediment than the north, and this decrease in sediment thickness may be due to the lack of such transport, as suggested by sediment accumulations on SEIR crust to the west. Trench sediment onlaps the MRC crust of the Hjort Ridge (Figure 2.7). This onlap indicates that at the eastern edge of the Trench, pelagic sediment was deposited directly on MRC crust, and that accretion has not been substantial. Farther east, the scarps in sediment deposits of the Hjort Plateau probably formed by erosion resulting from the Deep Western Boundary Current and the Antarctic Circumpolar Current [*Bernardel and Symonds*, 2001] as the Plateau was being uplifted (Figure 2.4).

2.5 ANALYSIS OF ACTIVE LITHOSPHERIC DEFORMATION

To better understand processes at depth in the Hjort region, including the possibility of subduction or oblique convergence, we investigated its seismicity. We considered all available events in the Harvard centroid moment tensor (CMT) catalog, *Engdahl, van der Hilst, and Buland, 1998* (EHB) relocations, and data archived by the International Seismological Centre (ISC) for the Hjort area (Figure 2.9). Because different characteristics are recorded in each catalog, we developed different criteria to define the more reliable events. ISC data provided information on the distribution of epicenters, EHB data on epicenters and focal depths, and CMT data on focal mechanisms. For events in the Hjort region, the closest station is on Macquarie Island, with other nearby stations in New Zealand, Australia, and Antarctica (Figure 2.1).

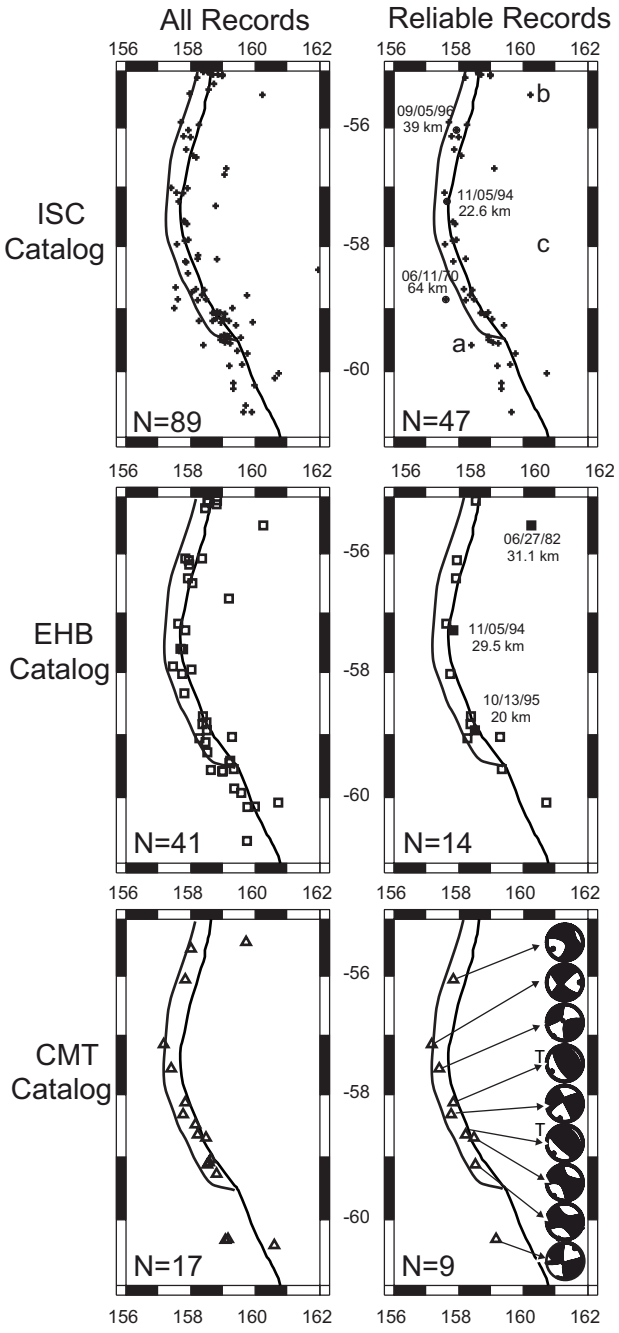

Figure 2.9. Seismicity in the Hjort region. Top: ISC data. Middle: EHB data. Bottom: CMT data, with focal mechanisms indicated for best constrained events (see text for criteria). Left: all available data for each catalog. Right: More reliable events (see text for criteria). Earthquakes are observed close to the plate boundary, and do not extend to the east, suggesting the lack of a well-defined Wadati-Benioff zone extending eastward beneath the MRC crust. Most events are shallower than 20 km. Well-constrained anomalously deep events are seen in ISC (top right) and EHB (middle right) catalogs. CMT catalog (bottom right) includes both thrusting (indicated with 'T') and dominantly strike-slip events (others), and suggests that strain partitioning is occurring at the Hjort Trench in response to oblique convergence.

2.5.1 International Seismological Center catalog (ISC)

The ISC uses P and other phase arrival data recorded at ~3,000 stations distributed around the world to constrain hypocentral locations [*Willemann and Storchak*, 2001]. The catalog contains 89 events in the Hjort region that occurred between 1964 and 1999. ISC epicenters are most reliable if the number of stations reporting phase arrivals is large. In this analysis, we considered phase recordings at twenty stations or more sufficient to provide more reliable epicenters. Using this criterion, 47 events are considered more reliable.

2.5.2 Engdahl, van der Hilst, and Buland (1998) relocations (EHB)

The EHB catalog relocates 41 earthquakes in the Hjort region between 1966 and 1999. We assessed events in the EHB catalog for hypocentral location and focal depth. Statistics related to observations considered important for reliably determining location and depth include the total number of stations reporting observations (N_{tot}), the number of teleseismic observations (N_{tel}), the standard error of the observations used (*se*), the largest station open azimuth (*openaz*), and the distance to the closest station (*rstadel*). We selected cutoff values for each statistic by evaluating the distribution for a given statistic and by choosing a cutoff value near the median, thereby eliminating approximately half the events. Our cutoff values are: N_{tot} ? 40, N_{tel} ? 20, *se* ? 1.3, *openaz* ? 90?, *rstadel* ? 8 degrees. Using these values, a subset of 14 events satisfied all the criteria and qualified as more reliable.

2.5.3 Harvard Centroid Moment Tensor Catalog (CMT)

The CMT catalog contains 17 events in the Hjort region from 1980 to 1999 [e.g. *Ekstrom et al., 1995*]. We assessed the quality of the focal mechanisms in the catalog following methods developed in *Frohlich et al.* [1997], focusing on three statistics. The first is f_{clvd}, a measure of the degree to which the mechanism approximates either a double-couple or compensated linear vector dipole (CLVD) mechanism. As a mechanism approaches a pure CLVD mechanism, the orientations of the B axis and either the T or P axis become indeterminate. Thus, low values of f_{clvd} indicate more reliable axial orientations and are therefore preferable for assessing focal mechanism. The second statistic, n_{free}, is the number (0 to 6) of moment tensor elements that are not constrained during the determination of the moment **M**. Larger values of this statistic allow more freedom in the axial orientations. A value of 6 means that the P, T, and B axes can assume any mutually orthogonal orientation. The third statistic is **E**, which compares the relative sizes of M and the standard error tensor **U**, essentially normalizing the size of the error to the size of the event, and thus ranges from 0 to 1. The orientations of the principal axes are more precisely constrained when values of E are low. In this study, we arbitrarily chose the following criteria to consider an event as reliable: f_{clvd} ? 0.20, n_{free} = 6, E ? 0.20. These criteria allow 9 events to be considered more reliable.

2.5.4 Active Lithospheric Deformation Discussion

All three datasets indicate that epicenters are generally proximal to the plate boundary zone, and events appear evenly distributed both to the east and

west of the plate boundary zone (Figure 2.9, left column). In addition, the more reliable events determined for each catalog are representative subsets of all available events (Figure 2.9, right column). These epicenters indicate that seismicity is restricted to the vicinity of the Hjort Ridge and Trench, and is therefore related to plate motion at or near the plate boundary zone. For each catalog, few epicenters lie east of the Trench (surrounding location c on Figure 2.9, top right), and no well-defined Wadati-Benioff zone is obvious. Of the more reliable locations, the events farthest from the plate boundary are ~100 km to the west and ~150 km to the east (locations a and b respectively in Figure 2.9, top right).

The nine better determined focal mechanisms (Figure 2.9, bottom right) reflect the diversity of the total 17 mechanisms in the CMT dataset. Of these, five were not included in analysis by *Frohlich et al.* [1997]. One event occurred after that publication was submitted, and two other events are included in this analysis because we chose a higher *E* value (E = 0.20 as opposed to 0.15). It is unclear why the remaining two events were not included in the previous analysis. Consideration of all nine events leads to a different conclusion for the general tectonic state at the Hjort Trench than that reached by *Frohlich et al.* [1997]. Thrust mechanisms (Figure 2.9, bottom right) indicate that the Hjort region is not a purely strike-slip boundary, but may be better described as a transpressional boundary.

Hypocenter determinations are more difficult to interpret. Focal depths reported by Harvard for all nine more reliable events are 15 km (Figure 2.9,

bottom right). Depth determinations from the EHB and ISC catalogs report data for these events that suggest the Harvard estimates may be too shallow. Six events from the ISC and EHB catalogs are deeper than 20 km and are more reliable (Figure 2.9, middle and bottom right). Twenty kilometers was chosen because it is significantly deeper than normal oceanic crustal thickness. Three ISC events are distinguished from the other ISC events as being deeper than 20 km and located using pP phase arrivals. The three ISC events have been constrained to 64 ? 3.5 km, 22.60 ? 1.55 km, and 39.26 ? 2.11 km (Figure 2.9, top right). Three EHB events are distinguished from the other EHB events as having m_b greater than 5.2 and being deeper than 20 km as determined using eight or more independent stations recording depth phases (Figure 2.9, middle right). The 06/27/82 event was located at 31.1 km using eight depth phases. A total of 18 depth phases were used to locate an event on 11/05/94 at 29.5 km. Fourteen depth phases were used to locate the 10/13/95 event at 20 km, which is a thrust event. Although the ISC typically located these three events at shallower depths, their reported depths were all greater than 15 km. Only one of these events is common to both catalogs: the 11/05/94 event recorded at 22.60 ? 1.55 km by ISC and 29.5 km by EHB. The event of 06/11/70 (Figure 2.9, top right) is not included in the more reliable EHB data because it has a standard error of 1.32, slightly higher than the cutoff criteria of 1.3. The focal depth of this event was located by EHB at 15 km, but perhaps, in this case, more reliably located at 64 km depth by the ISC using pP phase arrivals. These six records (five events) are not

deep enough to argue unequivocally for a subducting slab at depth, but in typical oceanic lithosphere would lie in mantle well beneath normal oceanic crust.

Considering arguments of *Parsons and Sclater* [1977], *Bergman and Solomon* [1980], and *Weins and Stein* [1983], the maximum depth of oceanic seismicity appears to be bounded by the ~700?C isotherm. Because the sub-seafloor depth to this isotherm increases with oceanic lithospheric age due to cooling, deeper earthquakes occur in older lithosphere. Relative to observations of intraplate earthquakes in oceanic settings [*Wiens and Stein*, 1983], the >~20 km events at the Hjort Trench would typically be found in oceanic lithosphere >30 Ma. The events at 64 and 39 km would be expected in lithosphere >60 Ma. Although the exact age of crust east of the Hjort Trench is not clear, tentative identification of anomalies 12 and 13 (*Weissel et al.*, [1977]; Figure 2.2) suggest it is younger than 30 Ma. The oldest oceanic crust generated by the MRC when it was a spreading ridge is identified as anomaly 18, adjacent to the Resolution Ridge (Figure 2.2), corresponding to a maximum age of 40 Ma. Magnetic anomalies 4 through 6 to the west of the Trench (*Weissel et al.*, [1977]; Figure 2.2) indicate that the portions of the crust there are younger than 25 Ma. Therefore the six deeper events that are most reliable (Figure 2.9, upper and middle right) are anomalously deep for Tertiary oceanic lithosphere. These deeper events likely indicate lithospheric deformation beneath the ridge complex and lithospheric underthrusting beneath the Pacific Plate.

Comparing the results of more reliable events for the three catalogs (Figure 2.9, right column), it is clear that the seismicity characteristics of the Hjort

Trench reflect neither established subduction nor purely strike-slip behavior. Events occur near the plate boundary and do not support the existence of a well-developed, eastwardly-dipping Wadati-Benioff zone, arguing against established subduction. The more reliable mechanisms illustrate thrust and strike-slip behavior, suggesting that the boundary is best explained by transpression in a zone of strain partitioning.

2.6 GRAVITY MODELING OF INTEGRATED CRUSTAL STRUCTURE

2.6.1 Data and Methods

To gain additional insight into crustal and upper mantle structure in the Hjort and adjacent Macquarie region, we selected four transects across the plate boundary for gravity modeling (Figure 2.3). The modeled transects combine 2000 *L'Atalante* and 1994 *Rig Seismic* gravity and bathymetry data with the satellite-derived free-air gravity field [*Sandwell and Smith*, 1997] and predicted bathymetry [*Smith and Sandwell,* 1997]. Bathymetry data were augmented with various USNS *Eltanin* cruises [*Houtz,* 1972; *Hayes and Talwani*, 1972] in the area. We use a two-dimensional forward gravity modeling approach [*Talwani et al*., 1959]. Where fracture zones intersect the transects (Figure 2.3), we have modeled vertical discontinuities in density contrast sub-seafloor (Figure 2.10). Density contrasts across fracture zones result from the crustal age differences [*Christeson and McNutt*, 1992; *Kamesh, et al.*, 1993; *Minshull et al.*, 1995; *Escartin et al.*, 1999]. Magnetic data do not allow the relative age differences across fracture zones to be determined accurately in the Hjort region. The only constraint is the tentative identification of anomalies 12 and 13 (30-35 Ma using

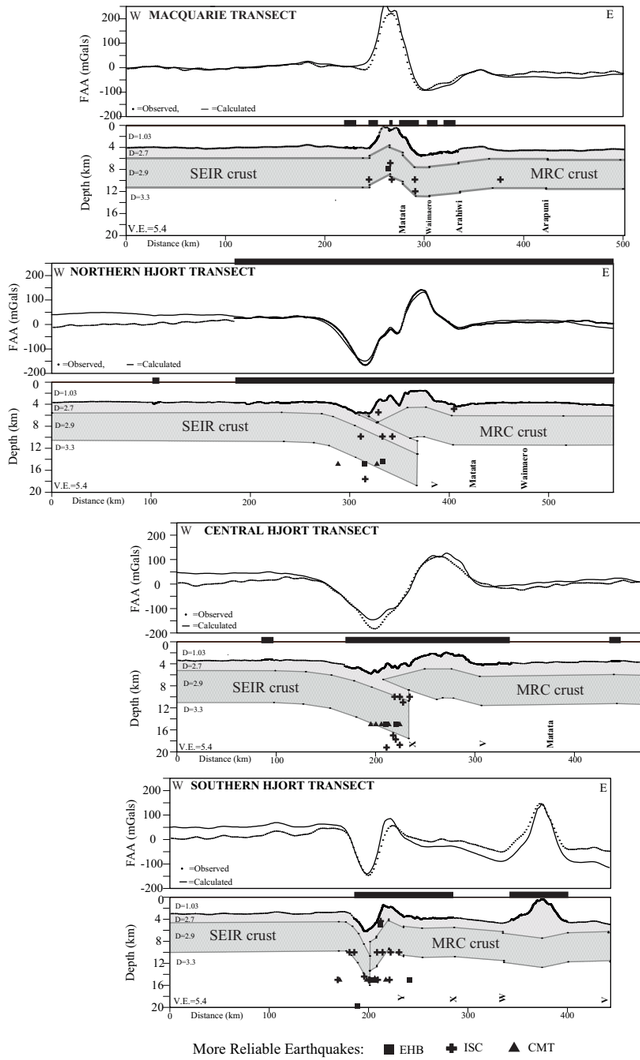

Figure 2.10. Gravity transects across the Hjort and Macquarie regions aligned on the crest of the ridge complex (see Figure 2.3 for locations). The gravity models include four layers: water (1030 kg/m3); upper crust (2700 kg/m3); lower crust (2900 kg/m3); and mantle (3300 kg/m3). Away from the MRC, we employed an oceanic crustal section ~7 km thick, consisting of ~2 km of upper crust and ~ 5 km of lower crust. These thicknesses are appropriate for crust of the ages implied by the available magnetic anomalies [White et al., 1992; Wood et al., 1996] and estimated spreading rates [Bown and White, 1994; Lodolo et al., 1996]. The models emphasize changes in subsurface geometry of the three layers, keeping layer densities constant, rather than introducing intra-layer density variability. Cross, square, and triangle symbols are projected hypocenters of better-constrained earthquakes within 100 km north and south of each transect. Horizontal black bars above transects represent extent of ship-derived data; Otherwise, the bathymetry and gravity values are satellite-derived. Portions of the transects that use satellite-derived gravity and predicted bathymetry utilize one-minute (latitude/longitude) data sampling values, which reflect the resolution of the free-air gravity anomaly and predicted bathymetry maps of Sandwell and Smith [1997] and Smith and Sandwell [1997], respectively. Discontinuities occur at transitions between shipboard gravity and bathymetry data to satellite-derived data; because shipboard data are more accurate, our gravity models more closely mimic the shipboard data. Fracture zone locations are labeled below the MRC crust (see Figure 2.3). For the southern Hjort and Macquarie transects, the gravity high occurs above the ridge complex adjacent to the Trench. For the central and northern Hjort transects, the gravity high is ~50 km east of the ridge complex. These two transects suggest limited underthrusting of SEIR oceanic crust beneath MRC oceanic crust. The other two transects indicate less developed underthrusting. In the Hjort transects, SEIR oceanic crust is being underthrust, whereas in the Macquarie transect, MRC crust appears to be more prone to underthrusting. Our models suggest progressive underthrusting that involves the deformation of MRC oceanic crust within the ridge complex to accommodate oblique convergence and underthrusting.

the geomagnetic polarity timescale of *Cande and Kent* [1995]) in the Pacific crust east of the Hjort Plateau (Figure 2.2; *Weissel et al.*, 1977). We used bathymetric offsets to estimate vertical offsets in subsurface densities across fracture zones, i.e., offsets in density contrasts in the subsurface mimic the sense and magnitude of bathymetric offsets. Although the seafloor expression of fracture zones is in many cases obscured by volcanism on the Hjort Plateau (Figure 2.4), where seafloor offsets across fracture zones are observed, they vary from 200 to 500 m. For ~30-35 Ma crust, these offsets represent a 5-12 Myr age difference across the fracture zones [*Parsons and Sclater*, 1977; *White et al.*, 1992], which is reasonable given *Massell et al.*'s [2000] model of spreading center evolution of the MRC north of the Hjort region, where this crust originated. For each transect, the best agreement between calculated and observed gravity values occurs with the inclusion of fracture zones modeled as vertically offset density contrasts. It is important to point out that these fracture zones have only been mapped in the Pacific crust east of the Trench, and neither gravity anomaly nor bathymetric data indicate the presence of fracture zones on the Australian plate immediately west of the Trench. No smaller scale faults (e.g., those in Figure 2.4) are included in the modeled transects, as the seismic reflection data do not allow extrapolation of these features to crustal or lithospheric scales.

2.6.2 Integrated Crustal Structure Results

The positions of the maximum and minimum bathymetric and gravimetric values highlight some general similarities and differences in the transects (Figures 2.3 and 2.10). The Trench is a bathymetric and gravimetric low west of the ridge

complex in all of the transects except the Macquarie transect, which exhibits a significantly shallower bathymetric low to the east of the ridge complex. South of 56°S, a gravity high parallels the Trench to the west. This 'outer bulge' is commonly observed in gravity and bathymetry data at convergent margins and has been ascribed to crustal flexure [*Watts and Talwani*, 1974]. The highest gravity values do not correspond to the same bathymetric sub-region along each transect. For the southern Hjort and Macquarie transects, the highest gravity values not associated with a volcano occur over the ridge complex. For the central and northern Hjort transects, the highest values occur over the volcanic Hjort Plateau, ~50 km east of the ridge complex (Figure 2.10).

Because we are concerned mainly with local crustal structure around the plate boundary zone, our models attempt to explain the observed gravity field using short wavelength (100's of km) variability in bathymetry and crustal distribution. In general, the fit between observed and modeled gravity is very good in the area of most interest, i.e., at the trenches, trough, and ridges comprising the MRC. The most obvious discrepancies between observed and modeled gravity are the ~50 mGal offsets at the western ends of the three Hjort transects, and at the eastern ends of the central and southern Hjort transects (Figure 2.10). Although we could modify crustal thickness to improve the fit of the modeled to the observed gravity, we chose to keep crustal thickness constant in the absence of any seismic data for crustal thickness control. We attribute the discrepancies to intermediate and long wavelength gravity anomalies possibly associated with geoid lows (e.g., Antarctic Discordance *[Marks et al.*, 1990,

Marks and Sandwell, 1991]) and highs. We did not attempt to incorporate variations in the geoid into our models, which have an infinitely flat, four-layer geometry.

Our crustal models fall into two categories, those with limited eastward underthrusting of SEIR crust beneath MRC crust (central and northern Hjort) and those without (southern Hjort and Macquarie) (Figure 2.10). The northern Hjort transect has the best shipboard gravity, bathymetry, and seismic reflection control, and it crosses the Trench where we interpret underthrusting in the 6-CS data. The crustal models are consistent with the depth and location of the majority of the earthquakes (Figure 2.10). Along the strike of the MRC, hypocenters 100 km north and south of each transect have been projected into the plane of the gravity transects. Aside from the deeper events in the Southern Hjort Transect, hypocenter depths generally complement the crustal models in the gravity transects. The central and northern Hjort transects suggest a maximum depth of 16 to 18 km for the underthrust SEIR crust. The gravity models do not explain the five better-constrained events deeper than 20 km (including the event at 64 km) (Figure 2.9), but they could result from either sub-crustal flexure or brittle failure in the mantle.

2.6.3 Integrated Crustal Structure Discussion

Topography at convergent and transpressional plate boundaries may be explained by plate flexure [e.g., *Watts and Talwani*, 1974; *De Bremaecker*, 1977; *McAdoo et al*., 1978] and dynamic support [e.g., *McAdoo*, 1981; *Davies*, 1981; *McAdoo*, 1982; *Hager*, 1984; *Wdowinski* 1992]. Our models suggest that

dynamic compensation is accompanied by faulting within the MRC crust as it was displaced upwards. *Collot et al.* [1995] proposed similar faulting and dynamic compensation as mechanisms for ridge formation east of the Puysegur Trench on the northern MRC. However, at least from the gravity models, it seems clear that deformation does not occur simply by vertical displacement on the fracture zones, but may involve diffuse strain such as that proposed for the Sumatran forearc [*McCaffrey,* 1991]. The progression of underthrusting suggested by the gravity models involves the elevation and faulting of the Hjort Ridge before underthrusting. Faulting is most likely to occur in crust with well-defined zones of pre-existing, crustal-scale weakness. In the Hjort region, the MRC crust has fracture zones, whereas the SEIR crust in the vicinity of the Trench does not. Fracture zones trending obliquely to subparallel to the ridge complex in the MRC crust may facilitate deformation by accommodating vertical displacement and allowing fluid circulation as deformation proceeds [*Bonatti,* 1978]. *Bonatti et al.* [1994] documented uplift at fracture zone settings due to compressional forces related to changes in relative motion across a fracture zone. The involvement of fracture zones in such deformation has been addressed by *Collot et al.* [1995], *Lebrun et al.* [1998], and *Deschamps et al.* [1998] for similar tectonic settings. *Chemenda et al.* [2000] identified pre-existing zones of weakness in physical models of the overriding plate as necessary for accommodating strain in obliquely convergent settings. *McCaffrey* [1992] did not require zones of pre-existing weakness to be present in the fore-arc to develop deformation, but noted that they would enhance this process.

In gravity models of the Hjort transects, SEIR crust broadly flexes downward as it approaches the plate boundary zone, whereas MRC crust deforms by a combination of faulting, upward flexure, and diffuse strain to accommodate the underthrusting. The differences in the style of crustal deformation for the SEIR and MRC crust may relate to crustal age. Although poorly constrained, some general age relationships are observed. The age of the SEIR crust west of the plate boundary generally increases from south to north (Figure 2.2). In contrast, the age of the MRC crust generally increases from north to south. According to *Massell et al.* [2000], the age of the MRC crust adjacent to the SEIR crust at the latitude of Macquarie Island may be relatively younger than that to the west. Anomalies 5 through 6 (10 – 25 Ma) have been mapped on the SEIR crust to the west of the ridge complex (Figure 2.2). The age of the crust composing the ridge complex south of Macquarie Island can be speculated upon as follows. Macquarie Island contains rocks that indicate that the crust of the island formed by spreading processes at the MRC [*Varne et al.*, 1969; *Varne and Rubenach*, 1972; *Kamenetsky et al.*, 2000; *Varne et al.*, 2000; *Goscombe and Everard*, 2001], and island basalt flows have yielded $^{40}Ar/^{39}Ar$ ages of 11.5-9.7 Ma [*Duncan and Varne*, 1988]. The ridge complex in the Hjort region is an extension of the ridge complex to the north, on which Macquarie Island rests. Thus, it is likely that the ridge complex in the Hjort region formed in a similar way. If the ridge complex in the Hjort region has a similar history as to the north, the age of the crustal material composing the ridge complex in the Hjort region can be estimated at around 10 Ma. The crustal material east of the ridge complex contains

interpretations of anomalies 12 and 13 (Figure 2.2; 30-35 Ma; *Weissel et al.*, 1977), and other currently unpublished locations of anomalies 9 through 18 east of the ridge in the Hjort region support an age increase to the southeast for crust east of the ridge complex (J. Stock, personal communication). The locations of those anomalies are consistent with the fracture zones interpreted in this study. Thus, the SEIR crust west of the ridge complex may be up to 10 Ma older than the MRC crust that composes the ridge complex. Crust of an age equivalent to the SEIR crust west of the northern end of the Trench (anomaly 6, ~20 Ma) is not likely to be encountered east of the Hjort Ridge for many tens of km. Therefore, the material forming the ridge complex is bordered to the east and west by older oceanic crust The younger, warmer, and weaker crust that composes the ridge complex likely deforms more readily than the flanking older crust. Thus, differences in deformation style between SEIR crust and MRC crust composing the ridge likely result from age differences.

The reversal of the position of the bathymetric low relative to the ridge in the Macquarie transect (Figure 2.10) may represent a change in polarity of underthrusting. Although deformation beneath the ridge complex along the Macquarie transect is typical of the other transects, here the MRC crust may eventually be involved in underthrusting. The Macquarie transect does not suggest flexure of the SEIR crust as in the three Hjort transects. Rather, it appears that the MRC crust is displaced downward. Thus, the MRC crust may eventually underthrust the portion of itself that is currently deforming under the ridge

complex. In contrast, along the Hjort segment of the MRC, SEIR crust is underthrusting the deformed ridge complex of the MRC crust.

Our gravity models argue against subduction as a likely source for the numerous volcanic edifices east of the Trench. Typically, volcanism in this position relative to a trench with underthrusting would be attributed to melt derived from the subducting slab or overlying mantle wedge. However, both the gravity models and seismicity suggest that underthrusting has not developed at the Hjort Trench to a stage consistent with a slab depth sufficient to generate melt. Thus, other sources for the volcanism are required, and as noted previously, the linear orientation of the volcanoes may indicate hot spot volcanism. Other possibilities include on- or off-axis volcanism associated with seafloor spreading and decompression melting resulting from flexural uplift of the Hjort Plateau. However, until these edifices are sampled and more is known about their age and composition, an unambiguous interpretation is not possible.

2.7 CONCLUDING DISCUSSION

The current tectonics of the Hjort region can be characterized as incipient oceanic-oceanic underthrusting in an obliquely convergent setting involving strain partitioning and fracture zone reactivation. Two main plate boundary fault systems, one in the Trench and the other in the ridge complex, parallel each other. Thrust and strike-slip focal mechanisms suggest that strain may be partitioned on and between these two fault systems. SEIR oceanic crust is underthrusting MRC oceanic crust along a fracture zone in the Trench. However, underthrusting is not as mature as previously thought (Figure 2.2). Earthquakes cluster at depths <20

km beneath the Trench and ridge complex, and provide no evidence for a Wadati-Benioff zone. However, five well-constrained events as deep as 64 km could suggest the initial response of the mantle to the underthrust slab. Gravity models suggest underthrusting to ~20 km depth and are consistent with all but the six deepest earthquake records. The Hjort region may or may not develop into a mature subduction zone, as relative plate motions predicted by the NUVEL-1A plate model [DeMets et al., 1994] suggest that the trajectory of underthrusting may be unfavorable for developing into self-sustaining subduction. Nevertheless, the following observations provide a modern example of incipient underthrusting that lends support for models of intra-oceanic subduction initiation at fracture zones.

Strain Partitioning

We interpret a low-angle decollement in the Trench and a high-angle fault system in the crest of the Hjort Ridge from multibeam and seismic reflection data. Thrust and strike-slip focal mechanisms suggest that strain is partitioned between thrusting in the Trench and strike-slip motion in the ridge system for the southern Hjort region. However, the absence of thrust mechanisms in the northern Hjort region argues against active underthrusting on the trench decollement north of 57.5ºS (Figure 2.9). In the north, both the decollement in the Hjort Trench and the fault system along the Hjort Ridge may accommodate strike-slip motion (Figure 2.11). The transition from thrusting to strike slip motion on the trench decollement likely results from changes in the orientation of the plate boundary with respect to relative convergence angles predicted by the NUVEL-1A plate

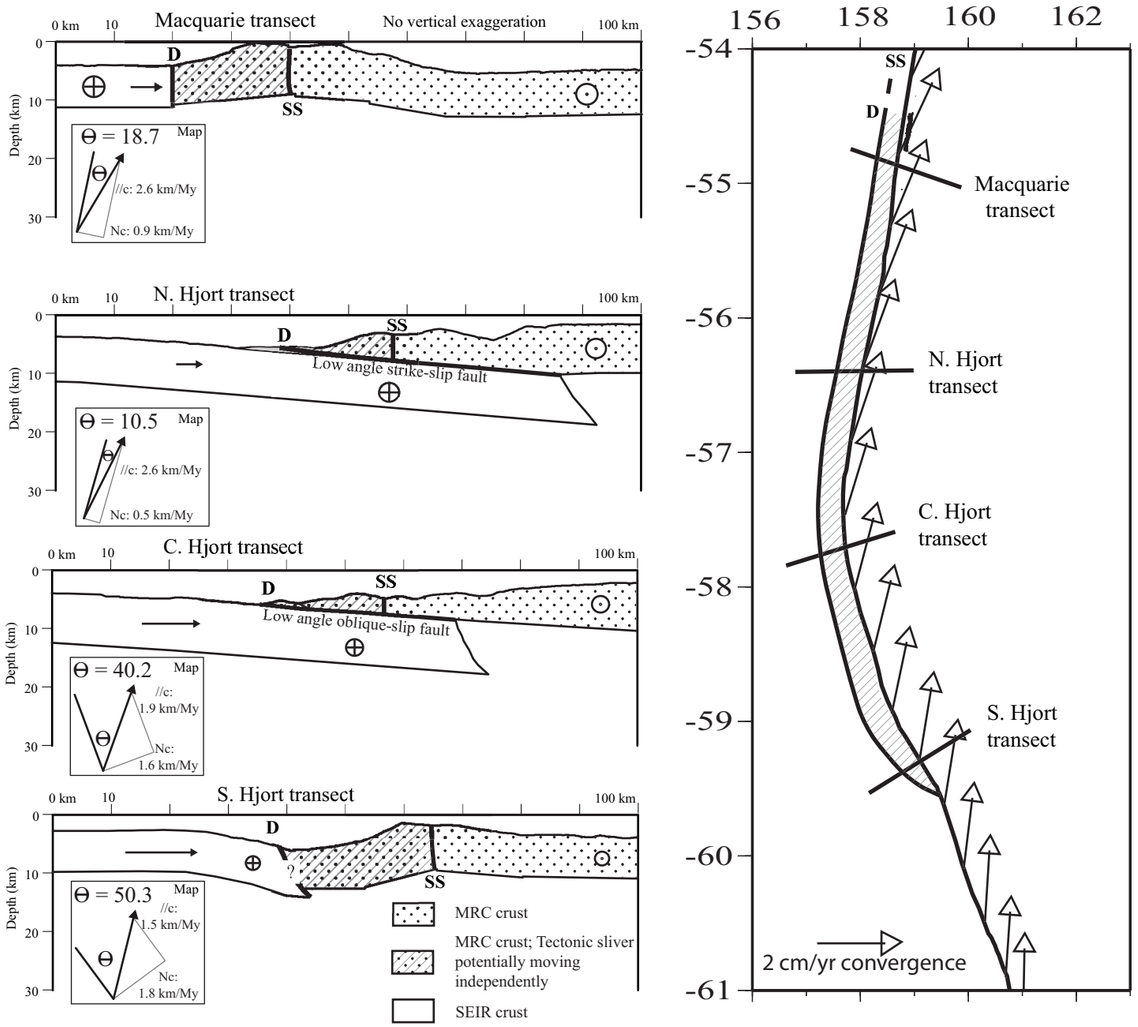

Figure 2.11. Cross sections of the plate boundary zone and relative plate convergence. Left: profiles extracted from the gravity models, with no vertical exaggeration. Stippled crust is interpreted to have formed at the MRC spreading center to the north; white crust at the SEIR to the south. Cross-hatched crust indicates tectonic slivers of MRC crust that are tectonically isolated from both the SEIR and MRC crust to the east, and belong to neither the Australian nor Pacific plates. Circled cross indicates interpreted right-lateral strike-slip motion perpendicular to the cross section away from the reader; circled dot toward the reader. Black-tipped arrows represent convergence. 'D' indicates decollement; 'SS' denotes strike-slip fault system in the crest of the Hjort Ridge. Boxes to lower left of each profile are map views showing the orientation of the trace of the decollement and the direction of relative motion of the Australian plate (SEIR crust) with respect to interior of the Pacific plate (MRC crust). Symbol is the angle between the strike of the decollement and the relative plate convergence vector. Relative convergence is visually separated into the component normal to the orientation of the decollement (Nc) and the component that is parallel (//c). Right: Map showing location of profiles and Australian-Pacific plate convergence vectors using the NUVEL-1A model [DeMets et al., 1994]. Cross-hatched region between decollement and strike-slip system may move independently if slip on two fault systems occurs at different rates. Both: from south to north, the decollement evolves from a thrust fault, to a low angle oblique-slip fault and eventually into a low angle strike-slip fault. Underthrusting has initiated in the southern half of the Hjort Trench, where convergence has the largest boundary-normal component. The underthrust SEIR crust in N. Hjort transect has been translated to its current position from the south.

model [*DeMets et al.*, 1994] (Figure 2.11). Gravity models support the existence of underthrust SEIR crust and can be used to infer crustal slivers of MRC crust between the two main plate boundary faults (Figure 2.11). All of these observations suggest that strain partitioning and the development of crustal slivers may accompany the earliest stages of underthrusting.

Strain partitioning between generally parallel-striking thrust and strike-slip faults has been interpreted in many other obliquely convergent settings [*Fitch*, 1972; *DeMets*, 1992; *Yu et al.*, 1993; *Malod et al.*, 1995; *Barnes et al.*, 1998; *DeMets et al.*, 2000; *Lamarche and Lebrun*, 2000; *Moore et al.*, 2000; *Bilich et al.*, 2001]. Furthermore, *McCaffrey* [1991, 1992, 1994, 1996], and *Platt* [2000] have emphasized that the degree of coupling of the interacting plates also affects the degree to which seismicity reflects partitioning. Coupling in the Hjort region may be influenced by the existence of structurally isolated blocks of crust between the two main fault systems identified. These tectonic slivers are inferred to be composed of MRC crust, but are not part of either the Australian plate to the west or the Pacific plate to the east, and may move independently of both plates. The slivers may be precursors to the generally wider forearc slivers observed at mature subduction zones (e.g. Sumatra, Kuril) [*Jarrard*, 1986b; *DeMets*, 1992; *McCaffrey*, 2000].

Fracture Zone Reactivation

We propose that reactivation of fracture zones has played an important role in the development of underthrusting in the Hjort Trench as well as deformation of the ridge system to the east. On the basis of seismic reflection

data, we interpret the crustal boundary between SEIR and MRC crust as a reactivated fracture zone. In the Hjort region, this and other fracture zones sub-parallel to the plate boundary provided crustal-scale (sub)vertical discontinuities. Upon reactivation, they accommodate thrusting in the Trench, upward displacement of portions of the ridge system during the early stages of underthrusting, and strike-slip motion in the ridge complex due to oblique convergence.

The fracture zone we interpret in the Trench, and those to the east, differ in their genesis. The former is the result of the complex evolutionary history of the Australian-Pacific plate boundary in the vicinity of the Hjort Trench. This boundary was an active transform at times when both the MRC and SEIR were actively spreading, but became a fracture zone with right lateral displacement when spreading ceased on the MRC. In contrast, fracture zones to the east of the Hjort Ridge are extensions of transform faults that separated individual spreading ridge segments on the extinct MRC spreading center to the north. Because the fracture zone in the Trench separates crust formed at two different spreading ridges (SEIR and MRC), with significant age differences, it is therefore a more significant crustal boundary. We argue that the Trench has formed via reactivation of this crustal boundary. Reactivation of the other fracture zones east of the Trench has resulted in deformation of the MRC crust.

For the Puysegur Trench (Figures 2.1 and 2.2) province of the MRC, just south of New Zealand, Lebrun et al. [1998] have speculated that reactivation of fracture zones within oceanic crust of the subducting MRC crust to the west of the

Trench may facilitate the development of strike-slip faults in the overriding MRC crust to the east. This could allow the formation and dispersion of terranes along this part of the plate boundary, as well as facilitate subduction erosion. However, in the Hjort region, trench-parallel fracture zones exist only in the MRC crust east of the Trench, not in the SEIR crust west of the Trench. Whereas the emphasis of Lebrun et al. [1998] was on the influence of fracture zone reactivation in the subducting plate on the overriding plate, in the case of the Hjort region, fracture zone reactivation may only be occurring in the overriding plate, and is not inherited from the underthrust plate. However, the effect of reactivated fracture zones on the bathymetry, gravity signature, and subduction initiation process may be similar.

Incipient Subduction

The Australian-Pacific plate boundary in the Hjort region is neither a well-established subduction zone nor a purely strike-slip boundary. Thrust and strike-slip events (Figures 24 and 2.9) are centered on the Trench and ridge complex and do not form a definitive eastwardly-dipping Wadati-Benioff zone. Moreover, the depths of these events are generally quite shallow (<20 km; Figure 2.10). Seismicity and gravity models suggest that less than 50 km of underthrusting has occurred toward the east, indicating that subduction and associated arc volcanism has not developed as previously proposed, and arguing against the seamounts northeast of the southern Hjort Trench (Figure 2.4) originating by ongoing subduction processes. As noted previously, the linear orientation of the volcanoes may indicate hotspot volcanism. An alternative hypothesis is that subduction has

occurred in the past, but is not active today. The few deep events could indicate a stagnant slab. However, the location of the two deepest events (39 and 64 km; Figure 2.9) west of the MRC is not consistent with a stagnant slab, which should lie to the east of the MRC. Moreover, the existence of thrust events argues for active underthrusting. Therefore, we conclude that underthrusting is ongoing, albeit at a highly oblique angle, and that the incipient subduction phase may have only just been achieved.

We propose that our gravity models represent a time series illustrating various stages of underthrusting leading to incipient subduction at the Hjort Trench. The southern Hjort and Macquarie transects represent less mature stages of underthrusting, whereas underthrusting is more fully evolved in the central and northern Hjort transects (Figure 2.11). The Macquarie transect shows extreme flexure but no offset, whereas the southern Hjort transect shows the beginning stages of offset. Underthrusting is developing from the south in a NNW direction (Figure 2.11, right), and is most evolved for the northern Hjort transect. The angle of convergence relative to the plate boundary and rate of convergence clearly influence the initiation of underthrusting. Initiation of underthrusting involves deformation leading to elevation of the MRC crust in the ridge complex and downward flexure of the SEIR crust (Figure 2.11, S. Hjort transect). Once a decollement is established, underthrusting proceeds and the ridge complex 'relaxes' to greater bathymetric depths (Figure 2.11, C. Hjort transect). Such deformation and the establishment of a decollement may be typical for young oceanic-oceanic convergent boundaries, but due to the close proximity of the pole

of rotation in the Hjort region, the evolution of underthrusting at the Hjort Trench may be relatively unusual. As the underthrust crust moves northward and the orientation of the plate boundary changes in the Hjort region, the decollement evolves into a low angle strike-slip fault. The lack of thrust events in the northern part of the Trench could indicate that all the underthrusting occurs in the southern part of the Trench. Northward translation of the underthrust crust has caused the bathymetric Trench to extend to the north. This interpretation suggests that the northern end of the Trench defines the extent to which underthrust crust has been translated northward (Figure 2.4).

Chapter 3: Tectonic geomorphology of an active, obliquely-convergent submarine plate boundary: Influence of convergence angles on topography and fault development in oceanic crust

3.1 ABSTRACT

Despite complex crustal interactions at the Australian-Pacific plate boundary south of New Zealand, a consistent relationship exists between topography in the plate boundary zone between 51ºS and 56ºS and the time-integrated convergence it has experienced. Anomalously shallow and deep bathymetry occurring within 70 km of the main plate boundary fault is proportional to the amount of plate boundary-normal convergence. Due to the variable orientation of the boundary and relatively close proximity of the Australian-Pacific poles of rotation, individual segments of the plate boundary have experienced different convergence histories since ~10.9 Ma (anomaly 5o). The topographic and structural development of the linear, NE-trending McDougall and NNE-trending Macquarie segments of the Macquarie Ridge Complex (MRC) is distinctly different from the arcuate NNE- to NW-trending Hjort segments to the south. The McDougall and Macquarie segments include a ~40 km-wide ridge rising 4000 m above the adjacent ocean basins, strike-slip faulting along the ridge crest, and bathymetric troughs as deep as 5500 m to the east. In contrast, the ridge in the Hjort region is ~4000 m deeper, has a trench 6,650 m deep to the west, and has a component of underthrusting in the southern trench in addition to strike-slip faulting along the ridge crest. These morphologic and structural differences can be attributed primarily to the variability in the angle

of convergence with respect to the plate boundary orientation since 10.9 Ma, when oblique convergence initiated for much of the boundary.

We quantify the amount of deformation along three segments of the plate boundary using geomorphologic techniques applied to swath bathymetry data. Between 51°S and 60°S we calculate anomalous volumes of oceanic crust relative to average local seafloor depths along transects normal to the plate boundary. We then compare these volumes to convergence angles and amounts of perpendicular convergence predicted by stage rotations and active seafloor faulting to characterize the geodynamic evolution of the different regions. Segments of the plate boundary with large volumes of displaced crust (> 7000 km^3) are associated with relatively high angles of convergence relative to the local plate boundary orientation (> 20º), whereas segments with smaller volumes of displaced crust are associated with smaller angles of convergence. A notable exception to this general observation involves segments of the boundary south of 56ºS that have experienced underthrusting. For the Hjort region, where convergence angles relative to the plate boundary orientation are highest (25-55º) for the southern MRC, displaced volumes are relatively low (< 7000 km^3) for the amount of convergence experienced. This suggests that above a critical convergence angle, underthrusting rather than crustal deformation accommodates convergence. For the MRC, a convergence angle of ~25° marks the transition from strike-slip dominated faulting and large displaced volumes to partitioned underthrusting and strike-slip faulting, and relatively low displaced volumes. We propose that convergence at angles >20° for =10 m.y, resulting in ~200 km of boundary-

normal convergence, represent conditions favorable for establishing incipient subduction in oceanic lithosphere at the Hjort Trench.

3.2 INTRODUCTION

The effects of oblique plate convergence on topography and structural development can be observed globally. Obliquely convergent continental plate boundaries are commonly characterized by regions of anomalous topography and partitioning of deformation between boundary-parallel strike-slip faulting, thrust and normal faulting, and folding oblique to dominant transform orientation, in addition to pervasive strain (e.g. the San Andreas Fault system in California [*Jones and Tanner*, 1995], the Alpine Fault in New Zealand [*Teyssier et al*., 1995; *Claypool et al*., 2002]. The influence of convergence angle on topography and structural development has been shown to be significant [*Bilham and Williams*, 1985; *Argus and Gordon*, 2001], although subaerial erosion complicates estimates of deformation recorded by the uplift of mountain ranges in continental settings.

Studies of oblique convergence at oceanic-continental plate boundaries document a similarly complex association of strain partitioning and deformation, which commonly involves a transition from strike-slip tectonics to subduction (e.g. the Puysegur Trench [*Melhuish et al*., 1999; *Lamarche and Lebrun*, 2000; *Lebrun et al*., 2000; *Moore et al*., 2000] and Hikurangi Margin (*Barnes et al.*, 1998] south and north (respectively) of New Zealand, southeastern Alaska [*Doser and Lomas*, 2000], Sumatra [*Yu et al*., 1993], and the northern Caribbean plate boundary [*Calais et al*., 1992; *DeMets et al*., 2000]. The style of transition from strike-slip faulting to subduction can vary from gradual (>100 km) (Hikurangi

Margin and southern Puysegur Trench) to quite abrupt (northern Puysegur Trench). Crustal heterogeneity across the plate boundary and erosion of the upper continental plate in these settings make it difficult to independently assess the contribution of variable convergence angles on topographic and structural development.

Oblique convergence at oceanic-oceanic plate boundary settings has generally received less attention (e.g. Shackleton Fracture Zone) [*Klepeis and Lawver*, 1996]. To our knowledge, only one attempt has been made to quantify oceanic crustal volumes across an obliquely convergent plate boundary and relate them to angles of convergence and structural development (e.g. the Clipperton Transform offshore southern Mexico) [*Pockalny*, 1997]. *Pockalny* [1997] focuses on the topographic, structural, and magmatic response of a fracture zone to transpression resulting from small changes in the direction of spreading (~5°) at a mid-ocean ridge over a short period of time (<0.5 Myr). Our research addresses the effect of a wider range of oblique convergence (>30°) on the topographic and structural evolution of an intraoceanic plate boundary over 10.9 Myr.

The 1600 km-long Australian-Pacific plate boundary south of New Zealand is ideal for investigating relationships among morphology, structural development, and convergence history at an obliquely convergent intraoceanic plate boundary (Figure 3.1). South of 51ºS, where gridded shipboard bathymetry has been integrated with predicted bathymetry, the interaction at the plate boundary involves only oceanic crust. In addition, subaerial erosion is minimized, although the occurrence of submarine slumps on the flanks of the

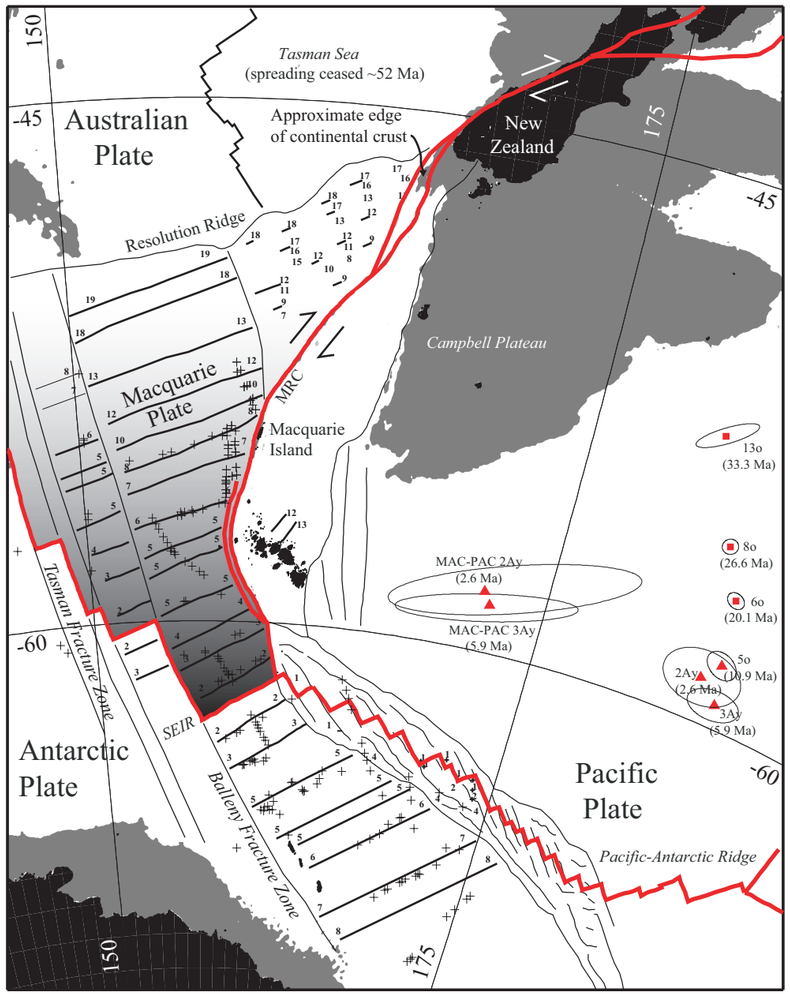

Figure 3.1. Geographic setting of the Australian-Pacific plate boundary and Macquarie Ridge Complex (MRC) south of New Zealand. Solid grey shading represents regions shallower than 2000 m. Euler pole locations and error ellipses for the rotation of Australian Plate with respect to the Pacific Plate (AUS-PAC) are from Cande and Stock [in review]. Square symbols indicate pole locations not used for calculating convergence in this study; triangle symbols are used (Table 1). Two westernmost pole locations are for rotation of the Macquarie Plate with respect to the Pacific Plate (MAC-PAC). The hypothesized Macquarie Plate (transitional shading) extends east of ~145°E and south of 52°S, bound to the east by the MRC and to the south by the SEIR [Cande and Stock, in review]. Interpreted schematic magnetic isochrons are numbered from Weissel et al. [1977], Wood et al. [1996], Cande et al., 2000, and the PLATES database [Lawver et al., 2001]. Weissel et al. [1977] and Ruff et al. [1989] interpreted ~200 km of underthrusting at the Hjort Trench based on the observed truncation of magnetic anomalies 5 through 8 (~10 to 25 Ma) [Cande and Kent, 1995] as compared to their conjugate anomalies on the south side of the easternmost segment of the Southeast Indian Ridge (SEIR).

MRC such as identified by *Massell et al*. [2000] may be another process modifying MRC morphology. Detailed mapping of such slump blocks has not yet been performed, but they represent a proportionally minor expression of the MRC. We investigate the possibility that the present morphology adjacent to the plate boundary may dominantly reflect the relatively recent (<10.9 Ma) history of transpression. Observed active faults along the central and southern MRC, including both strike-slip faulting and underthrusting [*Massell et al*., 2000; *Meckel et al*., in review], as well as localized normal faulting in the crest of the MRC and on Macquarie Island [*Daczko et al*., in review], may represent the primary structural response to transpression in oceanic crust. Complications associated with interactions of different crustal types (oceanic and continental) are avoided, and present morphology has not been significantly modified subsequent to its development. Furthermore, diverse orientations of the present plate boundary (Figure 3.1) allow analysis of the effects of changing angles of recent (<5.9 Ma) convergence over time. All of these characteristics suggest that studies of the MRC can yield fundamental relationships among topography, structural development, and variable convergence history in obliquely convergent intraoceanic settings.

In this paper, we analyze relationships along the MRC between quantitative estimates of crustal volume anomalies resulting from deformation and boundary-normal convergence magnitudes predicted by stage rotations, and investigate departures from that relationship in the southern Hjort region. We compare the distribution of thrust and strike-slip faults to convergence history to

characterize the geodynamic evolution of the MRC. Specifically, we document the angles of convergence that accompany the transition from partitioned underthrusting and strike-slip faulting to purely strike-slip faulting. Our analysis attempts to explain conditions that favor incipient subduction in intraoceanic settings.

3.3 DATA

The primary data for our analysis is swath bathymetry collected during three marine geophysical surveys of the MRC: the 1994 cruise of R/V *Rig Seismic* 124 [*Coffin et al*., 1994; *Frohlich et al*., 1997; *Schuur et al*., 1998; *Massell et al*., 2000], 1996 cruise of R/V *Ewing* 9513 [*Massell et al*., 2000], and the 2000 cruise of R/V *L'Atalante* AUSTREA-2 [*Bernardel, et al*., 2000; *Bernardel and Symonds*, 2001; *Meckel et al*., in review]. These swath data have been merged with predicted bathymetry [*Smith and Sandwell*, 1997] to create a digital bathymetry grid between 51°S to 61°S and 156°E to 162°E [*Bernardel and Symonds*, 2001] (Figure 3.2). A 2-D spline surface was fit to the bathymetry grid using cell resolution of 0.001°. Seafloor sediment accumulation is generally quite well known from reflectivity and multi-channel seismic surveys in the study area [*Schuur et al*., 1998], with the thickest accumulations in the Hjort Trench (up to 1.5 km) [*Meckel et al*., in review]. Magnetic anomaly interpretations used to infer the age of the crust adjacent to the MRC are from *Weissel et al.* [1977], *Wood et al.* [1996], the PLATES database [*Lawver et al*., 2001], and S. Cande [pers. comm.]. Stage pole locations and rotation angles for constraining relative motion

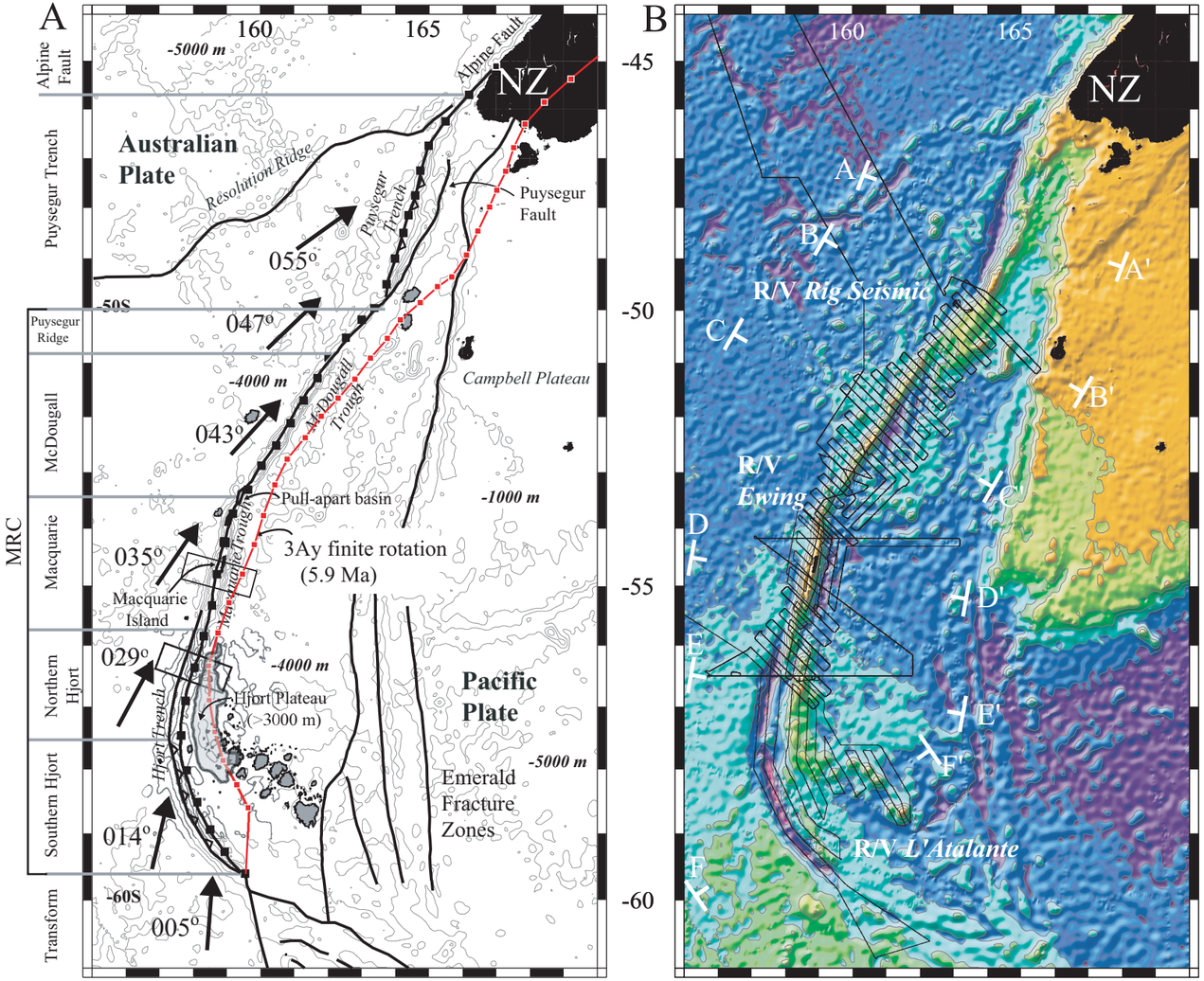

Figure 3.2. Physiography of the Macquarie Ridge Complex. Left: Alpine Fault, Puysegur Trench, Puysegur Ridge, Macquarie, McDougall, and Northern and Southern Hjort segments of the MRC indicated. Solid lines are the decollement (left) and strike-slip (right) plate boundary fault zones that accommodate oblique convergence within the plate boundary zone [Massell et al., 2000; Meckel et al., in review]. Bathymetry contoured at 2000 m intervals. Arrows indicate approximate direction of relative convergence at the plate boundary zone using the 2Ay to 0 stage pole rotation. Boxes on Macquarie and N. Hjort segments are representative swaths used to calculate volumes of crust displaced adjacent to the plate boundary (see Figure 3.7). Grey features with black outlines are mapped volcanic edifices on seafloor. Finite rotation of present plate boundary for anomaly 5o (10.9 Ma) (indicated) provides a visual estimate of the variable amount of convergence that has occurred along the boundary. Right: Combined L'Atalante, Ewing, Rig Seismic, and predicted [Smith and Sandwell, 1997] bathymetry shaded from the northeast [Bernardel and Symonds, 2001]. Letters A-F indicate lines of bathymetric profiles in Figure 3.4.

along and across the plate boundary since 10.9 Ma are calculated from the finite poles of *Cande and Stock* [in review].

3.4 TECTONIC SETTING

Changing relative motions between the Australian and Pacific plates south of New Zealand have resulted in a complex progression from seafloor spreading between the Campbell Plateau and Resolution Ridge (Figure 3.1) from ~40 to 10 Ma [*Molnar et al*., 1975; *Kamp*, 1986; *Wood et al*. 1996], to oblique convergence and strike-slip motion since ~10 Ma [*Lamarche et al*., 1997; *Massell et al*., 2000], and to subduction along the northernmost MRC (Puysegur) [*Christoffel and van der Linden*, 1972; *Walcott*, 1978; *Davey and Smith*, 1983; *Anderson et al*., 1993; *Delteil et al*., 1996]. Magnetic anomaly interpretations west of the northern MRC indicate seafloor spreading was established by 40 Ma [*Wood et al*., 1996], but divergence may have initiated as early as 53 Ma [*Marks and Stock*, 1997]. The southern Australian-Pacific boundary (south of ~56ºS) has experienced a distinctly different progression than the central and northern segments of the plate boundary, notably lacking an early divergent history. The southern boundary has evolved as a transform fault between the SEIR and MRC spreading centers (see Chapter One). Variable amounts of transpression along the transform resulted in deformation along the MRC and underthrusting at the southern Hjort Trench. Plate reconstructions [*Weissel et al*., 1977; *Stock and Molnar*, 1982; *DeMets et al*., 1990; *Sutherland*, 1995; *Royer and Gordon*, 1997; *Cande and Stock*, in review] suggest that a convergent component to relative plate motions along the entire length of the MRC initiated asynchronously between 20.1 and 10.9 Ma..

3.5 LOCATION OF THE MAIN AUSTRALIAN-PACIFIC PLATE BOUNDARY FAULTS AND ASSOCIATED TOPOGRAPHY

The southern extension of Australian-Pacific plate boundary south of 46°S between New Zealand's South Island and the Macquarie Triple Junction (MTJ) [*Falconer*, 1972; *Lodolo and Coren*, 1994 & 1997] (Figures 3.1 and 3.2) forms an shallow (commonly < 1000 m deep), ridge ~40 km wide with adjacent troughs that alternate sides along the length of the plate boundary (the MRC). The plate boundary can be divided into four main morphologic segments: the Puysegur (46ºS to 50.5ºS), the McDougall (50.5ºS to 53.5°S), Macquarie (53.5ºS to 55.8°S), and Hjort (55.8ºS to 59.5°S) (Figure 3.2) [*Massell et al.,* 2000]. The McDougall and Macquarie segments have troughs on the east side of the ridge, whereas the other segments have trenches on the west side. The transitions between these segments are distinct, distinguishable by breaks in the bathymetric ridge [*Schuur et al.,* 1998], and different orientations, morphologies, and structural characteristics.

The Puysegur segment includes both the Puysegur Trench (46ºS to 49.5ºS) and the Puysegur Ridge (47.5ºS to 50.5ºS) (Figure 3.3A). The Puysegur Trench is = 6300 m deep (average 5500 m) and is related to established subduction of oceanic lithosphere of the Australian plate beneath adjacent oceanic or continental lithosphere of the overriding Pacific plate [*Christoffel and van der Linden*, 1972; *Walcott*, 1978; *Davey and Smith,* 1983; *Anderson et al*., 1993; *Delteil et al*., 1996*Melhuish et al*., 1999; *Lamarche and Lebrun*, 2000; *Lebrun et al*., 2000]. Convergence north of 47ºS occurs between oceanic crust of the Australian plate

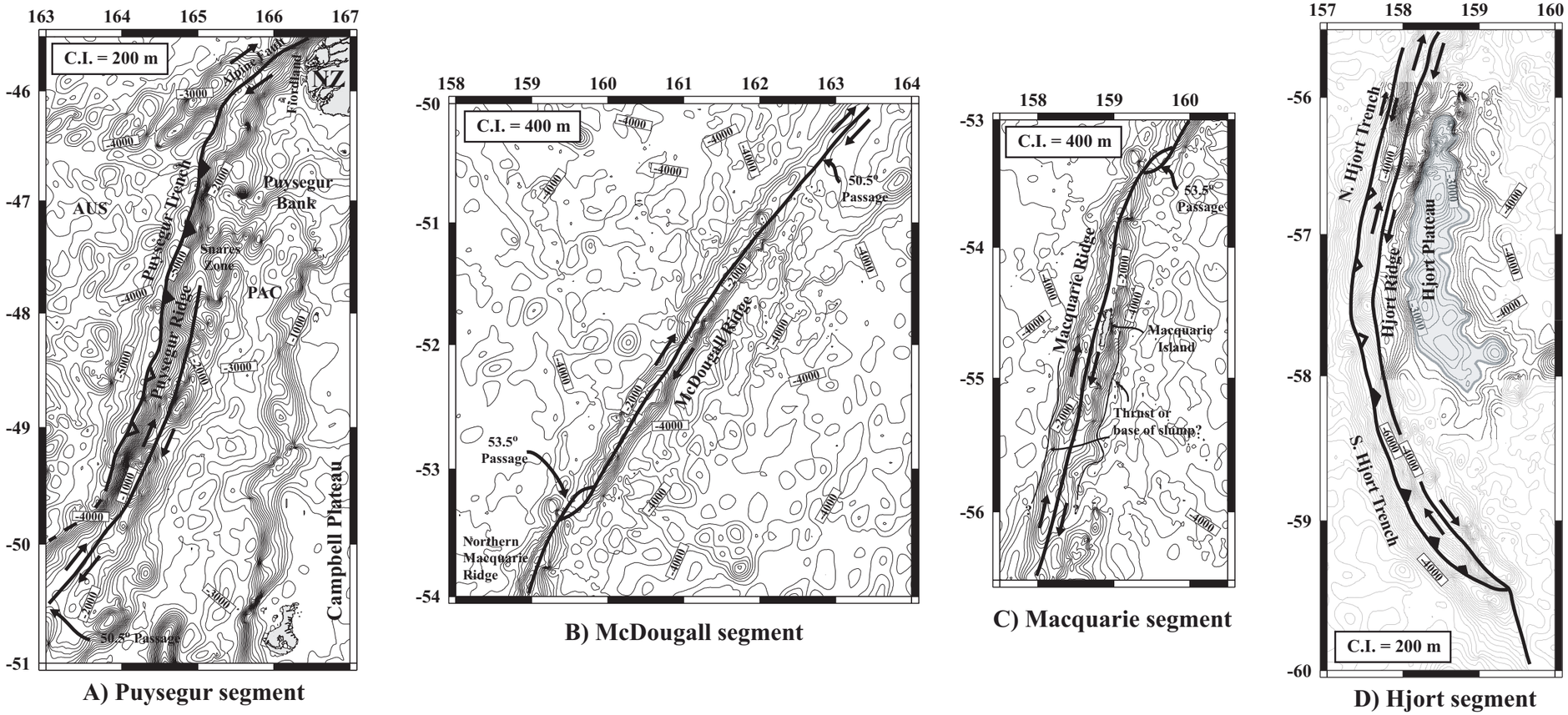

Figure 3.3. Contoured bathymetry for each of the various ridge segments along the length of the marine expression of the Australian-Pacific plate boundary south of New Zealand. Contour intervals indicated. Predicted bathymetry is from Smith and Sandwell [1997]. Major structural and bathymetric features discussed in the text are identified. A) Puysegur segment of the MRC. Oblique convergence that has occurred between the Australian and Pacific plates has resulted in ~150 km of subduction at the Puysegur Trench. Structures shown are modified from Lamarche and Lebrun [2000] and Lebrun et al. [2000]. Filled black triangle symbols represent thrust faults, and open triangles represent less developed thrusting. Black arrows represent strike slip motion at the plate boundary. B) McDougall segment of the MRC. The McDougall Ridge extends from the 50.5ºS Passage to the 53.5ºS Passage, and accommodates dominantly strike slip motion in the crest of the McDougall Ridge [Frohlich et al. 2000]. C) Macquarie segment of the MRC. The Macquarie Ridge extends between the 53.5ºS Passage and 55.8ºS, where the bathymetric deep changes from the east of the Macquarie Ridge to the Hjort Trench, west of the MRC. Oceanic crust is exposed at Macquarie Island (indicated). Plate motion is dominantly accommodated by strike-slip motion at the valley at the crest of the Macquarie Ridge. D) The Hjort segment of the MRC. The Hjort Ridge extends from 55.8ºS to 59.5ºS. The elevated Hjort Plateau is defined by the topography above the 3000 m bathymetric contour (indicated). Filled black triangles represent underthrusting in the Hjort Trench. Open triangles represent thrust offsets observed in seismic lines (see Chapter 2). The fault in the northern Trench accommodates an increasing amount of oblique slip due to the lower angles of convergence there.

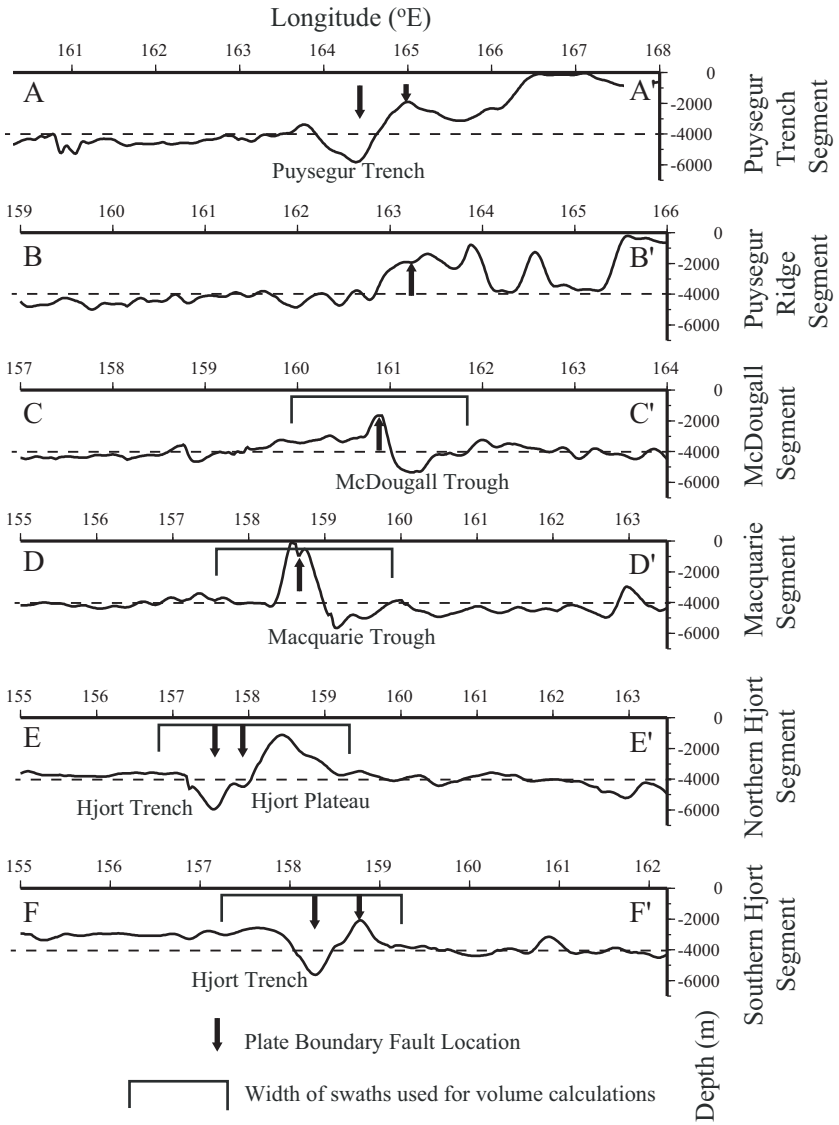

Figure 3.4. Bathymetric profiles perpendicular to the plate boundary orientation. Letters A-F refer to profile positions on Figure 3.2. Profiles use predicted bathymetry from Smith and Sandwell [1997]. Various segments of the MRC indicated at right. Dashed line indicates -4000 m. Black arrows indicated positions of plate boundary faults from Figure 3.2 that cross each profile. The widths of swaths of bathymetry data extracted for volume calculations are indicated. Swath widths traverse topography considered to be deformed as a result of convergence at the plate boundary.

and continental crust of the Puysegur Bank and Fiordland on the Pacific plate and subduction accommodates most of the plate convergence [*Lamarche and Lebrun*, 2000]. At the northern end, the Puysegur Trench terminates abruptly at ~46ºS, and the subduction zone and the Alpine Fault connect in a zone of strike-slip and thrust faults [*Delteil et al.*, 1996a, 1996b; *Lamarche and Lebrun*, 2000] (Figure 3.3A). Convergence in the southern Puysegur region is partitioned between the Puysegur subduction zone characterized by intraoceanic crustal convergence and strike-slip faults in the Snares Zone of the overriding Pacific plate. Southward, the Puysegur Trench gradually shallows, terminating at 49.5ºS (Figure 3.3A). Seismological studies and structural interpretations of the plate boundary zone of the central MRC indicate that no subduction is recognized south of 49ºS [*Frohlich et al.*, 1997; *Massell et al.*, 2000]. The Puysegur Ridge on the east side of the southern Puysegur Trench extends from 47.5ºS to 50.5ºS, forming the northernmost segment of the MRC [*Collot et al.*, 1995]. A 3200 m bathymetric gap in the MRC at the 50.5ºS passage [*Schuur et al.*, 1998] separates the Puysegur Ridge from the southern MRC ridge segments. *Lamarche and Lebrun* [2000] describe a gradual transition from subduction along the southern Puysegur Trench to dextral strike-slip faulting on the Puysegur Ridge. The Puysegur Ridge trends N25ºE and is ~2000 m deep (Figure 3.3A). A V-shaped valley along the crest is interpreted as a strike-slip fault zone (Puysegur Fault) [*Delteil et al.*, 1996], and this zone characterizes the crest of the MRC between the South Island of New Zealand and the southern end of the Hjort Trench (Figure 3.2). To the north, the Puysegur Fault terminates at ~47ºS, where dredged samples indicate that oceanic

crust of the Puysegur Ridge [*Summerhayes*, 1969] changes to the continental crust of the Puysegur Bank [*Mortimer*, 1994; *Lamarche and Lebrun*, 2000].

The McDougall and Macquarie segments consist of linear ridges varying from 30 to 50 km in width. The ridges are generally shallower than 2000 m, and >5000 m deep troughs to the east of the ridges (Figures 3.3B&C and 3.4). The change in position of the bathymetric trough at ~50.5ºS occurs at a ~3200 m bathymetric passage in the MRC, marking the transition from the Puysegur Ridge to the McDougall Ridge. The major distinction between the McDougall and Macquarie segments is the 18° difference in their orientations (Figure 3.3B, which occurs at 53.5ºS [*Massell et al*., 2000]. The notable break in the ridge >5100 m deep at the 53.5ºS Passage [*Schuur et al*., 1998] occurs at this transition and has been interpreted to be a 60 km-long and 20 km-wide pull-apart basin associated with a right step in the main plate boundary fault [*Massell et al*., 2000; *Daczko et al*., in review] (Figure 3.3B). The Australian-Pacific plate boundary fault at the crest of the ridge in the McDougall and Macquarie segments between 50°S and 56°S [*Massell et al*. 2000; *Daczko et al*., in review] (Figures 3.2 and 3.3B&C) is interpreted to accommodate primarily strike-slip deformation [*Frohlich et al*., 1997]. There is no indication from geophysical observations over the McDougall segment that any crust has been underthrust there. *Massell et al*. [2000] traced fracture zones and related spreading fabric adjacent to the MRC onto the crest of the MRC, where they intersect with the main strike-slip plate boundary fault. *Massell et al*. [2000] interpreted thrust faults at the base of the eastern and western slopes of the MRC in the southern Macquarie segment of the plate

boundary based on reflectivity data (Figure 3.3C), but seismic reflection profiles do not indicate any offset of the sediment/igneous basement contact for this region (Figure 2.8, upper profile). These linear features may be better interpreted as the toes of slump deposits. The dominance of normal faults on Macquarie Island [*Daczko et al*., in review] may also reflect active collapse of the MRC, but *Daczko et al*. [in review] identified a series of en-echelon strike slip faults separated by extensional relay zones in the submarine valley at the crest of the MRC. They attribute normal faulting on Macquarie Island to an extensional relay zone associated with these faults. The faults are thought to accommodate transpression, and their orientations are interpreted to be inherited from the pre-existing divergent setting of the Macquarie segment [*Daczko et al*., in review].

The Hjort region is characterized by a ridge that is the southernmost portion of the MRC, flanked to the west by the tectonically significant Hjort Trench (Figure 3.3D). The change in location of the trough on the east (Macquarie) side of the ridge to the trench on the west at ~56.5ºS corresponds with the ~3500 m deep bathymetric passage in the MRC identified by *Schuur et al*. [1998], marking the transition between the Macquarie and Hjort segments (Figures 3.3D and 3.4). The crest of the MRC in the Hjort region is = 4000 m deeper than in the McDougall and Macquarie regions to the north (Figures 3.2, 3.3, and 3.4). The southern Hjort Trench reaches depths of 6,650 m. In the Hjort region, the plate boundary zone contains two main faults, one at the crest of the ridge, which is a continuation of the dextral strike-slip plate boundary fault in the ridge of the McDougall and Macquarie segments, and another fault to the west in

the Hjort Trench thought to accommodate oblique convergence [*Meckel et al*., in review] (Figures 3.2, 3.3D, and 3.4). The amount of underthrusting in the Trench believed to result from that convergence is debated and varies between 50 and 200 km [*Weissel et al*., 1977; *Ruff et al*., 1989; *Meckel et al*., in review]. An additional topographic province (labeled Hjort Plateau; Figure 3.3D) unique to this region of the MRC lies east of the Trench and Ridge south of 56°S. The Hjort Plateau is defined to be the area shallower than 3000 m, as illustrated in Figure 3.3D. This plateau is populated with dozens of volcanoes, some rising = 3000 m above the regional seafloor (Figure 3.2).

Distinctions in interpreted fault behavior and orientation justify subdividing the Hjort region into northern and southern segments (Figure 3.3D). The northern Hjort segment is a transition between the Macquarie and the southern Hjort segment. Northern Hjort's orientation resembles Macquarie's, but morphologically northern Hjort more closely resembles the southern Hjort segment (Figure 3.3D). The southern Hjort segment strikes NW, which is distinctly different from the NE-striking segments to the north. *Meckel et al*. [in review] interpreted the fault in the northern Trench as a low angle strike slip fault that translates crust underthrust at the southern Trench northward. The fault in the southern Trench is interpreted as an oblique-slip thrust fault; two reliable thrust mechanisms in the southern Trench support active underthrusting in the region [*Meckel et al*., in review], although more detailed relocation of those events would be necessary to relate them to a specific fault.

3.6 CONSTRAINTS ON SEAFLOOR AGE ADJACENT TO THE MRC FROM MAGNETIC ANOMALIY INTERPRETATIONS

Favorably oriented magnetic anomaly data are sparse proximal to the MRC, but available data permit some general age constraints. The age of the crust west of the Hjort and Macquarie segments generally increases from south to north. Anomalies 3 through 8 west of the plate boundary between 53.5ºS and 59.5ºS (Figure 3.1) indicate ages from 4.2 to 26.5 Ma [all magnetic anomaly ages are from *Cande and Kent*, 1995]. The precise age of crust immediately (<200 km) west of the McDougall segment is unknown, but is younger than anomaly 7 (~25 Ma) [*Massell et al*., 2000] (Figure 3.1). In contrast, the age of the crust east of the MRC appears to increase from north to south. East of the MRC, interpretations of anomalies 12 and 13 (30.4 to 33.5 Ma; *Weissel et al.*, 1977; Figure 3.1), and other currently unpublished locations of anomalies 9y through 18o east of the ridge in the Hjort region also support an age increase to the southeast for crust east of the MRC (Keller, 2002; J. Stock, pers. comm.). The youngest anomaly identified east of the MRC is anomaly 9y (27.0 Ma).

The best age constraints for crust forming the ridge component of the MRC are derived from radiometric age dating of rocks on Macquarie Island (Figures 3.2 and 3.3C). Basalts and sheeted dikes exposed on Macquarie Island indicate that the island formed by spreading processes at the MRC when it was a spreading center [*Varne et al.*, 1969; *Varne and Rubenach*, 1972; *Kamenetsky et al.*, 2000; *Varne et al.*, 2000; *Goscombe and Everard*, 2001]. Island basalt flows have yielded $^{40}Ar/^{39}Ar$ ages of 9.7-11.5 Ma [*Duncan and Varne*, 1988] and 6.75

±0.09 and 6.1 ± 0.9 Ma [*Wertz et al.*, 2002; Wertz, unpublished data], suggesting that spreading continued until at least 6 Ma. Younger rocks may be present on the island, but have yet to be been identified. Thus, spreading on the Macquarie segment probably ceased sometime since ~6 Ma, and convergence since that time has resulted in deformation and uplift. The MRC in the Hjort and McDougall regions is an extension of the MRC to the south and north of the Macquarie segment, respectively, on which Macquarie Island rests. We assume that the crust composing the MRC's ridge north and south of Macquarie Island is of similar age to the island (6 to 11.5 Ma).

3.7 TIMING OF UPLIFT AT THE PLATE BOUNDARY

The timing of uplift at the Macquarie segment can be inferred from assumptions of topography that may have existed prior to convergence, the present topography, and the rates of uplift that have been determined for Macquarie Island. The MRC is emergent at Macquarie Island (Figure 3.2), which is ~4400 m above average adjacent seafloor. Topography at the plate boundary likely existed prior to convergence due to the young age of the crust that formed just prior to the cessation of spreading. Such topography can be assumed to have existed based on the observation of residual topography at extinct spreading ridges such as exists in the central Tasman Sea [*Gaina et al.*, 1998] and Pacific and Indian Oceans [*Mammerickx et al.*, 1980; *Mammerickx and Sandwell*, 1986]. Spreading in the Tasman Sea is known to have ceased at ~52 Ma [*Weissel and Hayes*, 1977; *Wood et al.*, 1996; *Gaina et al.*, 1998], yet bathymetric profiles across the extinct ridge at 46ºS show topography of the ridge flanks rising as

much as 500 m above the central trough of the extinct spreading ridge. Active and young ridges have topography of the same general wavelength [*Johansen et al*., 1984]. Numerical modeling studies of axial valley morphology at abandoned spreading centers [*Freed et al*., 1995] suggests that axial valley morphology may be preserved for tens of millions of years after the cessation of spreading. *Freed et al*. [1995] suggest that the removal of the axial valley topography can only be accomplished by reversal of regional extensional strains immediately after cessation, which occurred at the MRC. Thus, some hundreds of meters of topography may have existed on the flanks of the extinct spreading ridge at the Macquarie segment, but the transition to transpression may have inverted or enhanced any axial valley topography during convergence and increased flank elevations.

The typical depth for oceanic crust of a given age can be estimated using the relationships established by *Parsons and Sclater* [1977] and *Stein and Stein* [1992]. Using these models, oceanic crust with an age similar to Macquarie Island (6-11.5 Myr) typically reaches isostatic equilibrium around 3300-3800 m water depths. Thus the present elevation of Macquarie Island 400 m above sea level represents uplift of 3700-4200 m from a modeled seafloor elevation with equivalent age at equilibrium.

Selkirk et al. [1990] determined that Macquarie Island has been uplifting at a rate of 0.8 mm/yr since 0.6-0.7 Ma using thermoluminescence dating of wave-cut beach terraces. Palynological analyses and studies of marine terraces on the Island are consistent with these conclusions [*Selkirk et al*., 1983].

Extrapolating this rate, Macquarie Island could have been uplifted ~4400 m above the adjacent average seafloor depth since ~5.5 Ma. If the seafloor depth of the base of any pre-existing axial valley was only 3700 m, representing the shallowest modeled equilibrium depth prior to convergence, and had an additional 500 m of axial flank topography (making the shallowest region 3200 m), uplift could have occurred at Selkirk's rates since ~4 Ma. Shallow depths (< 50 m) and flat-topped morphology of the ridge crest elsewhere on the Macquarie segment suggest that a total of ~140 km of the ridge was previously at or above sea level [*Massell et al*., 2000], suggesting that long-term uplift may be punctuated by episodes of subsidence, essentially reducing the average uplift rate. In that case, it could have taken > 4-5.5 Ma for Macquarie Island to reach its current elevation. Alternatively, the erosion could have occurred during times of lower sea level. Unpublished GPS data from Macquarie Island that have been continuously collected since 1997 indicate uplift rates of 1.22 ± 0.12 mm/yr [http://www.auslig.gov.au/geodesy/argn/]. Using that rate and an elevation of 4400 m, Macquarie Island could have reached its present elevation in 3.3-4 Ma. Taking a depth of 3200 m, these rates would suggest uplift since approximately 2.5-2.9 Ma. These analyses indicate that the earliest uplift could have begun given the current data was 5.5 Ma, with the latest around 2.5 Ma.

3.8 STAGE ROTATIONS AND ESTIMATES OF CONVERGENCE

3.8.1 Methods

Estimates of convergence over time at the plate boundary can be made using interpreted orientations of the plate boundary (see Chapter One) and stage rotation poles. Previous research has used magnetic anomaly interpretations and fracture zone locations to constrain positions of finite poles of rotation for the Australian-Pacific two-plate system since 40 Ma. Positions for Australian-Pacific rotation poles (Figure 3.1) have been refined over the past decade due to increases in the amount and quality of relevant data [*Cande and Stock*, in review]. Convergence at the Hjort Trench since ~10.9 Ma is indicated by multiple efforts to locate Miocene pole positions [*Weissel et al*., 1977; *Stock and Molnar*, 1982; *DeMets et al*., 1990; *Sutherland*, 1995; *Royer and Gordon*, 1997]. Pole locations since 10.9 Ma (Chron 5o) or 5.9 Ma (Chron 3Ay) (*Cande and Kent* [1995]) and younger are most appropriate for estimates of total convergence experienced along the MRC (Figure 3.1). The location for the present pole of rotation between the Australian and Pacific Plates is from *DeMets et al*. [1994] (Figure 3.1).

Cande and Stock [in review] have calculated pole locations for anomalies 13o to 2Ay (33.5-2.6 Ma) for the Australian-Pacific two plate system (Figure 3.1). For anomalies 3Ay and 2Ay (5.9 and 2.6 Ma), they determined two sets of poles. One set is for the Australian-Pacific system (AUS-PAC), whereas the other considers the possible existence of an independently behaving Macquarie microplate and its interaction with the Pacific plate (MAC-PAC). The Macquarie plate, as delineated by *Cande and Stock* [in review], lies east of 145°E and south

of ~52°S, and its eastern and southern boundaries are the MRC and SEIR, respectively. Previously, the Macquarie plate has been considered to be the southeasternmost corner of the Australian plate (Figure 3.1). The existence of an independent Macquarie plate has significant implications for the tectonic history of the southern MRC, and we therefore include the MAC-PAC poles of rotation in our analysis (Table 1). However, for the northern part of the MRC, the AUS-PAC poles are relevant because these are the two interacting plates (Table 1).

We use stage rotations around Euler poles to predict the angles and amounts of plate convergence along the different segments of the MRC through time. We calculated stage rotations (see *Le Pichon* [1973]) for the anomaly intervals 5o-3Ay, 3Ay to 2Ay and 2Ay to 0 using the finite pole locations of *Cande and Stock* [in review] (Table 2). We generated two sets of stage poles, considering both the AUS-PAC and MAC-PAC finite poles. Choosing 33 arbitrary positions at ~50 km spacing along the plate boundary (solid black boxes in Figure 3.2), we applied the stage rotations describing the relative motion of the AUS-PAC and MAC-PAC systems (Table 2). Using new locations of the points for each stage rotation, we calculated angles of convergence relative to the plate boundary orientation for the 33 positions along the boundary south of 45ºS (Figure 3.5). In addition, we determined magnitudes of the plate-boundary-normal components of convergence (Figure 3.5D, inset).

Uncertainties in the positions of various finite rotation poles (Figure 3.1) result in uncertainties in positions of the stage poles used to calculate plate

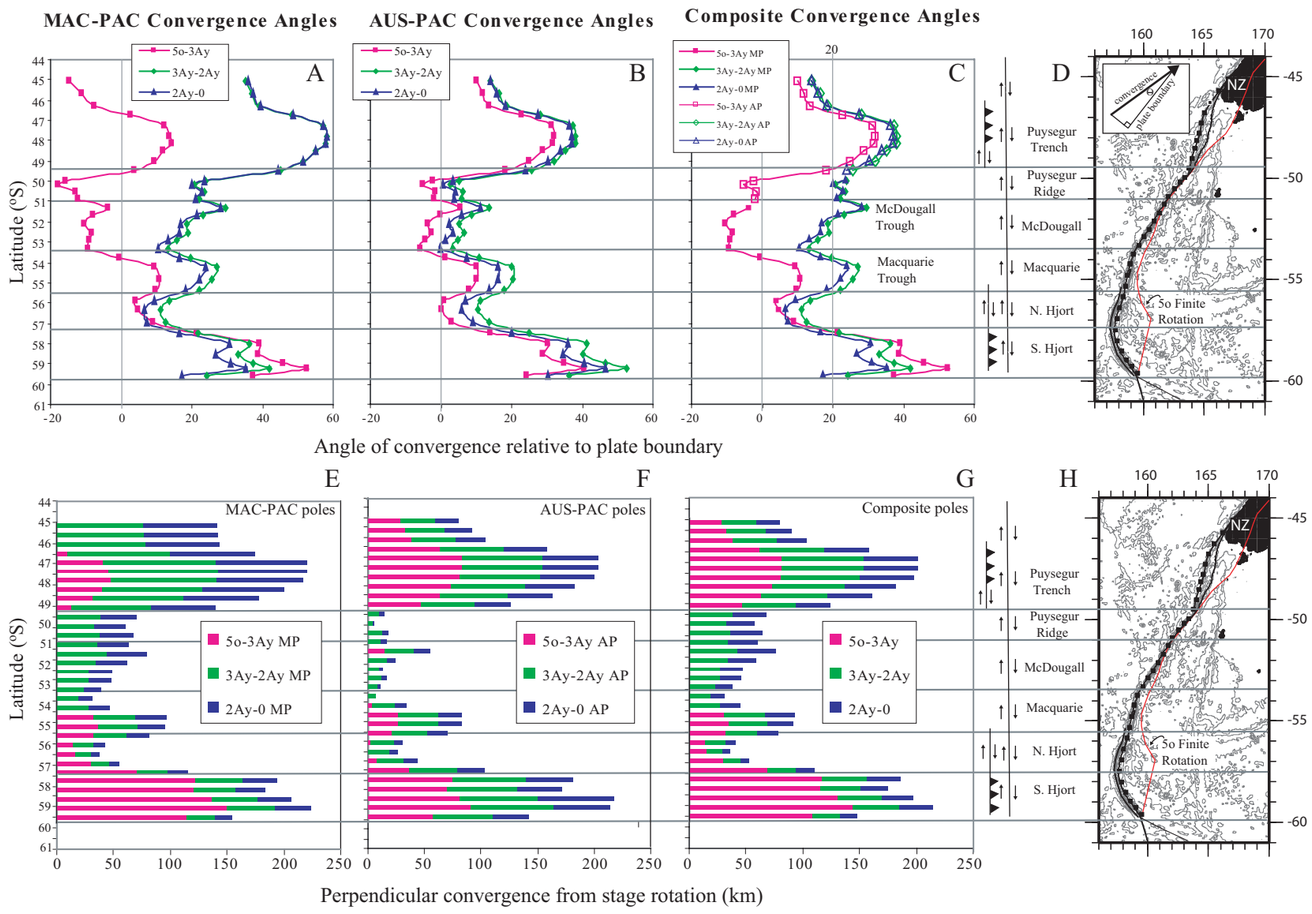

Figure 3.5. Comparison of angles of convergence with respect to the plate boundary orientation and boundary-normal convergence predicted by stage rotations from Table 2 for each of the segments of the boundary indicated to right since Chron 5o (10.9 Ma) with established fault systems. Top: Box, square, and diamond symbols represent locations at the crest of the MRC where calculations were made (Figure 3.2). Angles are between the convergence direction and plate boundary orientation (inset, D). Negative angles imply divergence and positive angles imply convergence. Bottom: Colored bars represent the boundary-normal component of convergence for each of the stage rotations. A: Convergence angles for different stages using the MAC-PAC stage rotations. Predictions for the Puysegur Ridge and Trench seem anomalous given the Alpine Fault was not divergent from 10.9 to 5.9 Ma. B: Convergence angles for different stages using the AUS-PAC stage rotations. Differences for the northern part of the plate boundary between A and B suggest that northern segments of the boundary are better described by AUS-PAC stage rotations. C: Composite curve using MAC-PAC stage rotations in the south and AUS-PAC stage rotations in the north. Analysis shown in Figure 3.10 indicates that MAC-PAC rotations are more appropriate south of ~51ºS. The transition is taken at 51ºS for the stage 50 to 3Ay and at 50ºS for younger stages, where the transition between curves is smoothest. D: Plate boundary faults that occur in different segments relate to convergence angles since anomaly 5o. Thrust faults are mapped where convergence angles have been higher than 20º since anomaly 5o. Strike-slip dominated segments have had a history of lower convergence angles. Macquarie and McDougall troughs occur where convergence angles have slightly exceeded 20º for stages 3Ay to 2Ay and 2Ay to 0. E-G: Plate boundary-normal components of convergence (inset, D) for the various convergence angles indicated in A-C. Except for the central MRC in F, all models arrive at a similar total amount of plate boundary-normal convergence. The main difference is in the timing of different magnitudes of convergence. Plate boundary-normal convergence of ~200 km is associated with thrust faults in the southern Hjort Trench and Puysegur Trench. H: Same as D.

Table 1. Finite rotation poles used in this study from Cande and Stock [in review].

Plate Pair (2nd plate fixed)	**Chron (Age) [Cande and Kent , 1995]**	**Latitude °S**	**Longitude °E**	**Rotation Angle (degrees)**
Australia - Pacific	5o (11.53 Ma)	-58.24	185.13	11.93
Australia - Pacific	3Ay (5.89 Ma)	-59.35	185.67	6.38
Australia - Pacific	2Ay (2.58 Ma)	-58.76	184.33	2.77
Australia - Pacific	Present Day (0 Ma) *	-60.08	181.74	1.07
Macquarie - Pacific	3Ay (5.89 Ma)	-58.64	171.98	9.18
Macquarie - Pacific	2Ay (2.58 Ma)	-58.28	171.55	4.29

* NUVEL -1A pole of *DeMets et al* . [1994]

boundary-normal convergence for each stage, thereby inducing uncertainties in the amounts of plate-boundary-normal convergence. For each finite rotation pole pair defining a stage rotation (e.g., 5o to 3Ay), we chose four points on the error ellipses for each finite pole that represent the maximum variability (in the 95% confidence zone) in the finite pole location (i.e the northernmost, southernmost, easternmost, and westernmost positions) (total of 8 points, 4 on each ellipse). We then calculated the stage pole position resulting from all 16 possible combinations of finite pole positions (Figure 3.6). These 16 points define the range of stage pole locations given the error associated with the finite pole positions, with the finite pole located in the center of the distribution. We used the northernmost, southernmost, easternmost, and westernmost of these stage pole positions (triangle symbols, Figure 3.6) to represent the maximum latitudinal and longitudinal error with respect to the stage pole at the center of the ellipses (Table 2). For stage 2Ay to 0, only 5 total estimates of stage poles were used, as there was only one error ellipse to evaluate. We then calculated the amount of plate-boundary-normal convergence at each point on the plate boundary (Figure 3.2) for five potential stage pole positions: the position derived using the center of each finite pole error ellipse (cross symbol, Figure 3.6), and those representing the maximum variability (triangle symbols, Figure 3.6). For each of the five potential stage poles for a given stage, we summed the amount of convergence for the three stages considered (5o-3Ay, 3Ay-2Ay, and 2Ay-0). We chose the result from the stage pole position derived using the points at the center of each finite

Table 2. Stage poles calculated from finite poles [Le Pichon, 1973].

Plate Pair (2^{nd} plate fixed)	Stage anomalies (ages) [Cande and Kent, 1995]	Latitude °S (associated error)	Longitude °E (associated error)	Rotation Angle in Degrees (associated error)
Australia-Pacific	5o-3Ay (11.53-5.89 Ma)	-56.94 (+1.28, -1.25)	184.80 (+3.48, -3.45)	5.55 (+0.0052, -0.0024)
Australia-Pacific	3Ay-2Ay (5.89-2.58 Ma)	-59.82 (+1.34, -1.33)	186.68 (+4.52, -4.53)	3.61 (+0.0048, -0.0006)
Australia-Pacific	2Ay-0 (2.58-0 Ma)	-58.76 (+0.78, -0.76)	184.33 (+2.32, -2.22)	2.77 (N/A)
Macquarie-Pacific*	5o-3Ay (11.53-5.89 Ma)	-51.46 (+4.69, -7.81)	220.78 (+7.25, -16.28)	3.02 (+0.20, -0.21)
Macquarie-Pacific	3Ay-2Ay (5.89-2.58 Ma)	-58.97 (+2.47, -1.38)	172.31 (+14.82, -15.41)	4.89 (+0.06, -0.0001)
Macquarie-Pacific	2Ay-0 (2.58-0 Ma)	-58.28 (+1.81, -0.78)	171.55 (+8.71, -4.28)	4.29 (N/A)

* Uses 5o AUS-PAC finite pole and 3Ay MAC-PAC finite pole

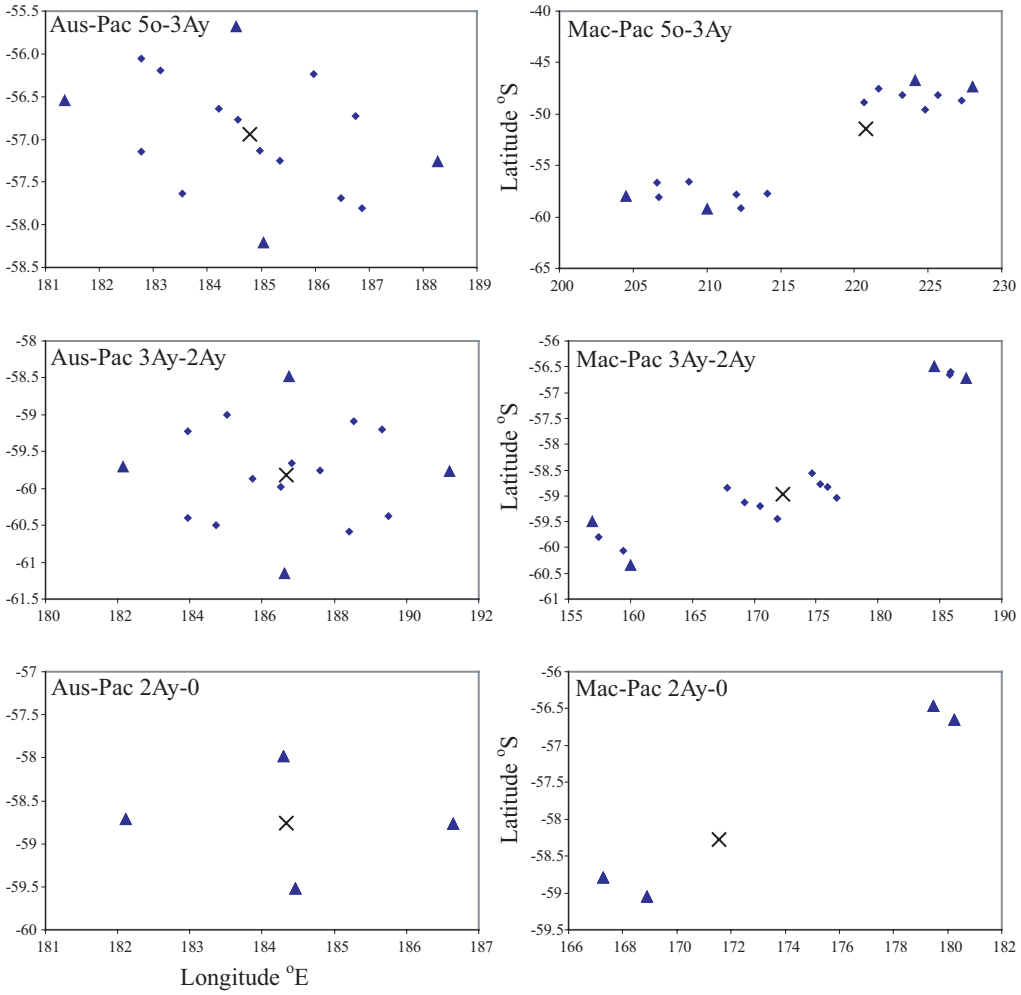

Figure 3.6. Plots of permissible stage pole locations used in assessing variability in amount of convergence at the plate boundary. Cross symbol denoted stage pole location using the pole positions seen in the center of the ellipses in Figure 3.1. All other symbols represent stage pole locations permissible given the error ellipses surrounding the finite rotation poles. Triangle symbols are northernmost, easternmost, southernmost, and westernmost stage pole positions used for assessing variability in predicted convergence at the plate boundary for each stage. Left: Australian-Pacific stage poles. Right: Macquarie-Pacific stage poles. Amounts of convergence perpendicular to the plate boundary orientation using these stage poles are reported in Table 3, columns 2 through 5.

Table 3. Amount of shortening perpendicular to the plate boundary orientation for the various models.

1	2	3	4	5	6	7	8	9	10
Latitude of point on crest of MRC (degrees south)	Cumulative predicted convergence since A5o from stage rotations using AUS-PAC poles (km)	Cumulative predicted convergence since A3Ay from stage rotations using AUS-PAC poles (km)	Cumulative predicted convergence since A5o from stage rotations using MAC-PAC poles (km)	Cumulative predicted convergence since A3Ay from stage rotations using MAC-PAC poles (km)	Average seafloor depth defined using bathymetric profiles perpendicular to the boundary (m)	Total volume displaced from average seafloor elevation (km^3)	Total predicted convergence using the volume & linear relationship in Figure 3.9A (km)	Difference between column 4 and column 8 (km)	Difference between column 5 and column 8 (km)
51.7	25 +13/-14	25 +13/-14	62 +15/-25	62 +15/-25	-4000	8095	55	7 +15/-25	7 +15/-25
52.1	13 +13/-12	13 +13/-12	49 +21/-18	49 +21/-18	-4000	8831	60	-11 +21/-18	-11 +21/-18
52.5	17 +13/-14	17 +13/-14	48 +19/-17	48 +19/-17	-4000	7502	51	-3 +19/-17	-3 +19/-17
52.9	11 +13/-11	11 +13/-11	40 +23/-13	40 +23/-13	-4000	6406	44	-4 +23/-13	-4 +23/-13
53.3	6 +18/-6	6 +18/-6	32 +26/-9	32 +26/-9	-4000	4795	33	-1 +26/-9	-1 +26/-9
53.7	35 +17/-17	31 +13/-13	47 +22/-19	47 +10/-19	-4000	6179	42	5 +22/-19	5 +10/-19
54.2	87 +21/-27	59 +14/-13	97 +8/-23	65 +5/-11	-4000	8219	56	47 +8/-23	9 +5/-11
54.8	87 +21/-27	59 +14/-13	97 +8/-20	60 +4/-9	-4000	9049	62	37 +8/-20	-2 +4/-9
55.3	73 +21/-27	52 +13/-14	83 +8/-21	49 +5/-9	-4000	7517	51	32 +8/-21	2 +5/-9
55.8	32 +20/-16	30 +13/-14	43 +12/-25	28 +12/-10	-4000	4320	30	13 +12/-25	2 +12/-10
56.4	28 +20/-14	27 +14/-13	38 +13/-21	22 +13/-8	-4000	7543	52	-14 +13/-21	-30 +13/-8
56.9	45 +22/-21	37 +13/-13	55 +11/-18	24 +7/-7	-3900	7385	51	4 +11/-18	-27 +7/-7
57.5	107 +25/-24	70 +11/-13	116 +12/-26	44 +10/-8	-3900	7097	49	67 +12/-26	-5 +10/-8
58.0	189 +26/-33	111 +16/-16	196 +29/-56	73 +27/-19	-3900	7239	50	146 +29/-56	23 +27/-19
58.5	179 +26/-34	106 +16/-16	185 +31/-56	64 +27/-18	-3800	5111	35	150 +31/-56	29 +27/-18
58.9	227 +23/-61	142 +12/-43	208 +41/-67	70 +34/-22	-3700	6450	44	164 +41/-67	26 +34/-22
59.3	224 +26/-39	129 +18/-22	226 +50/-72	74 +40/-20	-3700	5690	39	187 +50/-72	35 +40/-20
Min	6 +12/-6	6 +18/-6	32 +26/--9	22 +13/-8	-3700	4320	30	187 +50/-72	35 +40/-20
Max	227 +23/-61	142 +12/-43	226 +50/-72	74 +40-20	-4000	9049	62	-14 +13/-21	-30 +13/-8

pole error ellipse to be the best estimate of plate-boundary-normal convergence for a given stage, as it is the best constrained location given the available magnetic anomaly data [*Cande and Stock*, in review]. We then estimated cumulative convergence using the pints at the center of each ellipse, and its range (+/-) considering the four additional locations (triangles in Figure 3.6) (Table 3, columns 2-5). For example, at the latitude 51.7ºS, the best estimate of the amount of cumulative predicted convergence since anomaly 5o is 25 km using the AUS-PAC poles, but considering the error associated with the positions of the finite and stage poles, that number could be as high as 38 km and as low as 11 km (Table 3, column 2, row 1).

3.8.2 Analysis: Influence of variable convergence angles on observed faults

To understand the structural development of the entire MRC south of New Zealand over time, we compare the type of mapped plate boundary faults for each segment [*Melhuish et al*., 1999; *Moore et al*., 2000; *Lamarche and Lebrun*, 2000; *Lebrun et al*., 2000; *Massell et al*., 2000; *Meckel et al*., in review] to the angles of convergence and boundary-normal-convergence along the lengths of the boundary that correspond to the AUS-PAC and MAC-PAC stage rotations since anomaly 5o (Figure 3.5). We seek to understand the conditions that led to partitioned thrusting and strike slip motion versus those that led to only strike-slip faulting.

The diffuse northern boundary of the Macquarie plate lies at ~52°S, suggesting that different stage poles apply to different segments of the MRC. North of this boundary, we use AUS-PAC stage rotations, whereas to the south, we employ MAC-PAC stage rotations (Figure 3.5). For this reason, we have

created composite convergence angle curves by combining the AUS-PAC and MAC-PAC convergence curves and subsequently derived the associated plots of perpendicular convergence (Figure 3.5 C and G). The northern boundary of the Macquarie plate is difficult to identify precisely. Hence we selected positions on the profiles where the predictions of convergence angles and boundary-normal shortening from the two sets of stage poles allowed for a smooth transition between the AUS-PAC and MAC-PAC curves (Figure 3.5C). These composite curves use MAC-PAC stage rotations south of 51°S for the stage 5o to 3Ay, and AUS-PAC stage poles to the north. For younger stages, we used ~50°S for the transition.

Regardless of what stage poles are considered, convergence did not begin simultaneously along the MRC. For the 5o to 3Ay (10.9 to 5.9 Ma) stage rotation, the Puysegur Ridge, McDougall, and Macquarie segments were divergent, while the boundary to the north and south was convergent (Figure 3.5 A-C; exception of northern Puysegur noted above). Due to the orientations of the plate boundary in the Puysegur and Hjort segments, convergence began earlier than in the intervening segments of the MRC. The entire MRC south of New Zealand, however, has been convergent since chron 3Ay (5.9 Ma) (Figure 3.5C). The strike-slip fault in the crest of the MRC is continuous for the length of the MRC. The strike-slip fault probably originated during the transition from divergence to convergence (convergence angle of ~0º). Thus, we propose continuous strike-slip movement along the length of the MRC since 5.9 Ma, and it probably initiated earlier along much of the boundary.

All predictions include increased angles of convergence from stage 5o-3Ay to 3Ay-2Ay, and decreased angles from stage 3Ay-2Ay to 2Ay-0 (Figure 3.5 A-C). Except for MAC-PAC predictions of boundary-normal-convergence in the central MRC, all combinations of stage rotations result in similar cumulative amounts of convergence (Figure 3.5 E-G). Predictions of the various stage pole scenarios differ in the timing of boundary-normal-convergence. For example, MAC-PAC stage rotations suggest significant boundary normal convergence in the southern Hjort segment during the stage 5o to 3Ay, decreasing after that (Figure 3.5E), whereas the AUS-PAC stage rotations predict a more even distribution of boundary-normal convergence over time (Figure 3.5F). The opposite is true for the Puysegur Trench.

From 10.9 to 0 Ma, angles of convergence have been higher in the southern Hjort region and Puysegur Trench than for intervening segments of the MRC (Figure 3.5C). Thrust faults along the MRC [*Lamarche and Lebrun*, 2000; *Lebrun et al*., 2000; *Massell et al*., 2000; *Meckel et al*., in review] occur where angles of convergence have been significantly greater than 20° since 10.9 Ma (Figure 3.5C-D). These locations have experienced = 200 km of cumulative predicted boundary-normal-convergence. The southern Hjort Trench between 57.5°S and 59.5°S (Figure 3.5D) contains active thrust faults, where two reliable thrust mechanisms have been identified [*Meckel et al*., in review]. The Puysegur region has a well-defined Wadati-Benioff zone dipping at 80º to depths of 150 km between 47ºS and 49ºS [*Lebrun et al*., 2000]. *Collot et al*. [1995] identified minor thrust faults in the southern part of the Puysegur Ridge that evolve into the

established subduction zone of the northern Puysegur Trench. These minor thrust faults occur where convergence angles are increasing to the maximum values.

Strike-slip faults dominate the plate boundary where convergence angles are <25º, and boundary normal convergence is < 100 km. In these locations substantial convergence has only occurred since 5.9 Ma, or about half as long as for the trench segments at the southern and northern ends of the plate boundary.

3.9 CONVERGENCE AND DEFORMATION OF CRUST

We hypothesize that the anomalously shallow and deep regions of the seafloor at the plate boundary zone (ridges and troughs) represent deformation resulting from plate boundary-normal convergence that has occurred at each segment over the last 5.9 Ma. In this section we quantitatively compare the amount of deformation that is recorded in the topography within 70 km to either side of the MRC to the amount of perpendicular convergence.

We have made the basic assumptions that topography at the plate boundary that may have existed prior to convergence was minimal (100's of m) and that the equilibrium depth of the seafloor along the Hjort, Macquarie, and McDougall segments of the MRC was generally similar prior to convergence. It is recognized that the equilibrium depth of crust of different ages varies as a function of its age [*Stein and Stein*, 1992], and that some amount of topography may have existed at the spreading centers along the MRC when spreading ceased [*Mammerickx and Sandwell*, 1986] (see section 3.7). Equilibrium depths were determined from regional bathymetric profiles across the plate boundary, but the depths used have not currently been compared with modeled equilibrium depths.

It is likely that topography at extinct spreading ridges and crustal ages have influenced the observed morphology at the MRC, and this topic is being investigated.

Additionally, it is recognized that mass-wasting processes may contribute to morphology of the MRC [*Massell et al*., 2000] by transferring material down the flanks of the ridge. The volume of any slumped material is incorporated in our analysis of morphology, and treated as if it were part of the constructional history of the MRC, as it represents material that has been displaced from the average local seafloor depth.

3.9.1 Methods

We are interested in volumetric crustal displacement above and below the average seafloor depth along the boundary. Where bathymetry is well constrained by shipboard swath bathymetry, we extracted swaths oriented perpendicular to the plate boundary from the bathymetry data. Swaths have dimensions 50 km by 140 km, centered on points on the plate boundary with ~50 km spacing (two representative swaths are shown in Figures 3.2 and 3.7; Figure 3.4 shows representative swath widths). Swath area was chosen to span the variability in local topography both parallel and perpendicular to the plate boundary zone. Considered together, the swaths cover nearly all of the anomalous topography along the strike of the MRC south of 51°S.

For each of the swaths, the volume of crustal material above and below the average seafloor depth (horizontal datum) was determined using GIS software (ArcMap: 3D-Analyst surface analysis extension; see Appendix A). The average

seafloor depth was determined from local bathymetric profiles across the plate boundary (Figures 3.4 & 3.7). Although the age of seafloor adjacent to the MRC varies consistently within the study area (Figure 3.1), much of the seafloor adjacent to the MRC has an average depth around 4000 m (Figure 3.4). To the south, as the younger material near the SEIR is approached, the average depth shallows to 3000 m (Figure 3.4). The volume estimates take advantage of the highest resolution of the bathymetry grid (0.001° grid spacing) and allow the complexity of the surface to be fully incorporated to arrive at precise estimates of displaced volumes. In cases where sediment exists in the Hjort Trench, estimates of sediment thickness were determined from multi-channel seismic reflection profiles (Figure 3.2) by converting two-way travel times to depth using a velocity of 1500 m/s, and volumes of sediment were determined for each swath within the mapped extents of the sediments [Meckel et al., in review]. Sediment volumes within swaths ranged from 2 to 15 km3, equivalent to <10% of the total displaced volume for a given swath. Because we are interested in the amount of downward deflection of the oceanic crust adjacent to the plate boundary zone, the sediment volumes were added to the volume of material displaced below the average seafloor depth (Figure 3.7).

Modeling of the gravity profiles across the plate boundary indicates that the gravity signature can be explained using isostatic considerations (see Chapter 2). However, comparisons of shiptrack bathymetry and the predicted bathymetry of *Smith and Sandwell* [1997] differ by as much as 800 m in the Macquarie segment of the MRC. Such inconsistencies can be attributed to the lack of

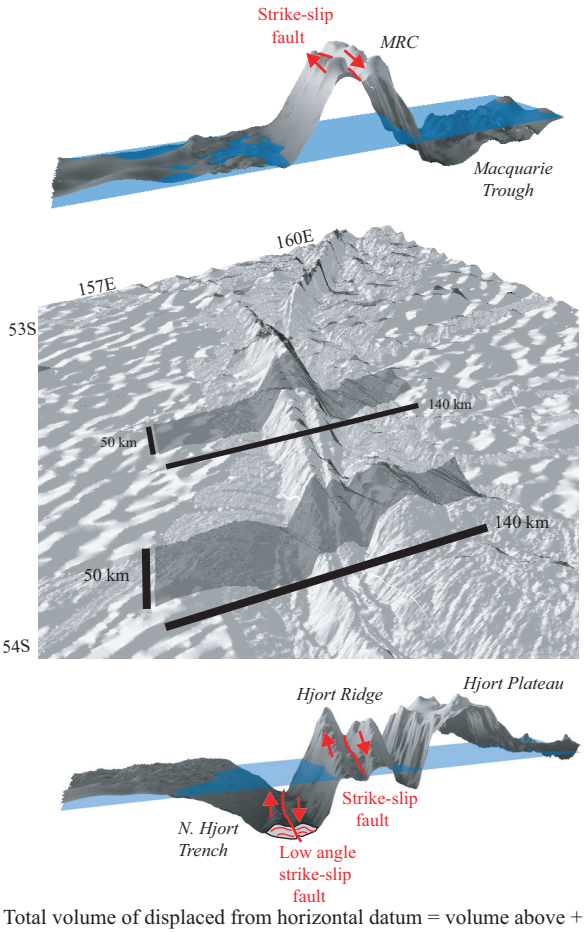

Figure 3.7. Method for calculating volumes of crust deformed during convergence adjacent to the plate boundary zone. Center: Bathymetry map with two representative swaths for Macquarie and Northern Hjort segments (see Figure 3.2 for locations). Swaths are oriented perpendicular to the plate boundary orientation and are 100 km by 280 km in dimension. Top: Perspective view of bathymetry swath from Macquarie segment of MRC. Bottom: Perspective view of bathymetry swath from northern Hjort segment. Horizontal datum is average seafloor elevation taken from 2D bathymetric profiles through the centres of swaths, and is -4000 m for both swaths shown. Strike slip fault runs in the valley at the crest of the MRC and interpreted low angle strike slip fault occurs in the northern Trench. Total volumes of displaced crust is the sum of the volume above and below the horizontal datum, including the volume of sediment in the trench. See Appendix A for details of calculation methodology.

calibration of the predicted bathymetry model with ship soundings given the remote location of the MRC and the assumption of a simple isostatic model for deriving predicted bathymetry from gravity data. The discrepancy in the bathymetry values suggests that the bathymetry of the MRC may not be in isostatic equilibrium. Thus, we suggest that dynamic forces related to convergence may influence the topography of the MRC. Although we have not constrained any of these forces for the Hjort region, numerical modeling of deformation at young convergent margins is most successful if dynamic forces are incorporated [*Toth and Gurnis*, 1998]. To differentiate between isostatic and dynamic components of MRC morphology, dynamic modeling needs to be considered, but is beyond the scope of this investigation.

We assume that some component of flexure of the crust forming the bathymetric depressions is a result of horizontal loading (shortening) during convergence, and that sediment accumulated in the Trench once the bathymetric depression was established. Sediment volumes in the Trench are not thought to constitute enough of a vertical load to contribute significantly to the observed amount of flexure. This assumption is supported by the observation that seamounts east of the Trench that are over 3 km tall do not result in flexure at the km-scale. Sediment volumes are far smaller than the volume of the seamounts; therefore, it is reasonable to assume their effect is minimal. More detailed modeling of the flexure of the oceanic lithosphere in the Hjort region and the influence of the sedimentary load on flexure in the Trench would require

estimates of the elastic properties of the crust in the Trench, and are beyond the scope of this investigation. This topic may be pursued in the future.

The sum of the volumes above and below the local datum depth represents the total volume in km^3 of oceanic crust that has been displaced from the local seafloor elevation during deformation adjacent to the plate boundary (Figure 3.7). These volumes vary with latitude (Figure 3.8; Table 3, column 7).

We attempted similar volumetric analysis north of 51ºS using predicted bathymetry from *Sandwell and Smith* [1997]. However, comparison of predicted bathymetry with measurements from shiptracks indicated that resolution of the predicted bathymetry was insufficient to obtain reasonable estimates of volumes displaced from the average seafloor depth. The average difference between predicted and measured bathymetry for a swath area is hundreds of meters, and these inconsistencies led to calculations of volumes that were an order of magnitude higher than volumes calculated using swath bathymetry.

3.9.2 Analysis - Relationship between convergence and crustal deformation

To investigate potential relationships between convergence history and deformation for oceanic crust at the MRC, we compare the cumulative amount of plate-boundary-normal convergence determined from stage rotations to calculations of anomalous volumes of crust (anomalous bathymetry) relative to average seafloor depths adjacent to the plate boundary. The anomalous volumes of crust along the plate boundary show a direct relationship to the amount of boundary-normal convergence for cumulative stage rotations since 3Ay (5.9 Ma)

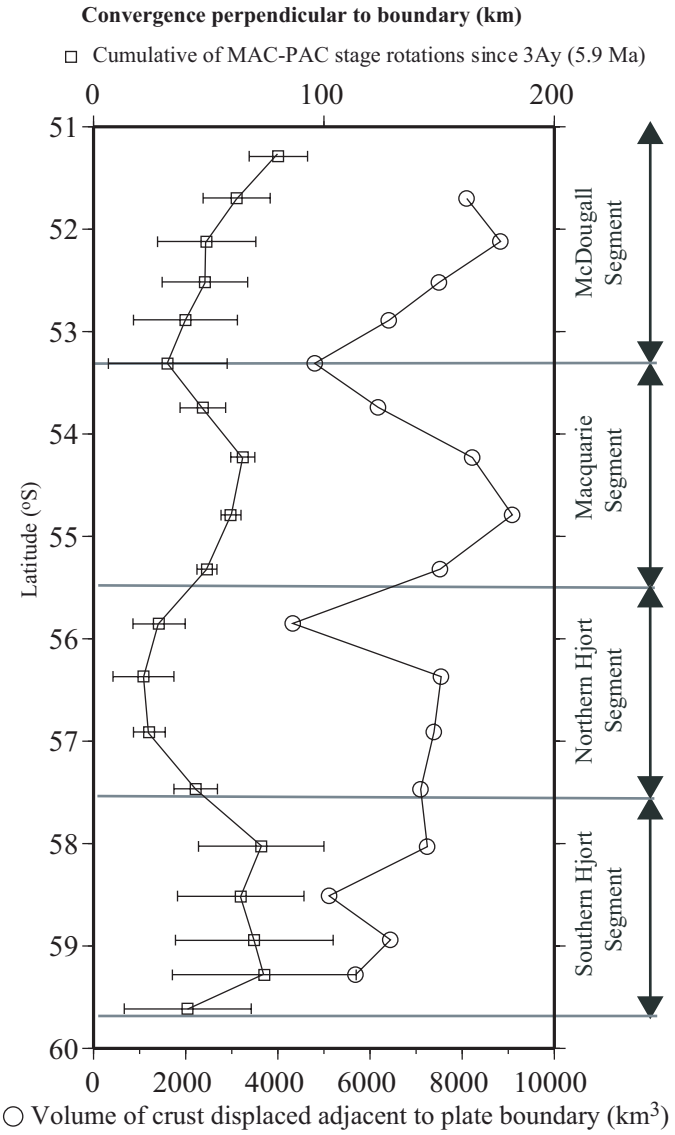

Figure 3.8. Comparison of cumulative plate boundary-normal convergence for each of the black boxes in Figure 3.2 using the AUS-PAC and MAC-PAC stage poles since anomaly 3Ay (5.9 Ma) (upper scale) with volume of crust displaced from average seafloor depth (lower scale). North of 56°S (N. Hjort, Macquarie and McDougall segments), displaced volumes correlate quite well with amounts of plate boundary-normal convergence. Displaced volumes south of 57.5°S correlate qualitatively with plate boundary-normal convergence predicted from finite rotations, but appear anomalously low.

(Figure 3.8). A similar relationship exists for cumulative stage rotations since 5o (10.9 Ma) (Figure 3.9) for most of the boundary, but decays in the Hjort region.

As discussed previously, the youngest age of spreading-related basalts on Macquarie Island indicates that the crust along the MRC north and south of the Island could be < 6 Ma. Thus, the anomalous bathymetry of the MRC should be dominantly the result of convergence post 6 Ma, as is suggested by the strong correlation between volumes of deformed crust and the cumulative boundary-normal convergence since 5.9 Ma (Figure 3.8). Furthermore, uplift data from Macquarie Island suggests that all the uplift occurred within the last ~6 m.y. Only the older crust (in Hjort Trench, on the west side of the Macquarie segment, and possibly part of Hjort Plateau) could have been affected by earlier convergence (i.e. 10.9 to 5.9 Ma; Chron 5o to 3Ay). Although earlier convergence occurred along the southern MRC (Figure 3.5), that crust was translated laterally along the boundary as much as 300 km since 10.9 Ma. Therefore, present day crust at those locations does not record the earlier convergence calculated for those same locations. Hence, it is not valid to ascribe anomalous bathymetry observed today at one of those locations to the earlier convergence. This discrepancy may explain the poorer correlation between volumes of deformed crust and cumulative boundary-normal convergence since 10.9 Ma in the Hjort region (Figure 3.9). For the reasons outlined above, the rest of our analyses use the cumulative perpendicular convergence from 5.9 to 0 Ma (3Ay to 0) for comparison with volumes of deformed crust.

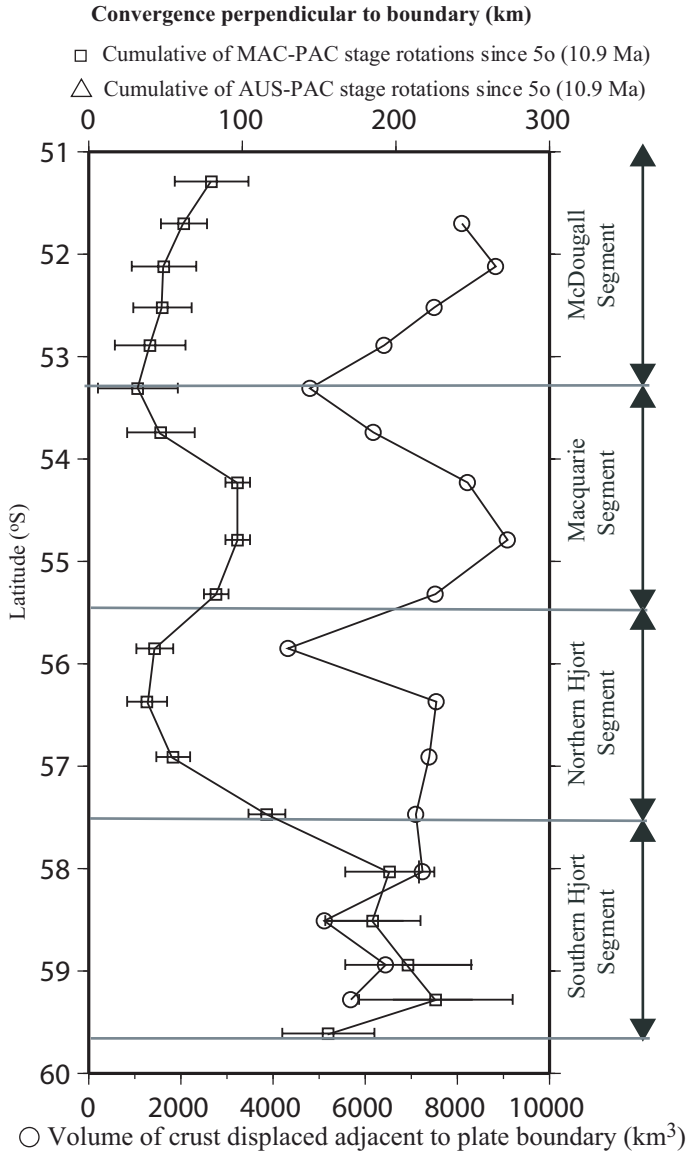

Figure 3.9. Same as Figure 3.8, but cumulative convergence is from anomaly 5o (10.9 Ma) to the present. Note scale change at top of plot. Additional convergence from 5o to 3Ay is only south of 54ºS. A similar correlation exists, but additional convergence in the southern Hjort Trench causes the inconsistency between convergence and volume to appear more drastic. For reasons given in the text, it is more appropriate to compare the convergence history and displaced volumes since anomaly 3Ay (Figure 3.8).

The relationship between the cumulative boundary normal convergence predicted by stage rotations and the volume of deformed crust is best seen between 51°S and 56°S (McDougall and Macquarie segments) (Figures 3.8 and 3.9). Considering only these segments (for which no underthrusting has been identified), a linear relationship can be established between the volume of crust displaced from the average seafloor depth and the cumulative amount of plate boundary-normal convergence predicted by the AUS-PAC stage rotations since 5.9 Ma (Figure 3.10). For our analysis of the Macquarie and McDougall segments, each kilometer of plate boundary-normal convergence (shortening) is associated with 146 km^3 of crustal displacement considering the MAC-PAC stage rotations (Figure 3.10A). The slope of this curve is dependent on the area of the swath chosen for determining volumetric displacements. However, swath areas remained constant for our analysis, and thus our analysis has been normalized to a constant swath area. Using this linear relationship for these two segments, observed volumetric displacements along the entire MRC can be used to predict convergence amounts perpendicular to the plate boundary (Figure 3.11).

No relationship can be confidently derived for the AUS-PAC stage rotations (Figure 3.10B). This indicates that the AUS-PAC stage poles do not accurately describe the amount of convergence suggested by the topography of the McDougall segment, whereas the MAC-PAC poles do. This supports the validity of the existence of the Macquarie Plate and position of the MAC-PAC pole of rotation proposed by *Cande and Stock* [in review]. Thus, we proceed with

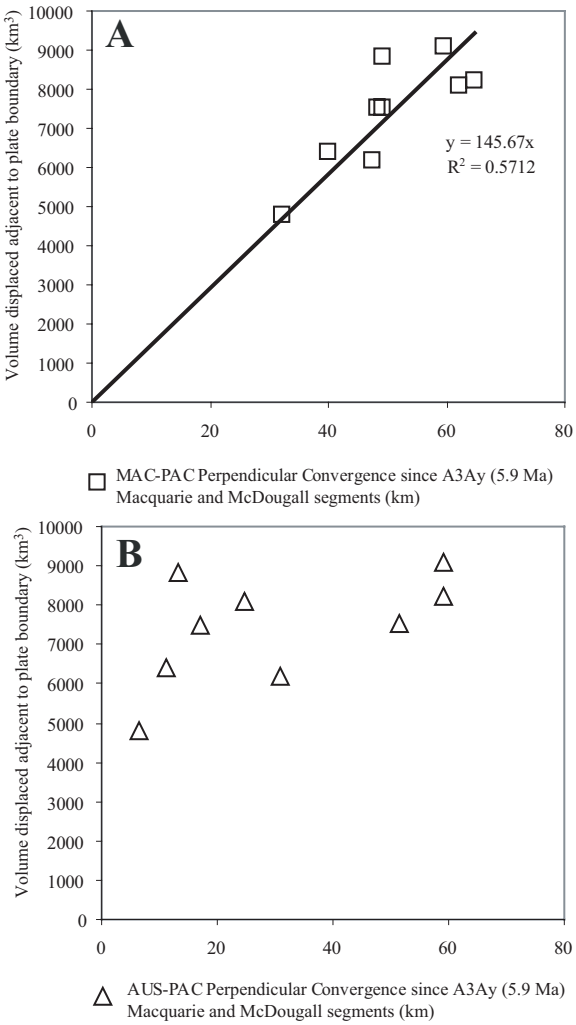

Figure 3.10. Plots of cumulative plate boundary-normal convergence for Macquarie and McDougall segments from stage rotations since anomaly 3Ay (5.9 Ma) vs. displaced crust adjacent to plate boundary. A: Boxes indicate relationship using the MAC-PAC stage rotations. A linear relationship can be established (best-fit lines forced through 0), providing a slope for converting displaced volumes adjacent to the plate boundary zone to amounts of inferred boundary-normal convergence (Figure 3.11). B: Triangle symbols indicate relationship using the AUS-PAC stage rotations. No linear relationship is evident, suggesting that the AUS-PAC poles do not predict an amount of convergence that is internally consistent with observed topography.

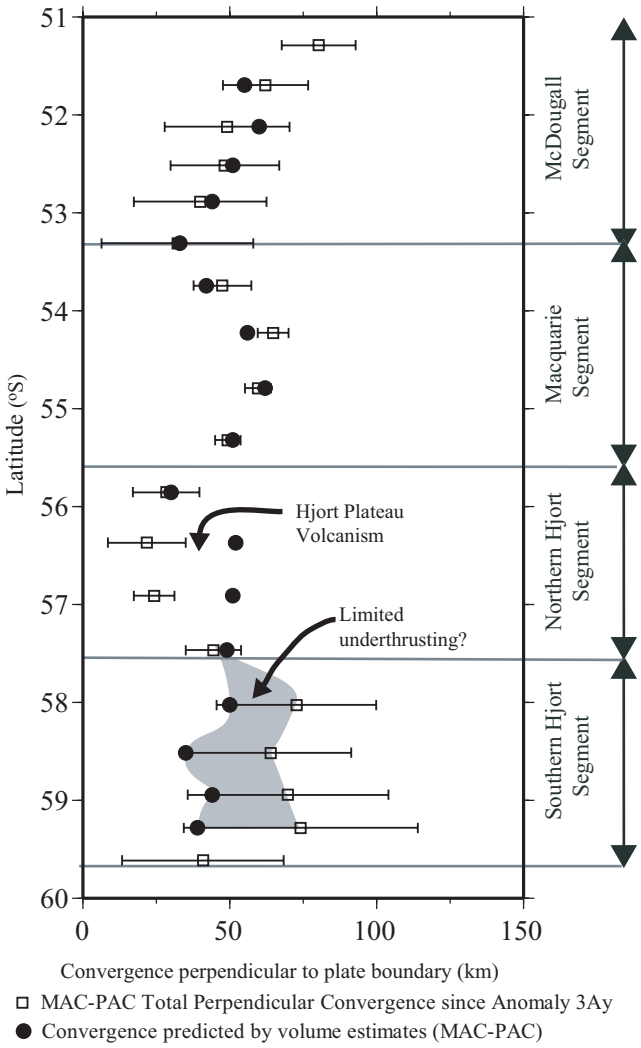

Figure 3.11. Comparison of calculated plate boundary-normal convergence from the linear relationships in Figure 3.10A with boundary-normal convergence estimates from cumulative stage rotations since 5.9 Ma. North of 56°S, linear shortening predicted from displaced volumes is internally consistent with the shortening predicted by the MAC-PAC stage rotations. South of 57°S, linear shortening derived from displaced crustal volumes is notably lower than the estimates from the AUS-MAC stage rotations (shaded region labelled 'limited underthrusting?'). The separation of the points at 56.4ºS and 56.9ºS is likely a result of volcanism in the Hjort Plateau that is not associated with deformation at the boundary.

the determination of underthrust crust in the Trench considering only the MAC-PAC rotation.

North of 56°S, the amounts of shortening predicted by the MAC-PAC finite rotation are internally consistent with the estimates of shortening derived from the observed volumetric displacements (Figure 3.11). The linear relationship between displaced volumes and convergence amounts decays to the south (Figure 3.11), where underthrusting is interpreted in the Trench [*Weissel et al*., 1977; *Ruff and Cazenave,* 1985; *Jones and McCue*, 1988; *Meckel et al*., in review]. Between ~56°S and ~57.5°S, the convergence predicted by volume estimates is greater than that determined from stage rotations. This area includes the Hjort Plateau, and some of the greater volume may result from volcanism. In contrast, the predicted amount of cumulative convergence from MAC-PAC stage rotations since anomaly 3Ay south of ~57.5°S is greater than in the north (Figures 3.8 and 3.9), but the corresponding volume of topography displaced is generally similar to the north. This suggests that, although most convergence in the Trench region is accounted for in the observed crustal deformation adjacent to the plate boundary, minor underthrusting of the Australian crust beneath the Pacific crust may have accommodated the remaining amount of convergence (identified as limited underthrusting in Figure 3.11). Given the error associated with the estimates of convergence from stage poles, it is possible (but less likely) that no underthrusting has occurred since 5.9 Ma.

Using the linear relationship in Figure 3.10A, displaced volumes adjacent to the Hjort Trench (south of 55.3ºS) correspond to plate boundary-normal

convergence of between 35 and 50 km (Table 3, column 8). These are the amounts of convergence that are consistent with the observed crustal displacements (deformation) in the Hjort region considering the linear relationship established for the McDougall and Macquarie segments (Figure 3.10A). South of 57.5ºS, these amounts are up to 35 km less than the amounts predicted by the MAC-PAC cumulative stage rotations. This difference represents the amount of shortening perpendicular to the boundary that is not explained by crustal displacement in the Hjort region. The length of these differences is inferred to have been underthrust at the Trench. South of 57.5ºS these lengths vary from 23 (+27/-19) to 35 (+40/-20) km (Table 3, column 10). We consider the difference to be notable, but recognize that, within the error of the analysis, the convergence at the trench since 5.9 Ma may be generally accounted for by the observed topography and may not require underthrusting. For the area between -56.4°S and -57.5°S, negative values in columns 9 and 10 of Table 3 imply that the calculated volumetric displacement of crust converted into convergence is more than is predicted by cumulative stage rotations using the MAC-PAC pole of rotation, as mentioned previously.

Meckel et al. [in review] proposed up to 50 km of underthrusting based on gravity modeling. We suggest above that 23-35 km may have been underthrust since 5.9 Ma. Thus, some underthrusting may be attributed to convergence older than 5.9 Ma. Since 5.9 Ma, limited underthrusting has occurred, and any previously underthrust slab was translated northward.

The Hjort Plateau may result from convergence and deformation in a restraining bend of the plate boundary east of the Hjort Trench (Figure 3.2), but the volcanoes indicate that some relief results from magmatism. In addition, the uplift of the Plateau may be a response to the limited eastward underthrusting of Australian crust beneath Pacific crust that is inferred at this latitude.

3.10 DISCUSSION

Variable angles of convergence and the corresponding amounts of cumulative plate boundary-normal convergence over the last 10.9 Ma control the morphology and fault development for the different segments of the MRC. Our analyses show that strike-slip faults dominate in regions of the MRC where the convergence angles are <25° and cumulative boundary-normal convergence is <100 km, whereas thrust faults dominate where convergence angles are significantly >20° and cumulative boundary-normal convergence as much as 200 km. Additionally, thrusting occurs in regions where convergence occurred between 10.9 and 5.9 Ma. Our results also show a strong relationship between the amounts of crust displaced above and/or below average seafloor level and cumulative boundary-normal convergence since 5.9 Ma. Below we consider the implications of variable amounts of convergence for each of the segments of the MRC south of New Zealand. We then address the differences that are observed between the Puysegur and Hjort subduction zones given their similar convergence history. Finally, we discuss the global implications of our results relating convergence angles to deformation and fault development. The tectonic history

of the MRC is compared to obliquely convergent continental systems. We conclude by considering the implications our results have for subduction initiation in intraoceanic settings.

3.10.1 Implications for individual segments of the MRC

Puysegur Trench segment: Convergence has occurred at the Puysegur Trench segment since at least 10.9 Ma (Figure 3.5C). Between 46ºS and 48ºS approximately 200 km of plate boundary-normal convergence is predicted during this time from stage rotations. North of 47ºS, subduction in the northern part of the trench accommodates most of the plate convergence [*Lamarche and Lebrun*, 2000]. Seismicity in the Puysegur Trench indicate a slab length of ~150 km [*Lebrun et al*., 2000], suggesting that at least 75% of the boundary-normal component of convergence has been accommodated by subduction in the Trench. Such a large percentage suggests that a thrust fault was established early in the convergence history of the Trench, and that only ~50 km of convergence may have been accommodated in deformation at the plate boundary zone prior to the establishment of the thrust fault. The southward transition from underthrusting in the northern Puysegur Trench to the partitioned thrust and strike-slip faulting in the southern part of the Trench is associated with decreased angles of convergence from ~40º to 25º. These angular changes correspond to a decrease in the amount of boundary-normal convergence from slightly greater than 200 km for the central and northern Trench to less than 150 km for the southern Trench (Figure 3.5G). The northern transition from subduction in the Trench to strike-slip deformation at the Alpine Fault occurs at a sharp change in the plate

boundary orientation at ~46ºS. This change in orientation results in a sharp decrease in the predicted convergence angles and a corresponding decrease in the boundary-normal convergence component (Figure 3.5 C and G). The southernmost Alpine fault is characterized by convergence angles less that 20º and approximately half of the amount of plate boundary convergence that is predicted for the Puysegur Trench.

Puysegur Ridge segment: Due to the orientation of the Puysegur Ridge compared to the Puysegur Trench, the Ridge segment has experienced less convergence normal to the boundary orientation than the Trench to the north. The composite convergence curve (Figure 3.5C) indicates that the Puysegur Ridge was divergent from 10.9 to 5.9 Ma. The Puysegur Ridge segment has experienced convergence angles of ~20º for the last 5.9 Ma, resulting in <100 km of cumulative boundary-normal convergence during that time. The relatively small angles of convergence compared to the Puysegur Trench resulted in deformation of oceanic crust at the plate boundary zone into the uplifted ridge feature, and the development of strike-slip faulting in the crest of the ridge. We conclude that convergence angles for the Puysegur Ridge segment have been too low and convergence has been occurring for too short a time period for thrust faulting to develop. This is demonstrated by the lack of observed underthrusting south of 49ºS [*Lamarche and Lebrun*, 2000].

McDougall and Macquarie segments: The evolution of the McDougall and Macquarie segments has been similar to the Puysegur Ridge segment. The strike-slip dominated McDougall and Macquarie segments are the result of

relatively low angles of convergence. Plate boundary-normal convergence has been accommodated through the deformation of oceanic crust into the Ridge feature, but convergence angles have not been high enough for thrust faults to develop.

Considering the angles of convergence from the composite curves during stages 3Ay to 2Ay and 2Ay to 0 (Figure 3.5C), a significant observation is that bathymetric troughs (>5000 m BSL) occur east of the McDougall and Macquarie segments, where convergence angles were only slightly greater than 20° (Figure 3.5C). These troughs occur where the convergence angles were greater than 20° since stage 3Ay-2Ay, but have since experienced a decreased angle of convergence. Even though the convergence angle has generally been decreasing toward the present, the regions where troughs occur have experienced convergence angles slightly greater than 20° for longer periods than sections of the Macquarie and McDougall segments just north or south of the troughs (Figure 3.5C). Such analysis suggests that those troughs began forming ~6 Ma, but did not develop to as mature a state as the Hjort or Puysegur Trenches because angles of convergence were so oblique that strike-slip faulting dominated over thrust faulting. However, no insight is gained as to why the crust on the east side of the MRC subsided rather than the west. More detailed identification of the age relationships across the MRC for these regions might clarify reasons for such observations. Perhaps of most significant is the orientation of pre-existing fracture zones [*Massell et al*., 2000] with respect to the relative convergence direction. Fracture zone orientations east of the MRC may be more favorably

oriented with respect to the convergence direction to accommodate vertical displacement than orientations of the west side of the MRC. This seems most likely for the Macquarie segment, where no fracture zones exist within 100 km west of the MRC, whereas multiple curved fracture zones occur to the east [*Massell et al*., 2000].

Northern Hjort segment: Despite the presence of a bathymetric trench similar to the southern Hjort Trench, the northern Hjort segment has experienced lower angles of convergence than the southern Hjort Trench (Figure 3.5C). The difference between the northern and southern Hjort segments is primarily a result of the difference in orientation between the two segments. The northern Trench has some of the lowest cumulative convergence amounts perpendicular to the boundary (Figure 3.5G). Thus, the deepening of the northern Hjort Trench cannot be attributed to plate boundary-normal convergence. The formation of the northern Trench is the result of crust underthrust in the southern Hjort Trench being translated to the north. The westernmost fault in the northern Hjort Trench has been interpreted as a low angle oblique-slip fault [*Meckel et al*., in review]. Crust that has been underthrust in the southern Trench is translated to the NNE, and the change in orientation of the plate boundary causes the thrust fault to evolve into a low angle strike-slip fault, eventually terminating at ~55.5ºS. No thrust earthquakes have been identified in the northern Hjort Trench [*Meckel et al*., in review], supporting the interpretation that the thrust in the southern Trench evolves into a strike-slip fault north of 57.5ºS. Northward translation of

underthrust crust has caused the bathymetric trench to extend to the north over time as limited underthrusting proceeds in the southern Trench.

Southern Hjort segment: Plate boundary-normal convergence at the southern Hjort Trench has consistently decreased since 10.9 Ma (Figure 3.5G). Over half of the total cumulative convergence occurred between 10.9 and 5.9 Ma. The decreasing amounts of convergence toward the present suggest that the Hjort Trench may not develop into a mature subduction zone if angles continue to decrease.

Where underthrusting has been interpreted, volumetric topography generated at the plate boundary is inconsistent with the linear relationship established (Figure 3.11); it is anomalously low considering the amount of cumulative convergence that stage rotations predict. This suggests that some convergence in the Hjort region since 5.9 Ma has been accommodated by underthrusting rather than the topographic construction that is observed along the Macquarie and McDougall segments of the plate boundary. The difference between the amount of convergence that is consistent with the observed topography adjacent to the southern Hjort Trench and the amount of convergence predicted by cumulative stage rotations since 5.9 Ma suggests that underthrusting at a decollement in the Trench has accommodated a maximum of 35 (+40/-20) km of boundary-normal convergence and the rest of the convergences was likely accommodated by flexure of the crust. Thus, we use morphologic arguments to derive amounts of underthrusting normal to the plate boundary that are ~50% less than cumulative stage rotations predict for the Hjort Trench since 5.9 Ma.

Hjort Plateau: Our analysis indicates that the broad uplift of topography of the Hjort Plateau is dominantly a result of convergence at the plate boundary. Swaths used for the volumetric analysis traversed the topography of the Hjort Plateau, and volumes of deformation include the uplift of the Plateau above the average seafloor depth. When the volumes calculated for the northern Trench region are converted to amounts of convergence perpendicular to the plate boundary using the relationship in Figure 3.10A, the amounts are larger than the estimates of cumulative convergence from stage rotations (Figure 3.11). The additional volume captured in the topographic analysis is considered to be a result of volcanism on the northern Hjort Plateau (Figure 3.11). It is unclear why deformation in the central and northern Hjort Trench is distributed over a wider distance than the more northern segments of the MRC, but it may relate to the restraining bend geometry of the plate boundary east of the northern Trench.

3.10.2 Regional implications

Differences in the Puysegur and Hjort Trenches: Convergence angles at the Puysegur and southern Hjort Trenches have exceeded 20º for at least 10.9 Ma (Figure 3.5C), and the result has been the formation of thrust faults. The amount of boundary-normal convergence that has occurred during this time for both these trenches is ~200 km (Figure 3.5G). Although the amount of boundary-normal convergence is similar for the two areas, the Puysegur Trench has a better-defined (geophysically) subduction zone than the Hjort Trench. The Puysegur Trench has a Wadati-Benioff zone extending to 150 km depth [*Lebrun et al.*, 2000], whereas the Hjort region does not and the deepest earthquake identified is

at 64 km [*Meckel et al*., in review]. The Hjort region is more isolated from established seismograph networks than the Puysegur region, which may result in many undetected earthquakes in the Hjort region. However, given the amount of underthrust crust is only ~35 km since 5.9 Ma, based on our morphologic arguments, the discrepancy in seismicity between the Hjort and Puysegur Trenches is not surprising. Furthermore, gravity modelling in the Hjort region did not define more than ~50 km of underthrust crust in the Hjort region [*Meckel et al*., in review].

One difference between the Puysegur and Hjort Trenches that may explain the different amount of subduction is the involvement of continental crust in convergence at the Puysegur Trench [*Lebrun et al*., 2000]. Convergence at the northern Puysegur Trench occurs between oceanic and continental crust, whereas in the Hjort Trench convergence is between oceanic crust. Where oceanic crust converges against continental crust, the establishment of subduction may occur earlier than for oceanic-oceanic interactions because of the rheological differences, allowing more subduction to occur (i.e. nearly all convergence would be accommodated by continued underthrusting). For interactions involving only oceanic crust, convergence may involve more complex deformation and faulting processes, as the rheology of the interacting crust is broadly similar, causing subduction initiation to be postponed. In these cases lateral translation of crust at the plate boundary on strike slip faults may efficiently translate crust involved in convergence to the north, limiting the amount of crust that can be potentially subducted.

3.10.3 Global Implications

Transpression at oceanic vs. continental settings: Broadly speaking, comparisons of the structural response of the MRC with continental boundaries of similar length such as the San Andreas and Alpine Fault systems reveal general similarities. *Teyssier et al*. [1995] demonstrated a quantitative relationship between the angle of convergence and structural development at transpressional continental plate boundaries. These two plate boundaries represent end member cases of strike-slip partitioned systems. The San Andreas system represents an extremely oblique convergent setting with a high degree of partitioning of convergence into boundary-parallel strike-slip faulting. *Argus and Gordon* [2001] document topography in the Coast Ranges adjacent to the San Andreas system that is generated at extremely oblique convergent boundaries. Convergence angles are less than 20° on the San Andreas Fault system, resulting in dominantly wrench tectonics and strike-slip faulting. Deformation related to more orthogonal convergence at the Alpine system of the South Island of New Zealand is not as strongly strike-slip partitioned [*Tessier et al*., 1995]. For the Alpine Fault system, angles of convergence are generally greater than 20° and are associated with pure-shear-dominated tectonics and active thrust faulting and crustal thickening.

The observations of changes in angle of convergence at the MRC over the last 10.9 Ma are largely consistent with the results of *Tessier et al*. [1995]. The observed distribution of strike-slip faulting on the Macquarie and McDougall segments [*Massell et al*., 2000, *Frohlich et al*., 2000] corresponds to areas where convergence angles have generally been less than ~25º. Regions of thrust faulting

in the southern Hjort and Puysegur Trenches [*Lebrun et al*., 2000; *Meckel et al*., in review] (Figure 3.5D) correspond to angles of convergence that have been greater than 20º for at least 10.9 Ma, and thrust focal mechanisms are observed [*Moore et al*., 2000; *Meckel et al*., in review]. Low convergence angles result in a high degree of partitioning of convergence into boundary-parallel strike-slip faulting. Higher convergence angles are associated with a decrease in the amount of convergence accommodated on strike-slip faults and a greater degree of accommodation on thrust faults. The similarities between the structural responses in obliquely convergent settings involving oceanic crust and those involving continental crust suggest that convergence angles result in a generally similar initial tectonic response in the two crustal types.

Subduction initiation: The initiation of subduction involves the combined effects of plate convergence angles, convergence rates, crustal heterogeneity and time. Our observations of the MRC suggests that convergence angles >20º for ~10.9 Ma resulted in established underthrusting in a convergent setting involving oceanic crust. The variable angles and rates of convergence that have occurred at the MRC over the last ~10.9 Ma imply that a discrete amount of boundary-normal convergence must have occurred prior to initiation. The Macquarie and McDougall segments have experienced as much as 50 km of convergence without any underthrusting (Figure 3.11). Thus, for the MRC, the amount of plate boundary-normal convergence required for subduction initiation appears to be greater than 50 km, but less than 200 km.

Various locations on the MRC can be used to infer the incremental stages leading to established thrust faulting and subduction initiation. The morphology and structures of the Macquarie and McDougall segments reflect a less advanced response to convergence, having experienced smaller convergence angles than the Hjort or Puysegur Trenches over shorter periods of time. Convergence angles have reached but not significantly exceeded 20º for at least 5.9 Ma (Figure 3.5C). The morphologic result is a 4000 m high ridge and ~6000 m BSL bathymetric troughs. Strike-slip faulting occurs in the crest of the ridge feature, but thrust faulting has not developed. This can be attributed to decreases in the convergence angle since 5.9 Ma (Figure 3.5C). The development of significant troughs adjacent to the Macquarie and McDougall segments suggests that these segments attained conditions very close to those favourable for thrust fault development, but did not develop underthrusting.

The Clipperton Fracture Zone (CFZ) west of southern Mexico illustrates the morphology and structural development associated with extremely young convergence of oceanic crust, perhaps representing the earliest stages of the evolution of the MRC. The CFZ has experienced extremely oblique convergence (5º) over a fairly short time period (0.4-0.5 Ma) [*Polkalny*, 1997], resulting in the formation of a 600-700 m high ridge, and minor downward flexure of the lithosphere near the transform fault. Faulting related to this convergence is observed as obliquely oriented normal and strike-slip faults. The topography and structural development of the CFZ can be considered to be an initial response to oblique convergence. Further increases in convergence angle would likely result

in the formation of a ridge feature similar to the Macquarie or McDougall segment.

3.11 CONCLUSIONS

Deformation at the MRC accounts for a considerable amount of plate convergence. Based on our observations of the Macquarie segment since 5.9 Ma, up to 50 km of boundary-normal convergence seems to be accommodated entirely in volumetric displacement within ~70 km to either side of the plate boundary when convergence is less than 20º. Convergence angles <~20º are associated with relatively large volumes of displaced crust and a dominance of strike-slip faulting at the plate boundary.

Thrust fault extents on the MRC occur where convergence has been >20º since 10.9 Ma. Regions where convergence angles approach 20º but are not significantly greater correspond to significant bathymetric troughs. The troughs adjacent to the Macquarie and McDougall segments represent failed attempts to develop thrust faults due to more recent decreases in convergence angles. This suggests that the MRC can be used to constrain conditions for which underthrusting will be established at obliquely convergent intraoceanic settings. Incipient subduction should occur when convergence angles exceed 20º for ~10 Ma, or for any combination of convergence angles, rates, and durations resulting in between 50 and 200 km of boundary-normal convergence.

Simple finite rotations do not adequately predict the amount of underthrusting at the Hjort Trench. Finite rotations (and cumulative stage rotations) assume that all the translation that is predicted actually occurs. These

rotations do not account for deformation at the plate boundary zone and the development of topography. Our analysis incorporating morphologic information along the MRC indicates that the amount of underthrusting at the southern Hjort Trench since 5.9 Ma is a maximum of 35 km. Calculated amounts of underthrusting incorporating deformation at the boundary are 50% less than predicted by cumulative stage rotations.

Development of the Macquarie Plate is consistent with the analysis done here. Comparisons of plate boundary-normal convergence and volumetric displacement are most consistent if rotations between Macquarie and the Pacific plates are considered rather than if the Australian-Pacific rotations are used.

Chapter 4: Evolution of the Macquarie Triple Junction since the Oligocene and Implications for Tectonics of the Southern Macquarie Ridge Complex

4.1 INTRODUCTION

The Macquarie Triple Junction (MTJ) exists at the intersection of the Australian, Pacific, and Antarctic plates south of New Zealand (Figure 4.1). *Falconer* [1972] determined the current position of the MTJ to be 61.5ºS and 161ºE, where the easternmost segment of the Southeast Indian Ridge (SEIR) terminates (Figure 4.1). Previous studies have constrained the Australian-Pacific-Antarctic plate configuration south of New Zealand during the inception of the MTJ at Anomaly 21 (47.91 Ma) [*Marks and Stock*, 1997] and for the most recent history of the triple junction since Anomaly 3A (5.9 Ma) [*Lodolo and Coren*, 1994 & 1997]. Very little research has been devoted to the behavior of the MTJ in the intervening 40 Myr. The ~1200 km-long offset of SEIR spreading segments across the Tasman and Balleny fracture zones (Figure 4.1) suggests significant southward migration of the MTJ with respect to the Australian plate since approximately anomaly 13o (33.3 Ma). Models of MTJ evolution presented here are used to document the complex crustal interactions that occurred at the southern Australian-Pacific plate boundary during this time, and to constrain the tectonic evolution of the Hjort Trench (Figure 4.1).

This chapter presents reconstructions illustrating the configuration of the MTJ and vector diagrams of relative plate motion at 7 times from 33.3 Ma to the present (A13o, A8o, A6o, A5o, A3Ay, A2Ay, and 0). For a given reconstruction,

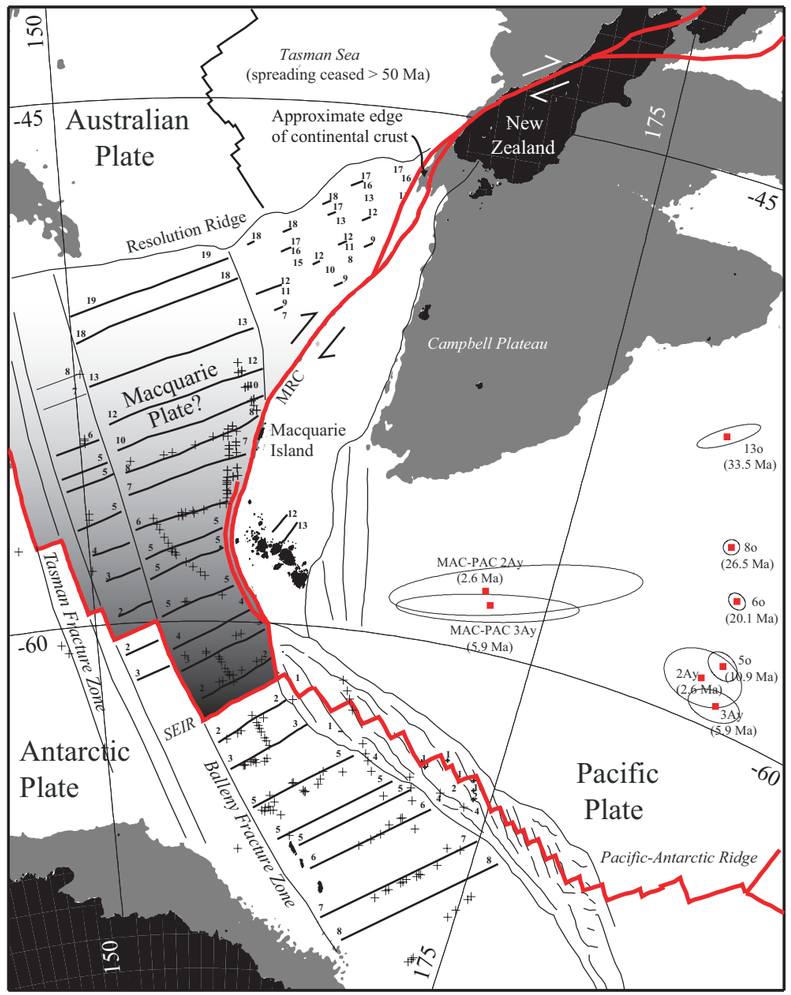

Figure 4.1. Geographic setting of the Australian-Pacific plate boundary, Macquarie Ridge Complex (MRC), and Macquarie Triple Junction (MTJ) south of New Zealand. Solid gray shading represents regions shallower than 2000 m. Euler pole locations (red squares) and error ellipses for the rotation of Australian Plate with respect to the Pacific Plate (AUS-PAC) are from Cande and Stock [in review]. The two westernmost pole locations are for rotation of the Macquarie Plate with respect to the Pacific Plate (MAC-PAC). The hypothesized Macquarie Plate (transitional shading) extends east of ~145°E and south of 52°S, bound to the east by the MRC and to the south by the SEIR [Cande and Stock, in review]. The offset of Southeast Indian Ridge (SEIR) spreading segments across the George V, Tasman, and Ballaney Fracture Zones suggests the Macquarie Triple Junction (MTJ) migrated ~1200 km southward with respect to the Australian plate. Interpreted schematic magnetic isochrons are numbered from Weissel et al. [1977], Wood et al. [1996], Cande et al., 2000, and the PLATES database [Lawver et al., 2001].

plate boundary orientations are interpreted using repositioned locations of previously interpreted magnetic anomalies and fracture zones. For comparison, both un-interpreted and interpreted reconstructions are presented for each time. However, the density of magnetic anomaly data is often insufficient to precisely locate the triple junction or constrain plate boundary orientations in the area immediately surrounding the triple junction. Vector diagrams of relative plate motion are constructed for each time in order to help constrain the position of the triple junction in reconstructions. Beginning with the present location of the triple junction, the previous location of the triple junction is inferred using relative motion information from the vector diagram. The relocated position of that point in the reconstruction for the previous stage represents the triple junction location for the previous stage. The interpreted plate boundary orientations together with the relative plate motion illustrated in the vector diagrams is then used to characterize the tectonic processes occurring at the three plate boundaries at each time and to deduce the migration history of the MTJ.

Significant conclusions from this analysis include (i) the MTJ migrated ~1100 km with respect to the Australian plate since 33.3 Ma resulting in the formation of a transform plate boundary between the Australian and Pacific Plates; (ii) Migration of the MTJ between 26.6 Ma and 5.9 Ma caused the length of the easternmost SEIR spreading ridge (east of the Balleny Fracture Zone; Figure 4.1) to decrease in length by 300 km. Decreases in the ridge length appear to partially accommodate convergence; (iii) No seafloor spreading occurred on the Hjort segment of the Australian-Pacific plate boundary south of the present

day latitude of 56ºS; the Hjort boundary has been a transform fault throughout its history; & (iv) Since 10.9 Ma, the Hjort segment of the Australian-Pacific transform evolved into the obliquely convergent incipient subduction zone of the Hjort Trench, where it is estimated that 220 km of convergence has occurred based on the reconstructions.

4.2 METHODS

4.2.1 Reconstructions

Tectonic reconstructions of the Australian-Pacific-Antarctic three-plate system are presented for the times 33.3, 26.6, 20.1, 10.9, 5.9, 2.6, and 0 Ma (all times derived from magnetic anomalies are from *Cande and Kent*, 1995). The Pacific plate has arbitrarily been held fixed in a present-day coordinate system throughout the reconstructions. These reconstructions relocate interpreted magnetic anomaly positions and fracture zone locations using the PLATES reconstruction software. Stage pole locations and rotation amounts for relative motion between the Australian, Pacific, and Antarctic plates were calculated from the finite rotation poles presented in *Cande and Stock* [in review] (Figure 4.1).

For comparison with the interpreted reconstructions presented here, the un-interpreted hardcopy output from the PLATES program for each reconstruction can be found in Appendix A.

For the reconstructions presented, two complications arise when considering the relative motion of the three plates. *Cande and Stock* [in review] have proposed the existence of the Macquarie plate for times younger than 5.9 Ma, which is thought to exist south of ~52ºS and east of 145ºE (Figure 4.1).

Therefore, reconstructions for times older than 5.9 Ma incorporate stage poles for the Australian-Pacific system. Reconstructions younger than 5.9 Ma use stage poles for the Macquarie-Pacific system (Figure 4.1). The second complication involves the treatment of the motion of Antarctica with respect to the Australian and Pacific plates. East and West Antarctica are thought to have had a component of divergence at the Adare Trough prior to anomaly 10o (28.5 Ma) [*Marks and Stock*, 1997; *Cande et al*., 2000]. This results in different finite poles of rotation (and therefore stage poles) for East and West Antarctica relative to the Australian and Pacific plates prior to 28.5 Ma. For constraining instantaneous relative motion at the triple junction, stage rotations for the Pacific and Australian plates with respect to West Antarctica are used for stages prior to anomaly 10o (28.5 Ma) (affecting only the 33.3 Ma reconstruction). For times younger than 28.5 Ma, East and West Antarctica behaved as one coherent plate and stage rotations of the Australian and Pacific plates relative to East Antarctica (which is fixed to West Antarctica for times younger than anomaly 10o; *Cande et al*., 2000) are used.

4.2.2 Determining instantaneous relative motion and estimates of error

For each reconstruction, directions and rates of instantaneous relative motion of the Australian, Pacific, and Antarctic plates at the mapped position of the MTJ were determined using stage rotation poles. The instantaneous vectors determined are tangent to the small circle around the rotation pole that passes through the triple junction. The vectors are used to characterize relative motion for the three plates in the vicinity of the triple junction for an entire stage.

Without additional stage poles, this is the simplest assumption that can be made for relative motion during a stage.

The vectors describing relative motion of the Australian, Pacific, and Antarctic plates at 33.3 Ma are the least constrained for all the reconstructions. The oldest pole of rotation between the Australian and Pacific plates presented by *Cande and Stock* [in review] is for anomaly 13o (33.3 Ma). It is not possible to define a stage pole for the stage preceding A13o (33.3 Ma) with their data. *Sutherland* [1995] provides an Australian-Pacific stage pole for the period 35-30 Ma, which is used to constrain the relative motion between these two plates for 33.3 Ma. For stages younger than A13o, the instantaneous relative motion between the Australian, Pacific, and Antarctic plates can be determined using stage pole positions derived from finite pole positions presented by *Cande and Stock* [in review].

Cande and Stock [in review] only provide error ellipses for the Australian-Pacific and Macquarie-Pacific finite poles (Figure 4.1), so estimates of error in instantaneous rates and direction associated with the variability in the positions of the stage poles are only assessed between those plates. Methods used for estimating the variability in the location of the Australian-Pacific stage poles are presented in Chapter 3. With regard to the instantaneous direction and rate of relative motion of the Australian-Pacific (Macquarie-Pacific for times < 5.9 Ma) plates at the mapped locations of the MTJ, the variability is reported in Figures 4.3 through 4.8. Generally, angles of instantaneous relative motion vary by less than 10º for the triple junction location, but can be up to 26º for the large errors

associated with the Macquarie-Pacific finite poles younger than anomaly 5o (10.9 Ma) (Figure 4.1). Errors associated with the rates of Australian-Pacific (Macquarie-Pacific < 5.9 Ma) relative plate motion are typically less than 1 cm/yr, but again vary by as much as 2.3 cm/yr for times younger than 5.9 Ma. Errors associated with the reported values for the instantaneous motion of the Australia-Antarctica and Antarctica-Pacific systems are considered to be broadly similar to values calculated for the Australian-Pacific system, but are undetermined.

4.2.3 Construction of vector diagrams

A point on a vector diagram represents an individual plate. The scales of a vector diagram are units of relative motion, and are cm/yr for the diagrams constructed here. The diagrams represent a map view of relative motion of the plates. The relative positioning of the points representing the individual plates indicates the direction of relative motion with respect to each other. The distance between the points represents the rate at which the plates are moving relative to each other.

For a three-plate system involving a triple junction, the triple junction is located by the intersection of various lines related to the type of plate boundary that exists between each plate (see *McKenzie and Morgan* [1969]). For the purposes of this analysis, lines related to transform fault, spreading ridge, and subduction boundaries apply. For two points (plates) that are spreading apart, a triple junction is located on the perpendicular bisector of the points. The perpendicular bisector represents the spreading ridge between two plates. For a

transform fault plate boundary, a triple junction is located on the line connecting the two points. The line connecting the two plates represents the transform fault between the two plates. For two points in an extremely convergent state, the triple junction is located on the line that is oriented parallel to the convergent boundary, passing through the overthrust plate (assuming underthrusting occurs). This line represents the convergent boundary between the two plates. Since a stable triple junction represents a point that is common to all plates involved, it exists at the intersection of the lines representing the different plate boundaries.

4.2.4 Determination of previous triple junction locations

The rates and directions of triple junction migration with respect to the individual plates can be inferred from a vector diagram. Knowing the amount of time between reconstructions, various distances can be determined on the reconstructions. Calculations of distance using the vector diagrams assume that rates and directions indicated in the diagram remained constant during the time period between reconstructions. Beginning with the present day location of the triple junction, the vector between the Australian point and the triple junction was used to determine the direction and distance from the triple junction location on the reconstruction to a point from which it appears that the triple junction migrated. This point was then rotated with the Australian plate to identify that location in the next older reconstruction. In the older reconstruction, the location of the rotated point was used as the position of the triple junction at that time. Thus, for a given reconstruction, the position of the triple junction was inferred using information from the vector diagram for next younger reconstruction, which

is taken to represent constant conditions of relative motion using the stage rotation pole. This position in the older reconstruction must be consistent with the available magnetic anomaly and fracture zone data.

As an example, the following procedure uses the present location of the triple junction (bold circle in Figure 4.8A), which is well constrained from regional gravity and predicted bathymetry maps, and the vector diagram for the present (Figure 4.8A) to determine the location of the triple junction at anomaly 2Ay (2.6 Ma) (bold circle in Figure 4.7B). Considering the vector diagram for the present (Figure 4.8A), the vector between the triple junction (open circle in Figure 4.8A) and the Australian point (blue diamond in Figure 4.8A) was determined to have an orientation of 335º (155º+180º). The length of the vector is 3.2 cm/yr, as determined from the scale on the vector diagram. If that rate is assumed to be constant since the last reconstruction (2.6 Ma), the triple junction has traveled ~85 km with respect to the Australian plate. A point is then determined on the present day reconstruction that is 85 km from the present day location of the triple junction location in the 335º direction (light gray circle in Figure 4.8B). This point was then rotated with the Australian plate into the reconstruction for 2.6 Ma (Figure 4.7B), where its position corresponds to the bold circle (Figure 4.7B), which is taken to be the location of the triple junction at that time. This procedure was then replicated for 2.6 to 5.9 Ma to find the location of the triple junction at 5.9 Ma, and continued backward in time until 33.3 Ma.

Although previous triple junction locations were determined starting with the present and working into the past, the reconstructions are presented beginning

at the oldest reconstruction. Once the active triple junction is located for a reconstruction, the plate boundary orientations are interpreted based on the location of the triple junction and the available magnetic anomaly and fracture zone data. The lack of interpreted magnetic anomaly locations adjacent to the Australian-Pacific plate boundary makes it difficult to confidently locate that plate boundary in many of the reconstructions.

4.2.5 Simulated magnetic anomaly locations

Due to convergence along the southern MRC, magnetic anomaly trends on the Australian crust west of the Hjort region are shorter than the analogous anomaly trends on the Antarctic plate (Figure 4.1) [*Weissel et al*., 1977; *Cande and Stock*, in review]. In order to investigate the interaction of the Australian and Pacific crust on the southern MRC at the times of the reconstructions, magnetic anomaly locations from the Antarctic side of the SEIR were artificially duplicated in the reconstructions when they formed at the SEIR and the duplicate set was attached to and rotated with the Australian plate. The anomalies chosen were those picked by S. Cande (personal communication), which are considered better locations than those from other sources. For a given reconstruction, the duplicate set of points was rotated as if it was part of the Australian plate. The assumption made is that crust equivalent to the south side of the SEIR was present north of the SEIR. This requires that spreading was essentially symmetric on the SEIR. *Lodolo et al*. [1996] used magnetic anomaly data to assess spreading rates on the SEIR east of the Balleny Fracture Zone. Their comparison of half spreading rates to the north and south of the SEIR indicate generally symmetric spreading for the

last 35 Ma. By attaching a duplicate set of Antarctic magnetic anomalies to the Australian plate, the convergence at the southern MRC at various times in the past can be better constrained than if only the magnetic anomalies on the Australian plate are used.

RESULTS

Anomaly 13o (33.3 Ma): The estimated triple junction location on the reconstruction for 33.3 Ma is 60ºS and 160.2ºE (bold black circle, Figure 4.2B), which agrees well with the rotated magnetic anomaly and fracture zone positions (Figure 4.2C). While the position of the triple junction is relatively well defined, the relative motion at this time is not. The instantaneous rates of relative motion were only calculated for the Australian-Pacific system for this time. Using the *Sutherland* [1995] pole for Australian-Pacific relative plate motion for the stage 35-30 Ma, the Pacific plate moved in a 120º direction at 3.4 cm/yr with respect to the Australian plate (Figure 4.2A). Repositioned magnetic anomaly data at 33.3 Ma indicate that spreading on the MRC and SEIR are approximately parallel at this time (Figure 4.2C), suggesting that the Australian-Antarctic plate motion was also directed generally in a 120º direction at this time. The amount of crust formed by the SEIR is generally greater than that of the MRC (Figure 4.2C), so spreading rates can be inferred to have been larger for the SEIR than for the MRC leading up to 33.3 Ma.

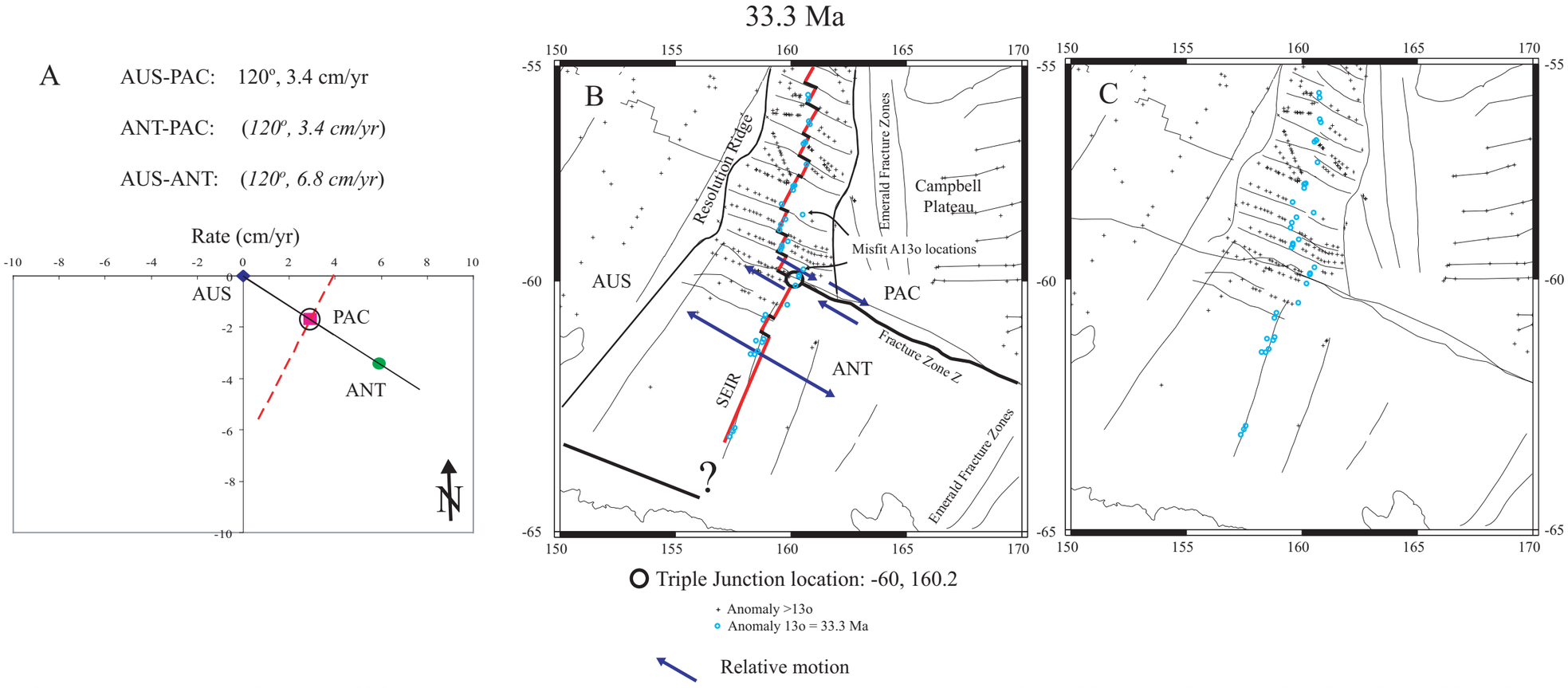

Figure 4.2. Reconstruction of the MTJ region at 33.3 Ma. A) Vector diagram of relative plate motion at the interpreted location of the MTJ. A stable Ridge-transform Fault-Fault (RFF) configuration for the triple junction is interpreted. Data used to generate the vector diagram are above the diagram, and were determined using stage poles calculated from the finite rotation poles of Cande and Stock [in review]. AUS refers to Australian plate; ANT to the Antarctic plate; PAC to the Pacific plate. Solid black lines represent transform plate boundaries; dashed red line indicate SEIR. Open circle indicates location of the triple junction in vector space. Only the AUS-PAC vector was constrained using a stage pole rotation; other vectors are estimated from fracture zone orientations and estimated of accreted crust from the map in B. B) Interpreted reconstruction of the geometry of the MTJ region. Symbols are indicated in the legend. Blue anomalies indicated as misfit locations suggest the 13o finite rotation pole is slightly mis-positioned and does not perfectly rotate the Australian plate with respect to the Pacific plate for 33.3 Ma. Bold red lines denote spreading ridges. Bold black lines denote fracture zones. The Emerald Fracture zones are offset in a sinistral sense across Fracture Zone Z. Bold black circle represents interpreted triple junction location. Relative motion between adjacent plates from the vector diagram in A indicated with blue arrows. Spreading north of the triple junction at this time is described as the Southeast Indian Ridge Extension (SIRE) by Kamp [1986] and Marks and Stock [1997], and separates the Resolution Ridge and Campbell Plateau. The 13o pole position of Cande and Stock [in review] (Figure 4.1) does not completely close spreading on the SIRE (indicated by misfit locations). C) Un-interpreted reconstruction of magnetic anomaly and interpreted regional structural lineaments.

Using directions of relative motion indicated by fracture zone orientation from the reconstruction (Figure 4.2C) and the direction and rate for the Australian-Pacific system from the *Sutherland* [1995] stage pole (Figure 4.2A), a permissible (but poorly constrained) vector diagram at 33.3 Ma indicates a stable Ridge-transform Fault-transform Fault (RFF) triple junction configuration (Figure 4.2A). The vector diagram suggests that the triple junction has migrated generally in a 120º direction.

Anomaly 8o (26.6 Ma): The interpreted triple junction location is 60.3ºS and 159.75ºE (bold black circle, Figure 4.3B). Relative motion vectors for all three plates at the triple junction were determined using stage rotations for the reconstructions younger than 33.3 Ma. For the stage from 33.3 Ma to 26.6 Ma, the Pacific plate was moving in a 132º (+9º, -10º) direction at a rate of 5.0 (+0.9, -0.8) cm/yr relative to the Australian plate. Relative to the Pacific plate, the Antarctic plate was moving in a 121º direction at 2.8 cm/yr. The Antarctic plate moved in a 149º direction with respect to the Australian plate at a rate of 7.1 cm/yr.

A vector diagram for anomaly 8o (26.6 Ma) (Figure 4.3A) indicates that one of the estimates of relative plate motion is slightly in error in order for the triple junction to be perfectly stable. An Australian-Pacific divergence rate approximately 1 cm/yr lower would lead to a stable configuration. Alternatively, an increase of 2 cm/yr in the Australia-Antarctic divergence would also satisfy stability. The error associated with the direction and rate of Australian-Pacific relative motion (Figure 4.3A) allows the position of the Pacific point to be

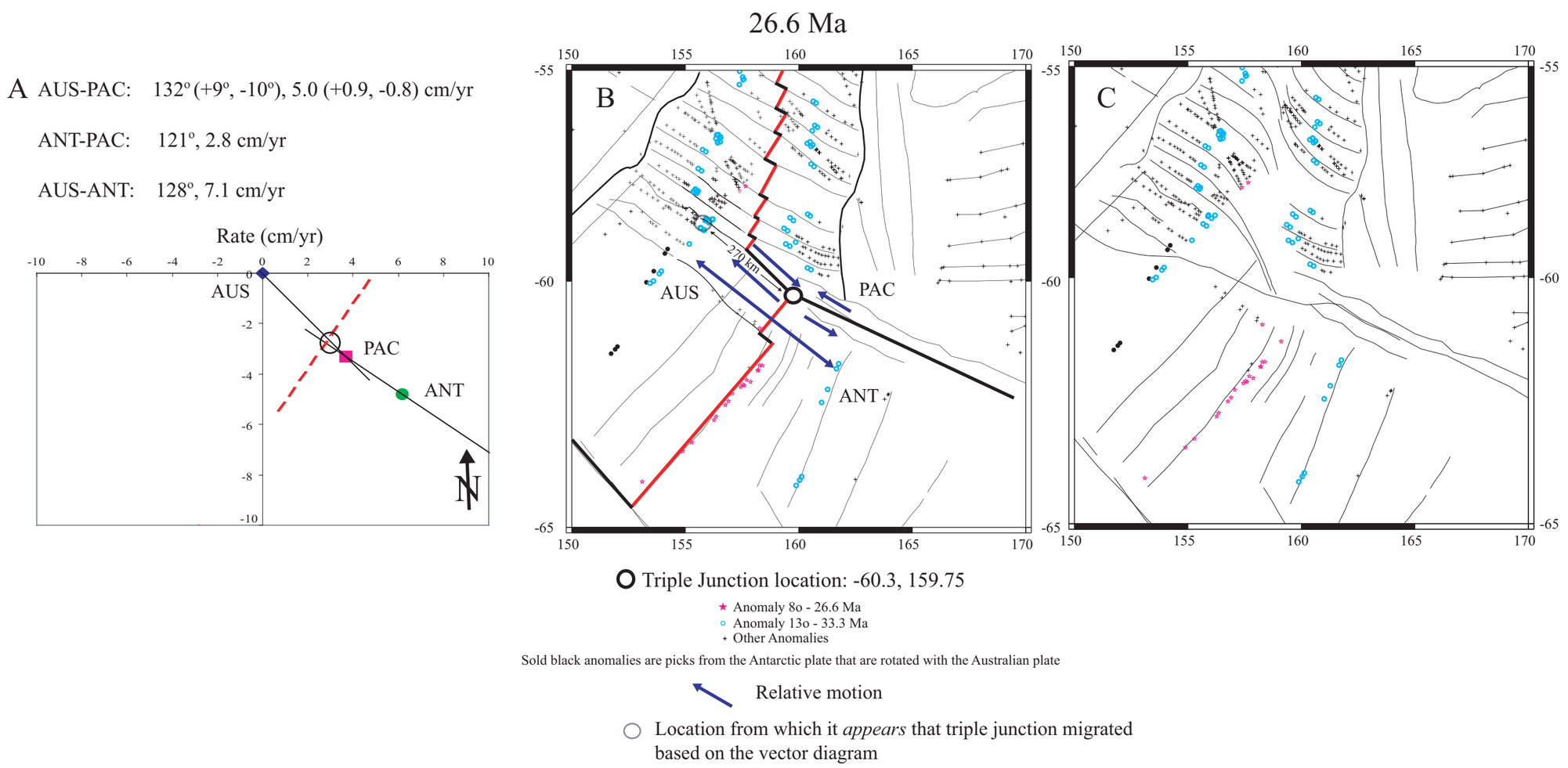

Figure 4.3. Reconstruction of the MTJ region at 26.6 Ma. A) Data, points and lines as in Figure 4.2A. Relative motion for all pairs of plates determined from stage rotation poles from Cande and Stock [in review]. A stable RFF configuration for the triple junction is interpreted. B) Pink stars indicate magnetic anomaly position with ages of 26.6 Ma, and others as indicated in key (below). C) Un-interpreted reconstruction of magnetic anomaly and interpreted regional structural lineaments.

consistent with a stable configuration, and the preferred location for the position of the Pacific point and triple junction location is indicated by the open circle (Figure 4.3A). The triple junction is characterized by a RFF configuration at this time.

Anomaly 6o (20.1 Ma): The interpreted triple junction location is 60.6ºS and 160.3ºE (bold black circle, Figure 4.4B). Relative to the Australian plate, the Pacific plate was moving in a 150º (+8º, -4º) direction at a rate of 3.4 (+0.9, -0.6) cm/yr. Relative to the Pacific plate, the Antarctic plate was moving in a 113º direction at 3.1 cm/yr. The Antarctic plate moved in the 132º direction with respect to the Australian plate at a rate of 6.0 cm/yr. From 26.6 to 20.1 Ma, the triple junction is characterized by a RFF geometry (Figure 4.4A).

Anomaly 5o (10.9 Ma): The interpreted triple junction location is 60.8ºS and 161.1ºE (bold black circle, Figure 4.5B). Rates of relative motion for all three plates are similar to the rates at 20.1 Ma. Relative to the Australian plate, the Pacific plate was moving in the 162º (+4º, -19º) direction at a rate of 3.3 (+0.2, -0.4) cm/yr. Relative to the Pacific plate, the Antarctic plate was moving in the 108º direction at 3.2 cm/yr. The Antarctic plate moved in the 135º direction with respect to the Australian plate at a rate of 5.8 cm/yr.

The complexity of the tectonics at this stage exposes the limitations of vector diagrams for characterizing transpressional boundaries. The configuration of the triple junction is theoretically stable with a RFF geometry (Figure 4.5A). However, the orientation of a transform between the Australian and Pacific points on the vector diagram is unreasonable given the geologic constraints on the map

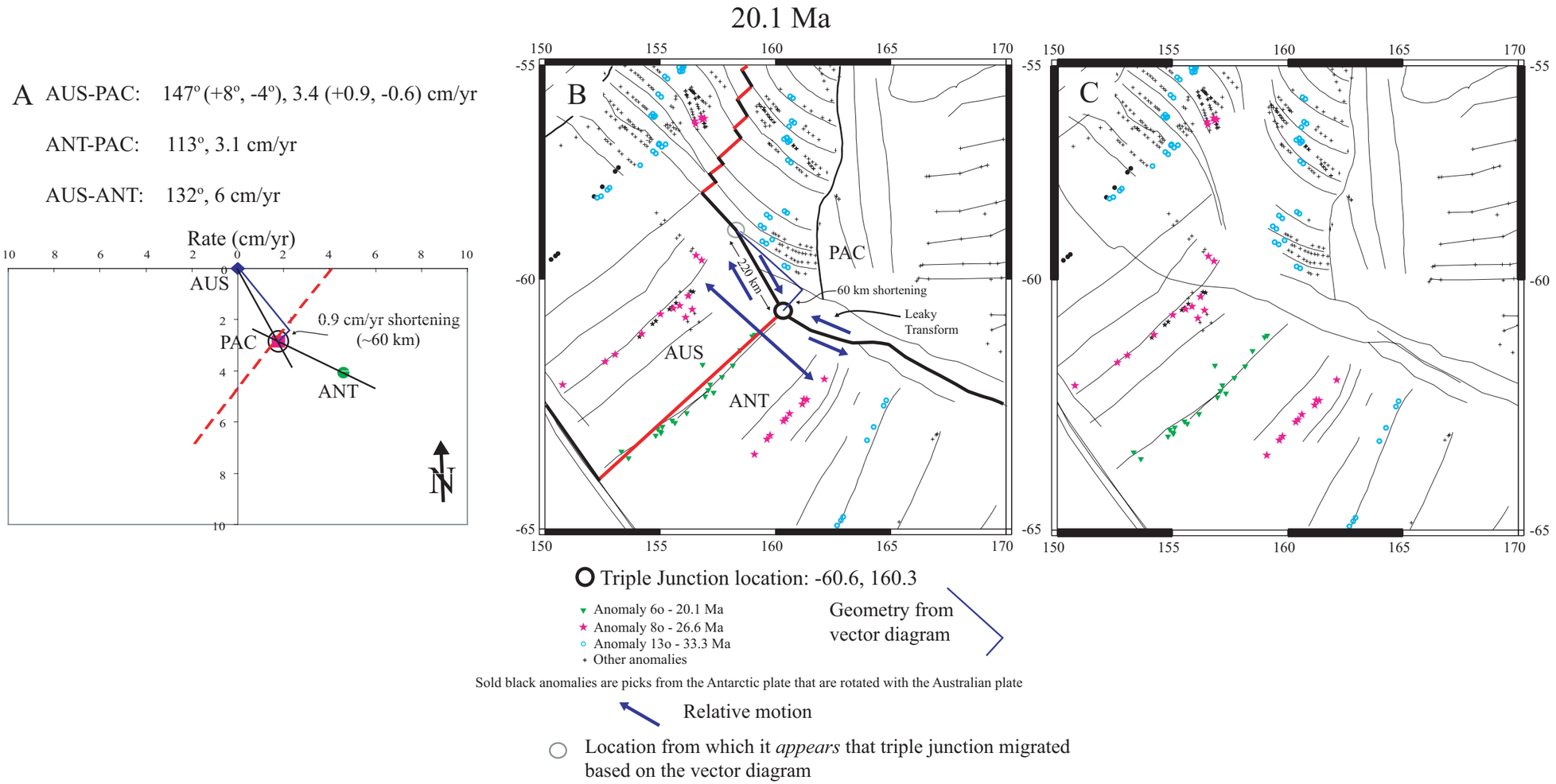

Figure 4.4. Reconstruction of the MTJ region at 20.1 Ma. A) Data, points, and lines as in Figure 4.3A. A stable RFF configuration for the triple junction is interpreted. Position of triple junction indicates that the SEIR shortened at 0.9 cm/yr, or ~60 km (indicated). B) Pink triangles indicate magnetic anomaly position with ages of 20.1 Ma, and other symbols as indicated in key (below). Blue lines are oriented and scaled based on the vector diagram in A. Vector diagram indicates the SEIR spreading ridge shortened by 60 km (indicated), and that the transform Australian-Pacific plate boundary lengthened by 220 km (indicated). Antarctic-Pacific boundary may be a leaky transform, as suggested by the separation of the lineaments used to define the boundary (see text). C) Un-interpreted reconstruction of magnetic anomaly and interpreted regional structural lineaments.

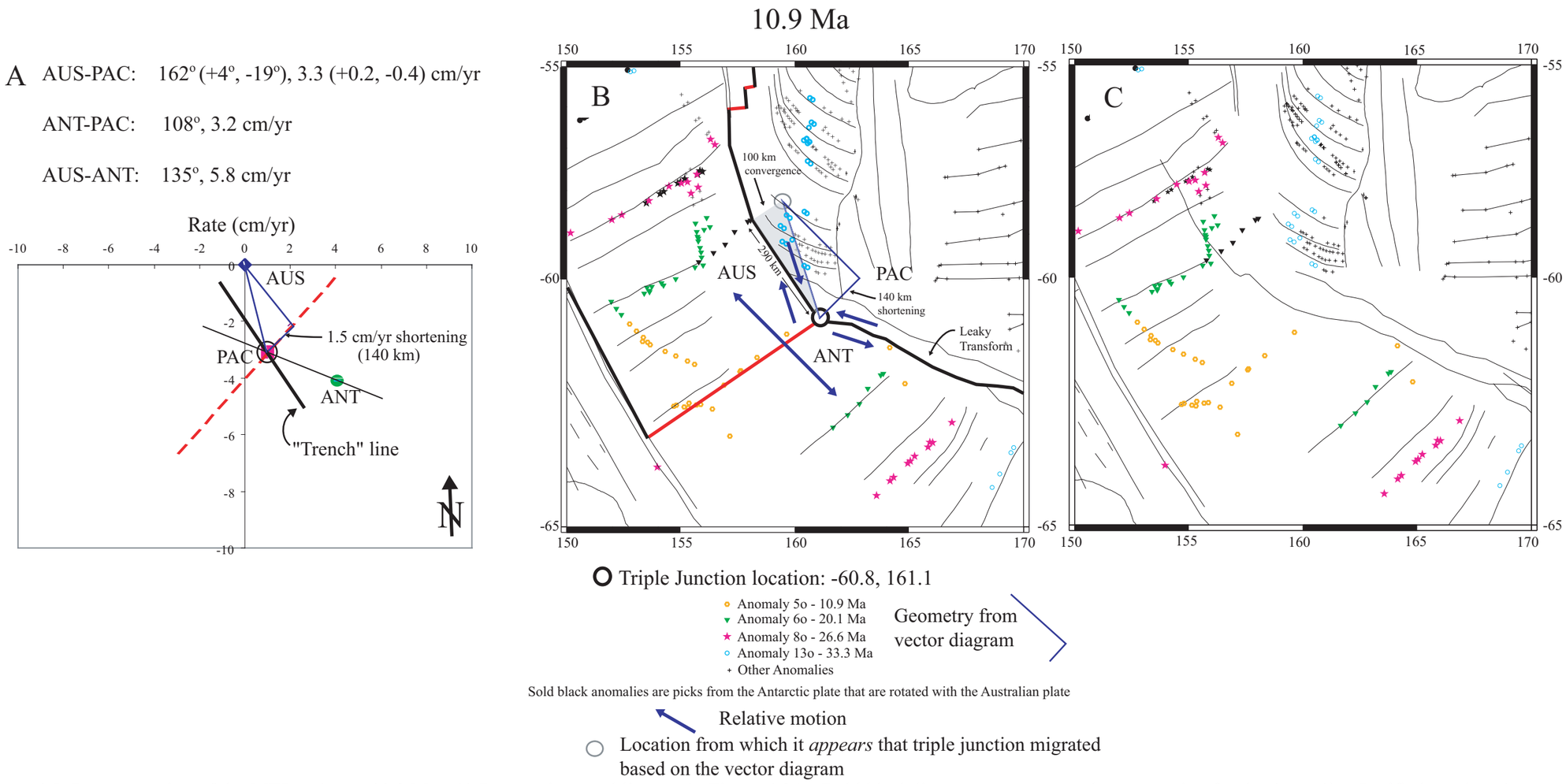

Figure 4.5. Reconstruction of the MTJ region at 10.9 Ma. A) Data, points, and lines as in Figure 4.3A. Bold black line represents a trench construction for the Australian-Pacific boundary (see text). A stable Ridge-Trench-transform Fault (RTF) configuration for the triple junction is interpreted. Position of triple junction indicates that the SEIR shortened at 1.5 cm/yr, or ~140 km (indicated). B) Orange hexagons indicate magnetic anomaly position with ages of 10.9 Ma, and other symbols as indicated in key (below). Blue lines are oriented and scaled based on the vector diagram in A, and emphasize the shortening of the SEIR by 140 km (indicated). The Australian-Pacific transform boundary lengthened by 290 km since 20.1 Ma (indicated). Shaded gray triangle emphasizes convergence that has occurred between 20.1 and 10.9 Ma. Position of light gray circle suggests a maximum of 100 km of convergence at the Australian-Pacific boundary between 20.1 and 10.9 Ma (indicated). C) Un-interpreted reconstruction of magnetic anomaly and interpreted regional structural lineaments.

(Figure 4.5B). Oblique convergence across the Australian-Pacific boundary justifies using a trench construction for the Australian-Pacific boundary in the vector diagram (labeled "Trench" line in Figure 4.5A; see methods section), resulting in a stable Ridge-Trench-transform Fault (RTF) configuration for the triple junction. This is not meant to imply that the boundary is a subduction zone at this time, only that a simple RTF geometry satisfies stability. The Australian-Pacific boundary at this time is a transpressional boundary, which is not modeled simply in vector constructions. However, stability is inferred (black circle, Figure 4.5A), and the relative motion vectors still provide important information for understanding the tectonics of the boundary (see discussion).

Anomaly 3Ay (5.9 Ma): The interpreted triple junction location is 61ºS and 160.5ºE (bold black circle, Figure 4.6B). Beginning at anomaly 3Ay, the Macquarie plate is thought to exist [*Cande and Stock*, in review]. Relative to the Macquarie plate, the Pacific plate was moving in a 192º (+6º, -3º) direction at a rate of 3.3 (+0.8, -1.2) cm/yr. Relative to the Pacific plate, the Antarctic plate was moving in a 121º direction at 3.8 cm/yr. Relative to the Macquarie plate, the Antarctic plate moved in a 156º direction at a rate of 5.8 cm/yr.

Complications similar to the previous reconstruction arise when modeling the Macquarie-Pacific plate boundary in vector space. By 5.9 Ma, the Macquarie-Pacific boundary is extremely convergent and the trench construction is used, suggesting a stable RTF configuration for the triple junction at 5.9 Ma (Figure 4.6A).

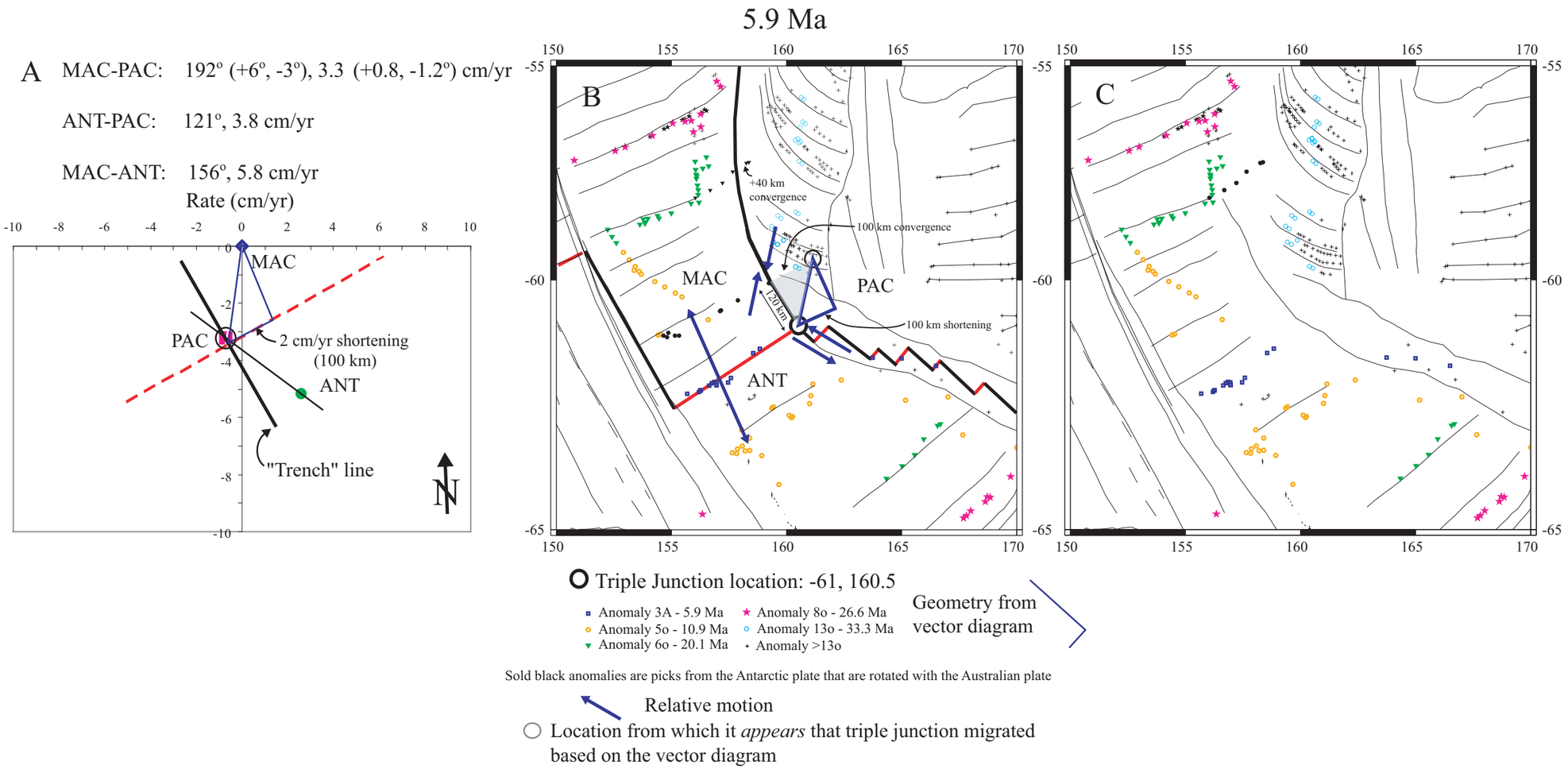

Figure 4.6. Reconstruction of the MTJ region at 5.9 Ma. A) Data, points, and lines as in Figure 4.3A. Bold black line represents a trench construction for the Australian-Pacific boundary (see text). A stable RTF configuration for the triple junction is interpreted. Position of the triple junction indicates shortening of the SEIR by 2 cm/yr, or approximately 100 km since 10.9 Ma. B) Blue squares indicate magnetic anomaly position with ages of 5.9 Ma, and other symbols as indicated in key (below). Blue lines are oriented and scaled based on the vector diagram in A, and emphasize the shortening of the SEIR by 100 km (indicated). The transform Australian-Pacific boundary lengthened by 120 km (indicated). Shaded gray triangle emphasizes convergence that has occurred between 10.9 and 5.9 Ma. Position of light gray circle suggests a maximum of 100 km of convergence at the Australian-Pacific boundary between 20.1 and 10.9 Ma (indicated). Solid black triangles (anomaly picks from the Antarctic plate that are rotated with the Australian plate) suggest 40 km of convergence at ~57ºS. C) Un-interpreted reconstruction of magnetic anomaly and interpreted regional structural lineaments.

Anomaly 2Ay (2.6 Ma): The interpreted triple junction location is 61.3ºS and 160.8ºE (bold circle, Figure 4.7B). Relative to the Macquarie plate, the Pacific plate moved in a 173º (+26, -8) direction at a rate of 1.7 (+2.3, -1.6) cm/yr. Relative to the Pacific plate, the Antarctic plate was moving in a 155º direction at 5.0 cm/yr. With respect to the Australian plate, the Antarctic plate moved in a 160º direction at a rate of 6.6 cm/yr.

The vector diagram indicates that one of the estimates of relative plate motion is inaccurate (Figure 4.7A). Given the error ellipses associated with the positions of the Macquarie-Pacific finite rotation poles for this time (Figure 4.1), it seems likely that the location of the Pacific point on the vector diagram is mis-positioned. The open black circle on the vector diagram (Figure 4.7A) is considered to be the most appropriate position of the MTJ, which suggests that the Macquarie-Pacific relative motion direction should be slightly more eastward and the rate should be higher by almost 2 cm/yr, which is within the error estimates. If so, the triple junction is characterized by a stable RFF configuration at 2.6 Ma (Figure 4.7A).

Present: The interpreted triple junction location is 61.5ºS and 161ºE. For the stage 2Ay to 0, the Pacific plate has moved in a 155º (+8º, -10º) direction with respect to the Macquarie plate at a rate of 2.1 (+1.5, -0.7) cm/yr. Relative to the Pacific plate, the Antarctic plate moved in a 160º direction at a rate of 4.5 cm/yr. Relative to the Macquarie plate, the Antarctic plate moved in a 158º direction at a rate of 6.5 cm/yr. With the estimated error, the configuration of the MTJ is stable with a RFF configuration (Figure 4.8A). The current location of the MTJ

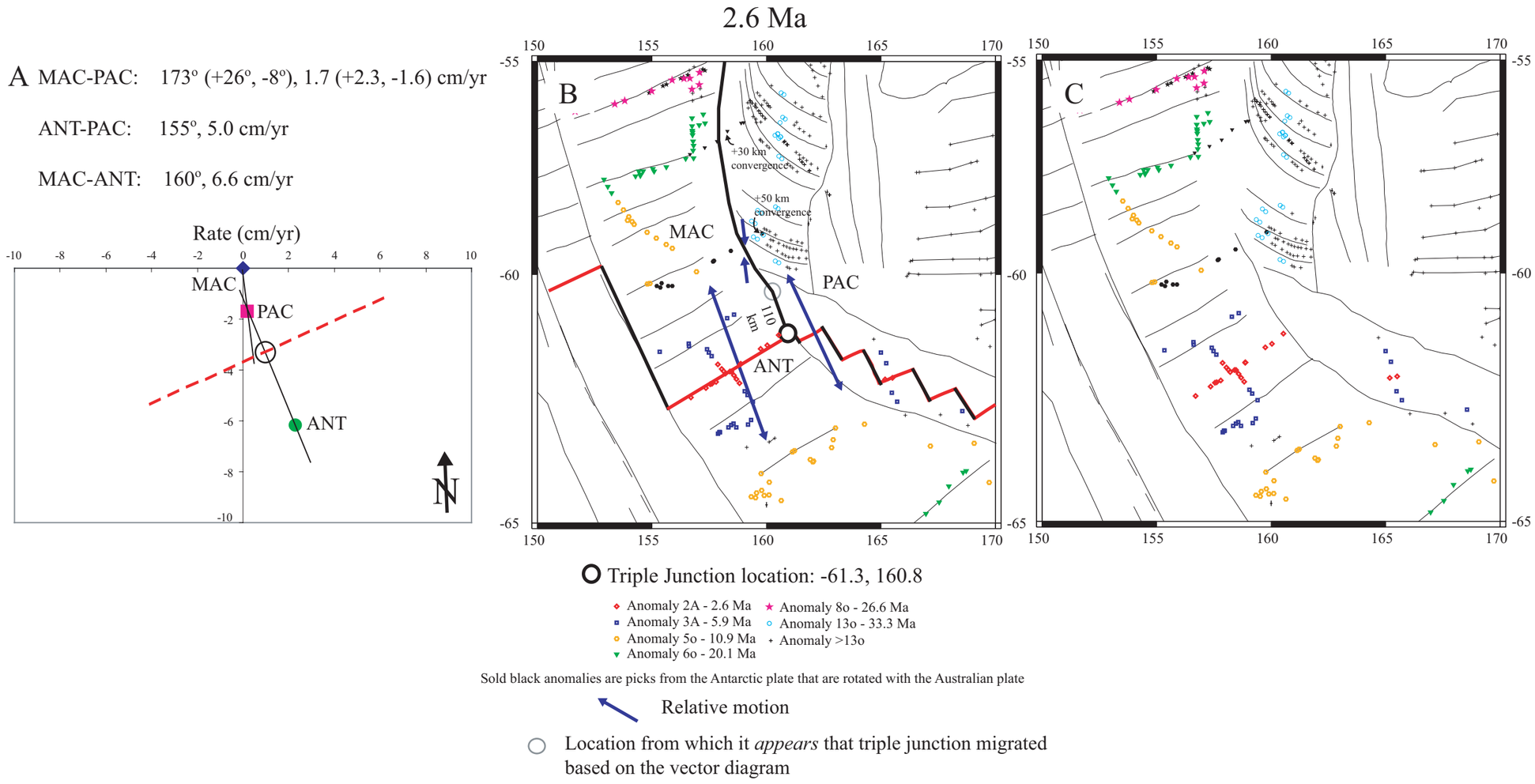

Figure 4.7. Reconstruction of the MTJ region at 2.6 Ma. A) Data, points, and lines as in Figure 4.3A. A stable RFF triple junction for the triple junction is inferred considering the position of the open black circle. B) Red diamonds indicate magnetic anomaly position with ages of 2.6 Ma, and other symbols as indicated in key (below). The Australian-Pacific transform boundary lengthened by 110 km, as indicated by the triple junction diagram (A). Solid black hexagons suggest an additional 50 km of convergence at ~60ºS since 5.9 Ma. Solid black triangles indicate an additional 30 km of convergence at ~56ºS since 5.9 Ma.

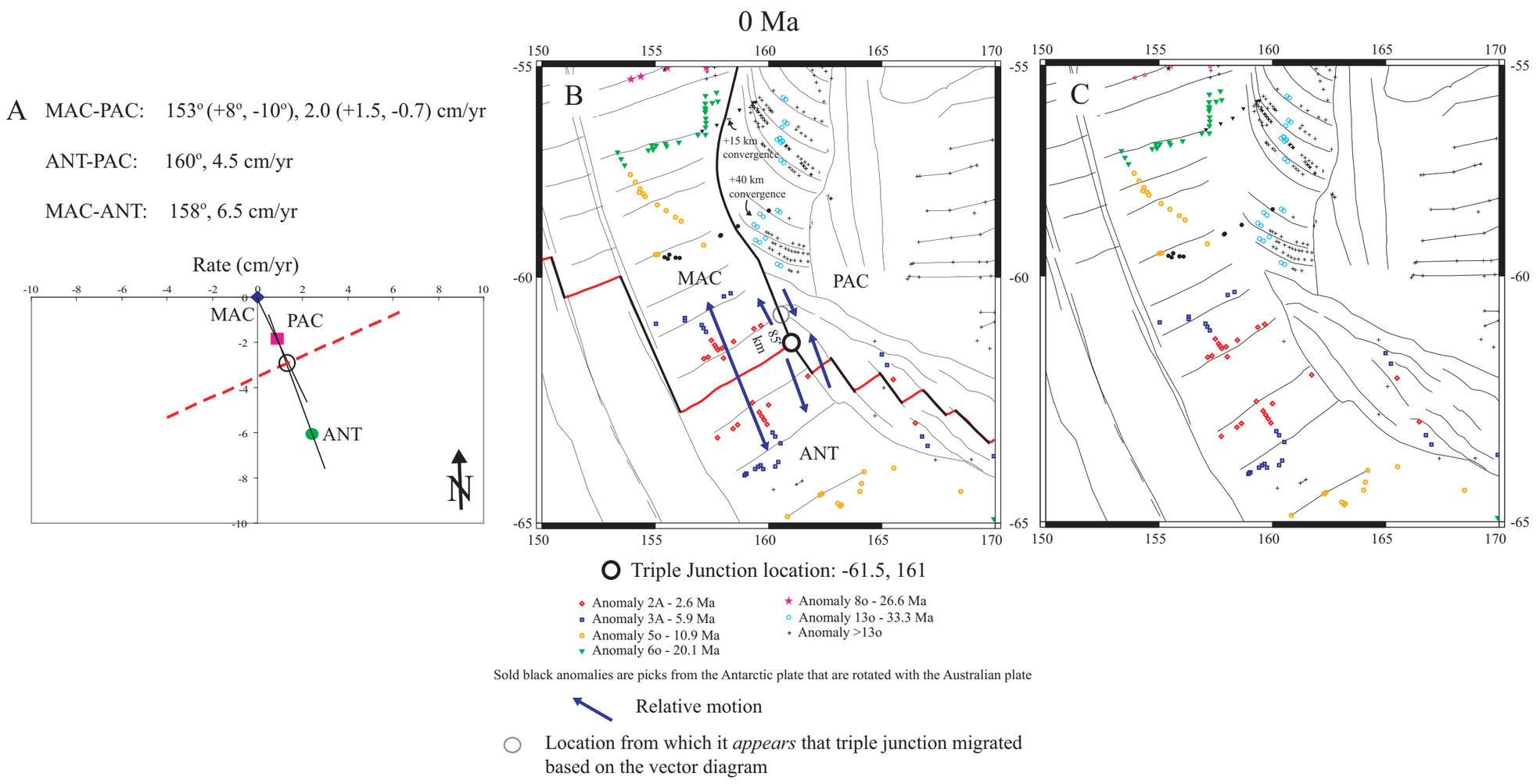

Figure 4.8. Present day map of the MTJ region. A) Data, points, and lines as in Figure 4.3A. A stable RFF triple junction for the triple junction is inferred considering the position of the open black circle. B) Symbols as indicated in key (below). The Australian-Pacific transform boundary lengthened by 85 km, as indicated by the triple junction diagram (A). Solid black hexagons suggest an additional 40 km of convergence at ~59ºS since 2.6 Ma. Solid black triangles indicate an additional 15 km of convergence since 2.6 Ma.

determined using the global marine gravity and predicted bathymetry maps [*Sandwell and Smith*, 1997; *Smith and Sandwell*, 1997] is 61.5ºS and 161ºE (Figure 4.8B).

DISCUSSION

Anomaly 13o (33.3 Ma): The SEIR and MRC spreading ridges are essentially continuous for the reconstruction at 33.3 Ma (Figure 4.2B). *Kamp* [1986] and *Marks and Stock* [1997] refer to the MRC spreading ridge at this time as the Southeast Indian Ridge Extension, indicating the close association between the two spreading systems. The mapped triple junction configuration for 33.3 Ma (Figure 4.2B) is consistent with the older Australian-Pacific-Antarctic configuration of *Marks and Stock* [1997] for anomaly 21 (47.91 Ma).

At anomaly 13o (33.3 Ma), the SEIR and MRC spreading ridges were offset from the Pacific-Antarctic spreading centers by a transform fault hundreds of kilometers long (Figure 4.2B). The orientation of the Antarctica-Pacific transform fault boundary to the southeast of the MTJ is well constrained at 33.3 Ma by the relocated position of the present boundaries of the youngest spreading on the Pacific-Antarctic Ridge (Figures 4.1 and 4.2C). *Kamp* [1986] previously identified the boundary separating the Antarctic and Pacific plates southeast of the MTJ as Fracture Zone Z (Figure 4.2B). This boundary is more accurately characterized as a transform fault at this time, as it had dominantly sinistral strike-slip displacement from 33.3 Ma until approximately anomaly 5.9 Ma [*Marks and Stock*, 1997], when oblique spreading began across the transform fault [*Lodolo and Coren*, 1997]. Sinistral offset on this transform fault led to displacement of

the Emerald Fracture Zones across this boundary [*Marks and Stock*, 1997] (Figures 4.1 & 4.2B).

A few of the magnetic anomaly locations located north of the triple junction location and east of the interpreted spreading ridge suggest the finite reconstruction pole for anomaly 13o of *Cande and Stock* [in review] may be slightly mispositioned (see anomalies labeled misfit in Figure 4.2B; 13o error ellipse, Figure 4.1). The anomalies east of the interpreted ridge location for the Southeast Indian Ridge Extension should plot closer to the other anomaly 13o positions that line up on the interpreted ridge segments. The potential mis-positioning of the Australian-Pacific finite rotation pole has consequences for the calculated Australian-Pacific relative motion vectors for the stage 13o-8o (see below).

Anomaly 8o (26.6 Ma): Since anomaly 13o (33.3 Ma), spreading became slightly more oblique at the MRC due to changes in relative motion between the Australian and Pacific plates [*Massell et al*., 2000] (Figure 4.3B). Error attributed to the position of the anomaly 13o finite pole (Figure 4.1) likely influences the position of the Pacific point on the vector diagram for 26.6 Ma (Figure 4.3A). The preferred location for the Pacific point is shown with the open circle, representing the triple junction location in vector space. The vector diagram indicates that the MTJ migrated in a ~130º direction with respect to the Australian plate from 33.3 to 26.6 Ma, resulting in the lengthening of the transform fault connecting the MRC spreading segments with the SEIR spreading segments (Figure 4.3B). Taking the best estimate of the triple junction position in vector

space (open circle in Figure 4.3A), the transform lengthened at 40 km/m.y. from 33.3 to 26.6 Ma. This equates to 270 km of increased length of the transform fault (Figure 4.3B). The transform connecting the SEIR and MRC spreading ridges is relatively short compared to the transform separating the Pacific and Antarctic plates (Figure 4.3B).

Anomaly 6o (20.1 Ma): During the stage from 26.6 Ma to 20.1 Ma spreading on the MRC rotated clockwise, continually adjusting to the changes in the Australian-Pacific relative motion. The spreading direction of the SEIR remained essentially NW/SE. The clockwise change in Australian-Pacific motion can be seen comparing Figures 4.2A through 4.4A as the clockwise rotation of the Pacific plate with respect to the Australian plate. This resulted in the formation of curved fracture zones adjacent to the MRC, lengthening of transforms between the oblique spreading centers, and a decrease in the width of spreading segments (Figure 4.4B) [*Lamarche et al*., 1997; *Massell et al*., 2000]. In the vector diagram for 20.1 Ma (Figure 4.4A), this rotation causes the direction of triple junction migration to begin a more SSE trajectory with respect to the Australian plate. Migration in a 150º direction with respect to the Australian plate at a rate of 34 km/m.y. results in an increase in 220 km for the Australian-Pacific transform boundary length (Figure 4.4B). The direction of lengthening of the transform fault connecting the SEIR and MRC spreading ridges changed in response to the more southerly migration direction of the triple junction.

An important consequence of the migration of the triple junction beginning around 20.1 Ma is that the length of the easternmost SEIR begins to

shorten. The triple junction is moving southwestward with respect to both the Australian and Antarctic plates. The rate of shortening of the ridge segment can be estimated using the vector diagram. The triple junction is migrating SW at a rate of 0.9 cm/yr with respect to the line connecting the Australian and Antarctic plates (Figure 4.4A). If this rate is taken as constant over the time interval since the last reconstruction (6.5 m.y.), the easternmost SEIR ridge segment shortened by 60 km (Figure 4.4B). The shortening of the ridge segment may have caused the development of a leaky transform on the Antarctic-Pacific plate boundary during this time (Figure 4.4B).

Anomaly 5o (10.9 Ma): The time between constructions for anomaly 6o and 5o (20.1 Ma to 10.9 Ma) represents the longest interval between reconstructions (9.2 m.y.). Relative motion of the Pacific plate with respect to the Australia plate rotated clockwise, to a more NNW/SSE direction (Figure 4.5A). Spreading on the central MRC was extremely oblique at this time [*Massell et al*., 2000] (Figure 4.5B). The change in motion resulted in an increase in the southward migration of the triple junction with respect to the Australian plate, observed as the lengthening by 290 km of the transform fault boundary connecting the SEIR and MRC spreading ridges (Figure 4.5B). The clockwise change in relative motion of the Pacific plate with respect to the Australian plate caused the transform connecting the SEIR and MRC spreading ridges to begin a transpressive phase. The location of the light gray circle (Figure 4.5B) indicates that 100 km of convergence has occurred adjacent to the anomaly 6o locations (Figure 4.5B). The easternmost of the anomaly 6o locations (solid black triangle

symbols, Figure 4.5B) abuts the transform separating the Australian and Pacific plates (Figure 4.5B). However, the 20.1 Ma reconstruction (Figure 4.4B) indicates that crust existed between the northeasternmost anomaly 6o location and the proposed triple junction location (between the open green triangles and triple junction in Figure 4.4B). This does not necessarily mean that 100 km of underthrusting has occurred, only that ~100 km of convergence has occurred. The convergence may have been accommodated by deformation at the boundary. All convergence estimates are of course dependent on the interpreted location of the plate boundary. The estimates throughout are meant to convey a general sense of the magnitude of convergence.

The length of the easternmost SEIR ridge segment can be seen to be 140 km shorter in the 10.9 Ma reconstruction than for the 20.1 Ma reconstruction (blue lines, Figure 4.5B). Considering the geometry of the vector diagram (Figure 4.5A), the location of the triple junction indicates that the easternmost SEIR shortened at a rate of 1.5 cm/yr from 20.1 to 10.9 Ma (Figure 4.5A), accounting for the difference in the observed lengths of the easternmost SEIR at 20.1 Ma and 10.9 Ma (Figure 4.5B). The amount of Australian crust involved in convergence that occurred at the Australian-Pacific boundary from 20.1 Ma to 10.9 Ma must decrease to the south (between anomaly 6o locations and the triple junction, Figure 4.5B) as a consequence of shortening of the easternmost SEIR (Shaded triangle in Figure 4.5B). This suggests that convergence between 20.1 and 10.9 Ma is accommodated both by deformation of existing crust and shortening of the ridge segment.

Anomaly 3Ay (5.9 Ma): At this time, *Cande and Stock* [in review] proposed the formation of the Macquarie plate in the southeast region of the Australian plate. The Macquarie plate is defined by *Cande and Stock* [in review] to exist roughly east of 145ºE and south of 52ºS (present day coordinates; Figure 4.1), with the eastern margin as the MRC and the southern Margin as the SEIR (Figure 4.1). The Macqaurie-Pacific stage pole of rotation is located in close proximity to the boundary (Figure 4.1), resulting in dramatic variability in the direction of Macquarie-Pacific plate motion with respect to the orientation of the MRC. By this time, spreading ceased on the central MRC due to the orientation of relative motion of the Pacific plate with respect to the Australian plate becoming sub parallel to the orientation of the plate boundary at the central MRC (Figure 4.6A). Between 10.9 and 5.9 Ma, the central MRC makes a transition from oblique spreading to strike-slip (and slightly convergent) motion. Thus, the Macquarie-Pacific plate boundary essentially becomes an obliquely convergent transform fault thousands of km long, connecting the SEIR spreading ridge to the Alpine Fault system in New Zealand.

Both of the transform faults have significant components of oblique motion across them (blue arrows, Figure 4.6B). The Pacific plate has maintained its clockwise rotation with respect to the Australian plate (Figure 4.6A), resulting in convergence across the transform fault at the boundary of the Macquarie and Pacific plates south of ~57ºS (Figure 4.6B). Positions of the duplicate Antarctic magnetic anomalies for anomaly 6o (solid black triangle symbols, Figure 4.6B) plot east of the Macquarie-Pacific plate boundary, indicating that an additional 40

km of convergence has occurred for the boundary at ~58ºS (Figure 4.6B). At ~61ºS, convergence of at least 130 km is demonstrated by the overlap of the previous triple junction location (Figure 4.6B). Again, this does not necessarily imply that 130 km of underthrusting occurred, only that 130 km of convergence occurred.

The instantaneous relative motion vector diagram at this time (Figure 4.6A) indicates that the MTJ migrated SSW with respect to the Macquarie plate. The length of the Macquarie-Pacific transform fault grew by 120 km (Figure 4.6B). Migration of the triple junction caused the easternmost SEIR to shorten at a rate of 2 cm/yr from 10.9 to 5.9 Ma (Figure 4.6A). This resulted in approximately 100 km of shortening in the length of the easternmost SEIR during this time (Figure 4.6B). Similar to the situation for the 10.9 Ma reconstruction, the amount of crust involved in convergence at the Macquarie-Pacific boundary decreases between the anomaly 5o locations and the triple junction (shaded triangle in Figure 4.6B). Thus, between 10.9 and 5.9 Ma, convergence at the Macquarie-Pacific boundary was accommodated by a complex combination of deformation of existing crust and shortening of the easternmost segment of the SEIR. The Hjort Trench is likely becoming well developed between 10.9 and 5.9 Ma due to the high angles of convergence.

A change in Pacific-Antarctic relative plate motion to a slightly more N/S orientation around anomaly 3Ay (5.9 Ma) caused the transform between the Pacific and Antarctic plates to develop into an oblique spreading center (Figure 4.6A). *Lodolo and Coren* [1997] identified magnetic anomalies for the crust east

of the triple junction location that support initiation of spreading on the Pacific-Antarctic transform at ~6 Ma (Figure 4.6A). They report spreading rates of ~3 cm/yr for the crust in this region, which is consistent with the estimates of instantaneous relative plate motion obtained from stage pole calculations (Figure 4.6B). The apparent asymmetry of the spreading is a result of previous extension along an interpreted leaky transform (Figures 4.4B and 4.5B). In the immediate vicinity of the MTJ, the Antarctic-Pacific boundary is a relatively short transform fault connecting the SEIR with the recently formed oblique spreading centers of the Antarctic-Pacific Ridge.

Anomaly 2Ay (2.6 Ma): The vector diagram for 2.6 Ma (Figure 4.7A) indicates that shortening of the easternmost SEIR ridge segment became insignificant by 2.6 Ma. The inferred triple junction location on the vector diagram (Figure 4.7A) does not plot significantly to the west of the line connecting the Macquarie and Antarctic points. The direction of triple junction migration with respect to the Macquarie plate was in a ~160º direction (Figure 4.7A), resulting in the lengthening of the Macquarie-Pacific plate boundary at a rate of 38 km/m.y., as determined from the vector diagram using the position of the triple junction shown. For the 3.3 m.y. since the last reconstruction, this rate resulted in the lengthening of the Macquarie-Pacific transform fault by 110 km (Figure 4.7B).

Angles between the convergence vector and the plate boundary orientation in the Hjort region become smaller at 2.6 Ma than for 5.9 Ma. Thus, deformation at the Hjort region likely decreased from 5.9 to 2.6 Ma. Relative motion caused

an additional 30 km convergence adjacent to the anomaly 6o locations (solid black triangles, Figure 4.7B), and an additional 50 km of convergence adjacent to the anomaly 5o locations (solid black hexagons, Figure 4.7B). From 5.9 to 2.6 Ma, the Antarctic-Pacific boundary continued spreading at an oblique angle, serving to more efficiently link the Pacific-Antarctic and SEIR spreading ridge systems.

The MTJ had a RFF configuration between 5.9 and 2.6 Ma (Figure 4.7B). However, sparse magnetic anomaly data directly east of the MTJ do not allow much constraint on the nature of the intersection of the Antarctic-Pacific boundary with the triple junction (Figure 4.7C). A small segment of transform fault is illustrated in Figure 4.7B, but it is also conceivable that the westernmost Antarctic-Pacific spreading segment intersected directly with the triple junction. The choice of a transform fault is illustrated in the vector diagram for 2.6 Ma (Figure 4.7A), although the geometry is only stable considering the errors associated with the Australian-Pacific relative motion. However, a transform Antarctic-Pacific boundary intersecting the MTJ is more probable than a spreading ridge. If an Antarctic-Pacific ridge intersected directly with the MTJ, the direction and rate of spreading would have to have been essentially the same as for the SEIR and Antarctic-Pacific spreading ridges in order for the MTJ to remain stable. Given the geometry of the vector diagram (Figure 4.7A), it seems unlikely that the spreading rates were equivalent.

Present: Relative motion of the Macquarie and Pacific plates resulted in an additional 15 km of convergence adjacent to the locations of anomaly 6o (solid

black triangles, Figure 4.8B), and an additional 40 km of convergence adjacent to anomalies 5o (solid black hexagons, Figure 4.8B). Convergence can be seen to decrease consistently since 10.9 Ma.

The estimates of relative plate motion determined from stage pole rotations compare well with previous estimates using interpreted magnetic anomaly data. *Falconer* [1972] determined the Australian-Antarctica relative motion to be 6.8 cm/yr in the 145º direction. Australian-Pacific relative motion was estimated to be 3.5 cm/yr in the 155º direction, and Antarctic-Pacific relative motion was determined to be 3.5 cm/yr in the 135º direction. The only significant discrepancy between those values and the calculations used in this analysis is the direction of Antarctic-Pacific motion, which differ by 25º. The Australian-Pacific vector calculated using the stage pole is considered to represent a more accurate direction of relative motion. *Falconer* [1972] located the triple junction at 61.5ºS, 161ºE, and also characterized it as having a RFF geometry. Between 2.6 Ma and the present, the MTJ migrated in the ~155º direction with respect to the Pacific plate at a rate of 32 km/m.y., resulting in an increase in the Macquarie-Pacific transform length of 85 km (Figure 4.8B). At this time, oblique convergence was still occurring on the Macquarie-Pacific plate boundary to the north.

CONCLUSIONS

The MTJ can be characterized by a Ridge-transform Fault-transform Fault (RFF) configuration from 33.3 Ma to 20.1 Ma, and from 2.6 Ma to the present. Between 20.1 Ma and 5.9 Ma, a Ridge-Trench-transform Fault (RTF) is more appropriate for constructing vector diagrams. For these times, the Australian-

Pacific (Macquarie-Pacific) boundary is an obliquely convergent transform. Since 33.3 Ma, the MTJ has migrated southeastward with respect to the Australian plate for a distance of over 1100 km, resulting in the lengthening of the Australian-Pacific transform plate boundary.

The Australian-Pacific (and Macquarie-Pacific for times younger than 5.9 Ma) plate boundary evolved from a spreading ridge to a strike-slip fault and eventually to an obliquely convergent plate boundary since the Oligocene. Spreading only occurred on the central and northern MRC and was never part of the evolutionary history of the MRC south of the present day coordinates on the MRC of ~56ºS and 160ºE. Convergence began in the Hjort region between 20.1 Ma and 10.9 Ma, while spreading was still occurring at an extremely oblique angle at the central MRC. Relative motion at the Australian/Macquarie-Pacific boundary eventually resulted in convergence of between 180 km (using anomaly 6o locations) and 220 km (using anomaly 5o locations). Between 20.1 and 5.9 Ma, convergence at the Australian-Pacific plate boundary was accommodated by a complex combination of deformation of existing crust and shortening of the easternmost segment of the SEIR. MTJ migration between 26.6 Ma and 5.9 Ma resulted in the decrease of the length of the easternmost SEIR spreading ridge by 200 km.

The Antarctic-Pacific boundary was a transform fault connecting the Antarctic-Pacific spreading ridge system with the SEIR for times between 33.3 and 5.9 Ma. Between 26.6 and 10.9 Ma the Antarctic-Pacific boundary was likely a leaky transform, accommodating some divergence between the two plates. At

5.9 Ma, a change in Antarctic-Pacific relative plate motion caused the transform fault to evolve into a spreading ridge. The spreading since 5.9 Ma served to more efficiently link the SEIR and Antarctic-Pacific spreading ridge systems, as the relative motion of the Antarctic-Pacific and Antarctic-Macquarie became similar in direction and magnitude.

Summary

Significant advances have been made toward understanding the present tectonic state and past evolution of the Hjort region of the southern Australian-Pacific plate boundary. Limited underthrusting is now recognized in the Hjort region based on the identification of a thrust fault in the trench accompanied by thrust focal mechanisms, anomalously deep seismicity for the age of the oceanic lithosphere interacting at the boundary, and a gravity signature consistent with ~50 km of underthrust crust. These observations have led to the conclusion that incipient subduction has occurred at the Hjort Trench. The Hjort region represents one of the best localities in the world for investigating the processes involved in subduction initiation, and provides an observational basis for models of subduction initiation in a marine setting.

The recognition that the Hjort boundary has seen more convergence than has currently been accounted for by underthrusting led to the search for additional processes that may have accommodated convergence. Topographic analysis identified a consistent relationship between topography and boundary-normal convergence, suggesting that most of the convergence since 5.9 Ma can be accounted for in the generation of topography at the plate boundary. In addition, the identification of strain partitioning between thrust and strike slip faults in the Hjort region highlights the potential for the lateral translation of crustal slivers along the plate boundary, limiting the amount of crust that can be potentially

underthrust. The accommodation of strain at the plate boundary through the formation of topography and lateral translation of crustal slivers are viable explanations for the observed differences between the amount of subduction at the Hjort and Puysegur Trenches. Convergence prior to 5.9 Ma may have resulted in underthrusting identified in the present gravity anomaly, but any underthrust crust has more recently been moving northwards, resulting in the migration of the Hjort Trench to the north. Although it is unclear whether the Hjort Trench will evolve into a mature subduction zone, convergence angles have been decreasing for the past 5.9 Ma, suggesting that mature subduction may not develop.

The evolution of the southern Australian-Pacific plate boundary is notably different than the segments of the boundary farther north. The southern boundary lacks a divergent history, and has evolved from a dextral transform into the current transpressional setting. Additionally, the complex interaction of oblique convergence and triple junction migration has resulted in the presently observed curved shape of the plate boundary in the Hjort region and the formation of the Trench.

This research highlights significant topics that remain to be explored. What is the relationship between the dynamic history of the overriding plate and convergence during incipient subduction? The strength of the Hjort region as an observational laboratory for understanding the processes and tectonic response during the earliest stages of subduction could be further exploited by using the topography at the plate boundary to constrain numerical models of subduction initiation. Finally, while significant advances have been made regarding where

subduction may initiate and how structures and topography respond to initiation, it remains unclear what mechanisms generated the forces responsible for the documented changes in relative plate motion that resulted in incipient subduction at the Hjort Trench.

Appendices

APPENDIX A: UN-INTERPRETED OUTPUT FROM THE PLATES PROGRAM FOR EACH OF THE RECONSTRUCTIONS

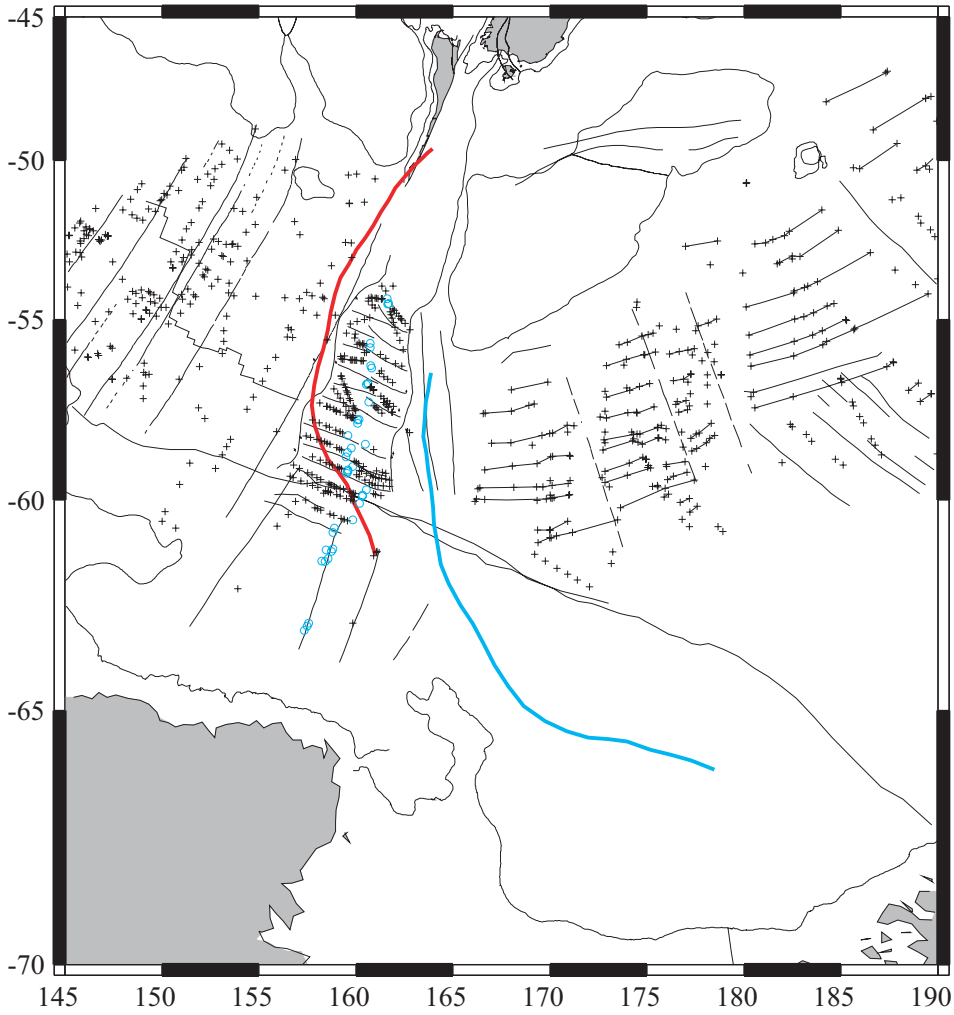

33.3 Ma - An13o
PAC fixed
Cande & Stock in review

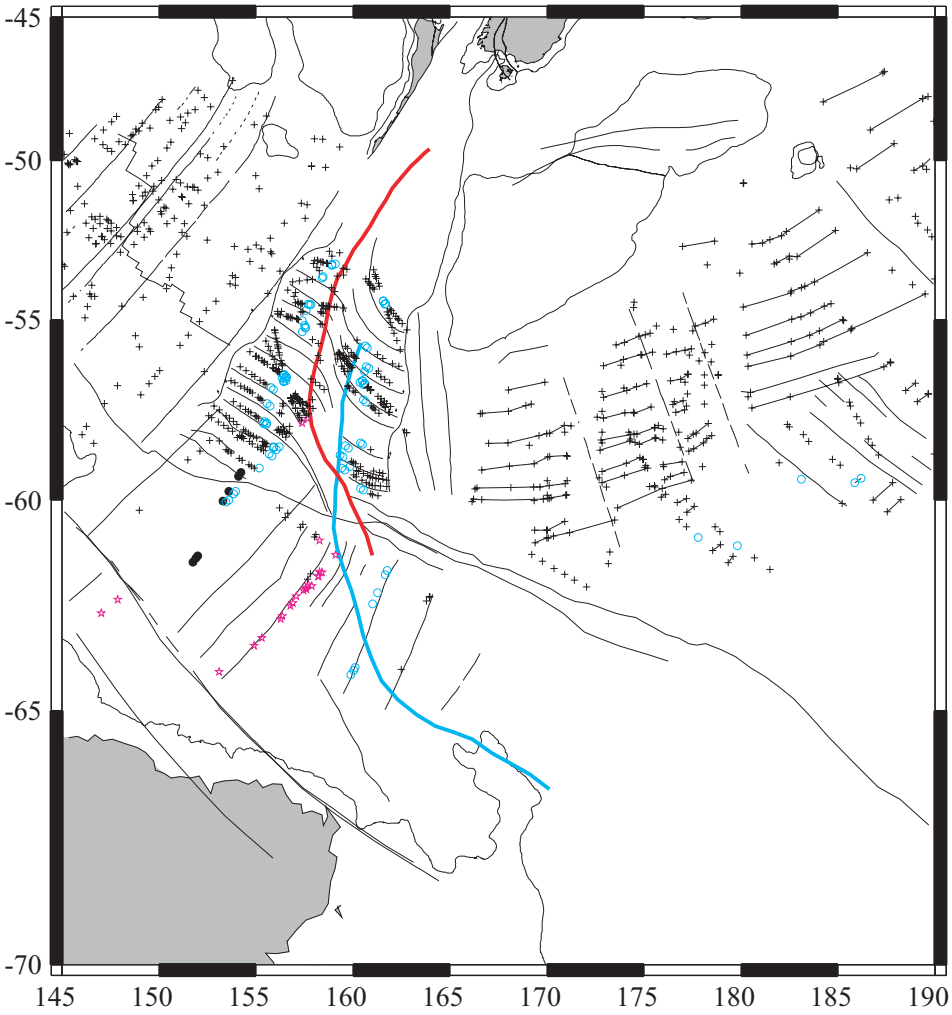

26.6 Ma - An8o
PAC fixed
Cande & Stock in review

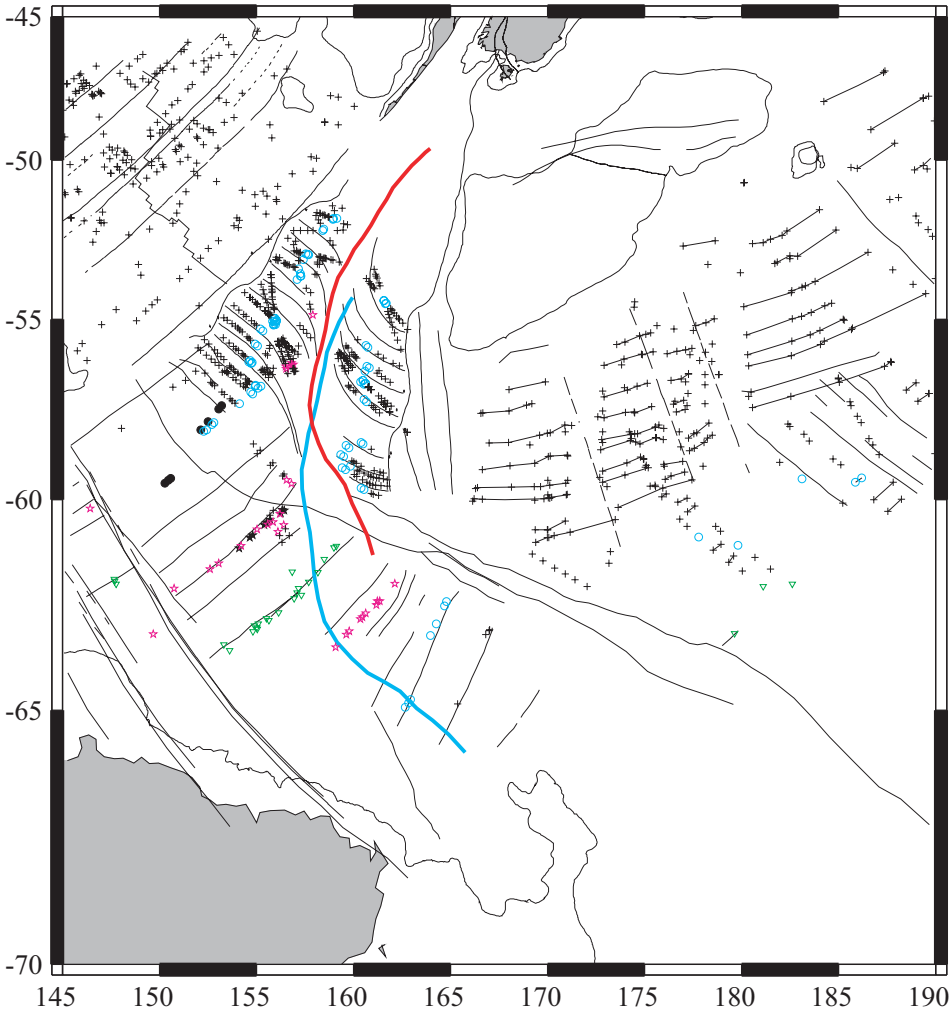

20.1 Ma - An6o
PAC fixed
Cande & Stock in review

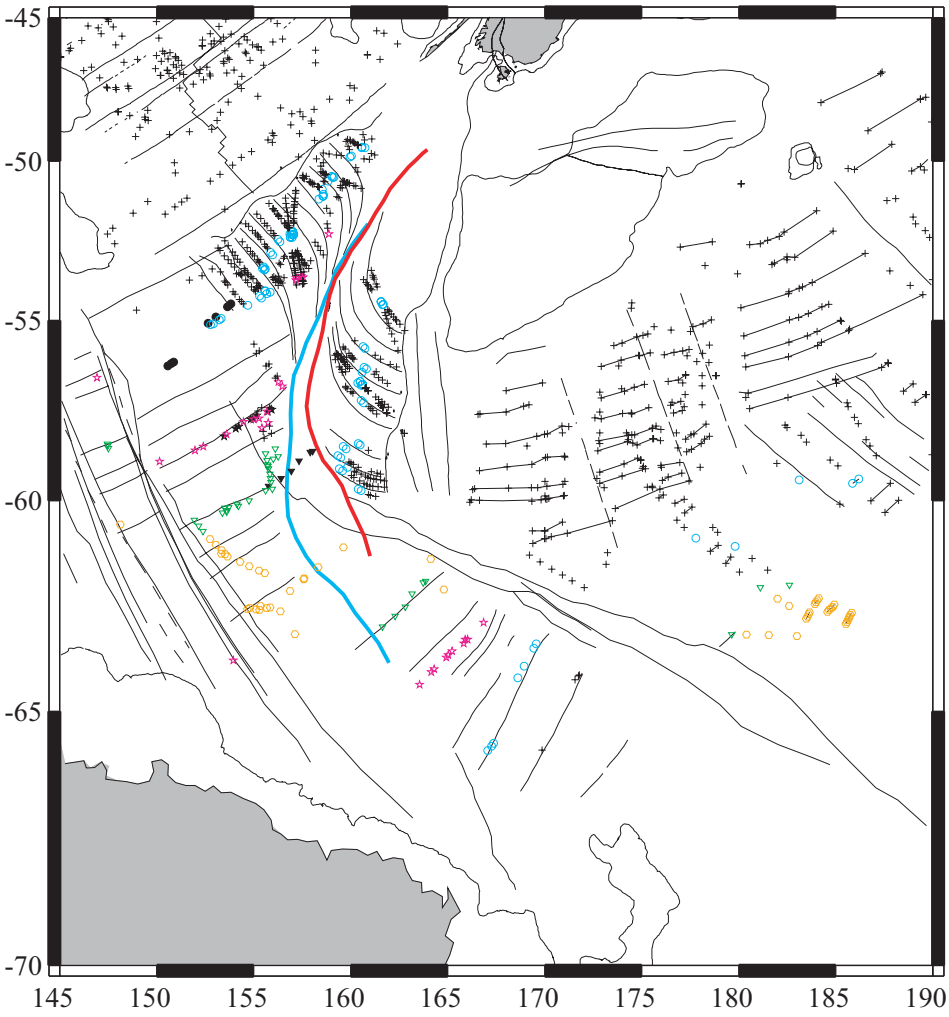

10.9 Ma - An5o
PAC fixed
Cande & Stock in review

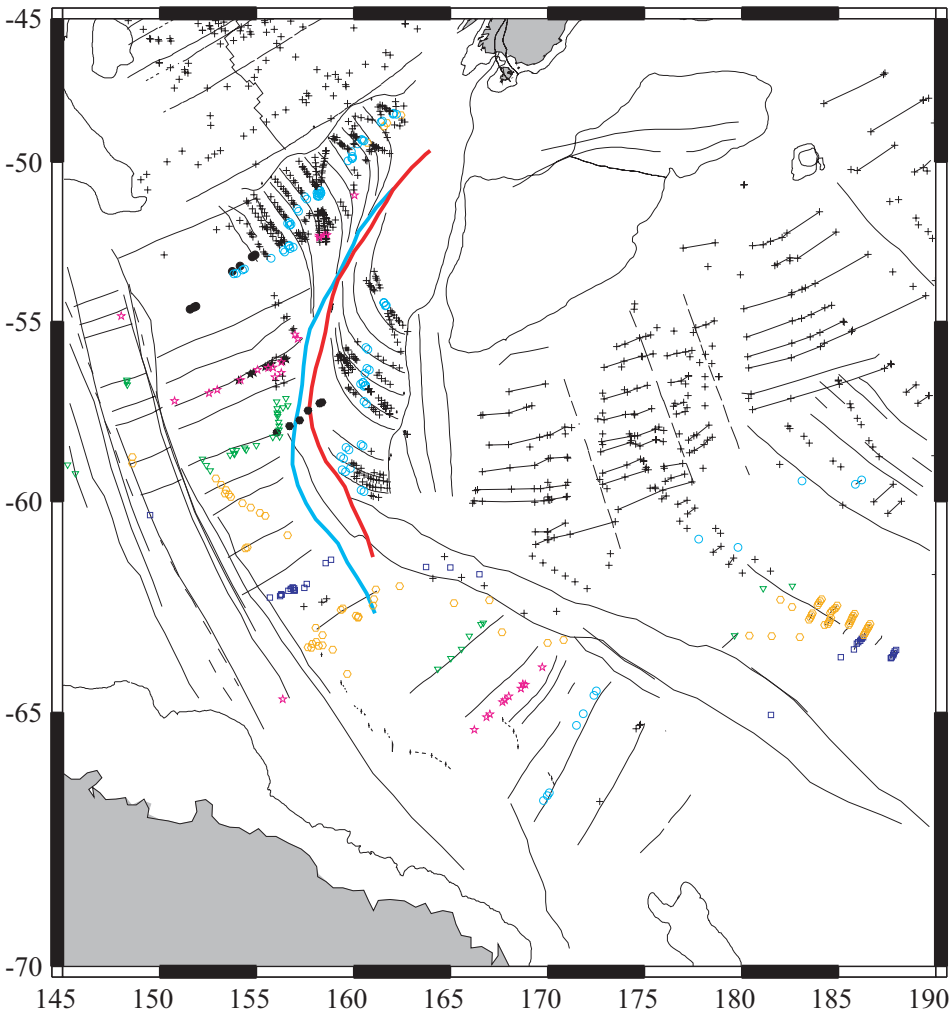

05.9 Ma - An3A
PAC fixed
Cande & Stock in review

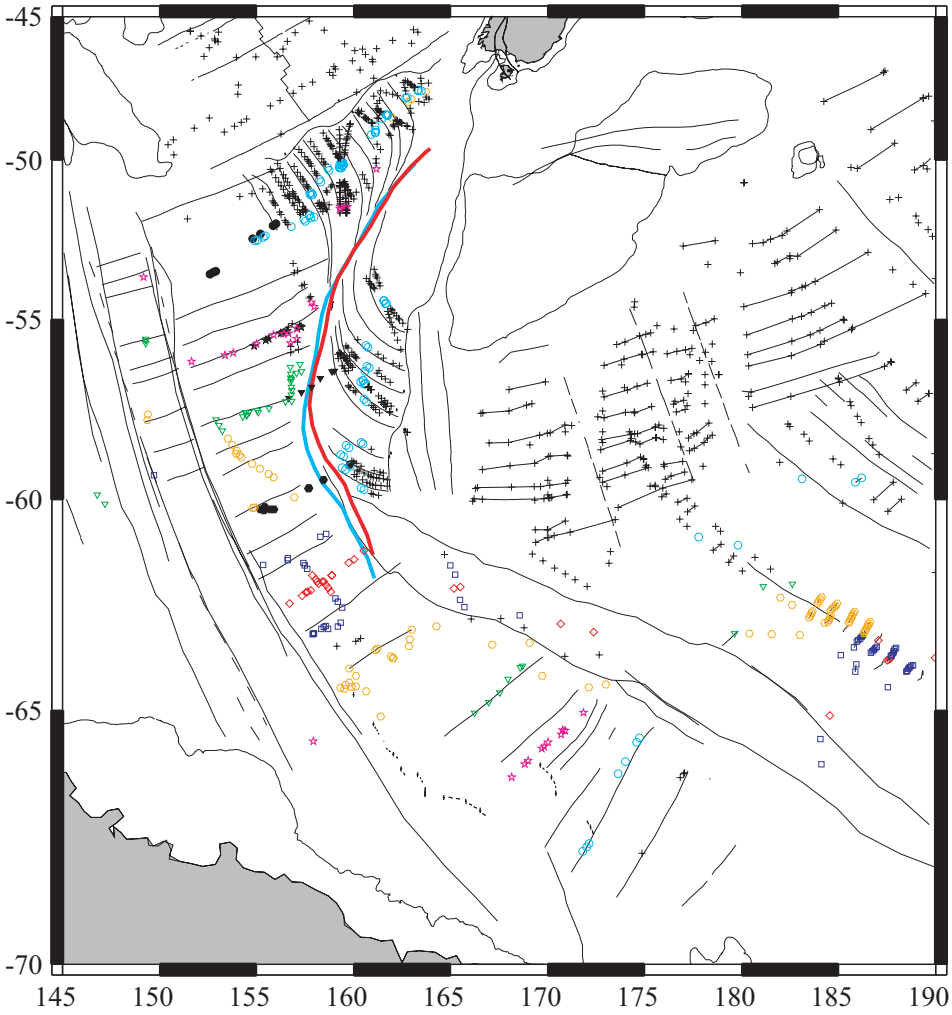

02.6 Ma - An2A
PAC fixed
Cande & Stock in review

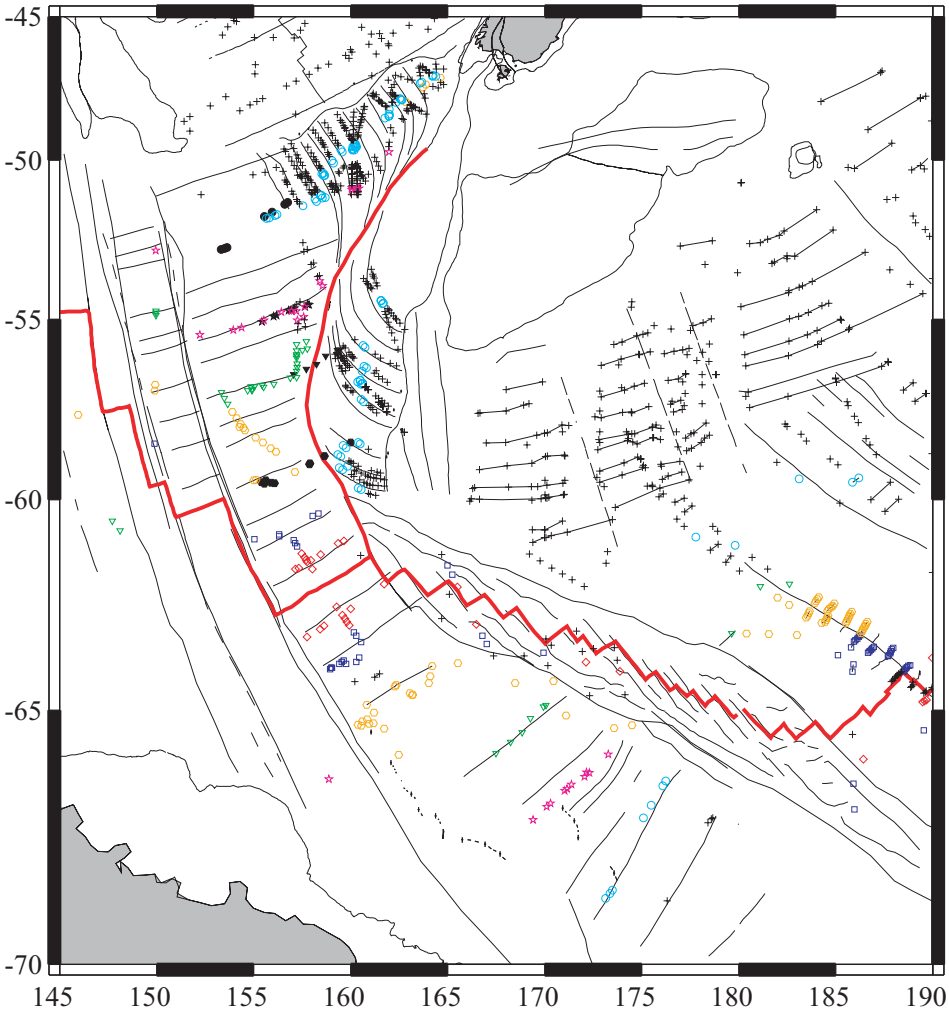

00.0 Ma - Present Day
PAC fixed
Cande & Stock in review

APPENDIX B: VOLUME CALCULATIONS

Calculations were made for 17 points on the plate boundary between 51ºS and 60ºS (latitudes reported in Table 3). Vertices of the rectangles that define swaths centered on each point were defined as follows. A swath area was arbitrarily chosen that would extend perpendicular to the plate boundary across all topography assumed to be related to deformation adjacent to the plate boundary. After considering various widths, I decided that 70 km on either side of the boundary was sufficient, resulting in a 140 km-wide swath. The 50-kilometer dimension was chosen because pre-determined points on the boundary had arbitrarily defined 50-km spacing. Thus, swath overlap for adjacent swaths was minimized. A Lambert Azimuthal Equal-Area (-Ja option in GMT) plot with gridlines every 0.1 degree was generated centered on each of the 17 points on the plate boundary. A rectangle overlay representing the desired swath width (50 km by 140 km) was placed on the map perpendicular to the boundary and the latitude and longitude vertices of the rectangle were recorded from the map.

Volume calculations use a digital bathymetry grid (hereafter referred to as regional grid) between 51º-61ºS and 153º-163ºE with a cell size of 0.001º by 0.001º. The regional grid contained merged data from the 2000 R/V *L'Atalante*, 1996 R/V *Rig Seismic* (see Chapter 2 for extents), and predicted bathymetry from *Sandwell and Smith* [1997]. For determining a value for each cell in the regional grid, *L'Atalante* data was given priority, then *Rig Seismic*, then predicted bathymetry. That is, bathymetry values were chosen from *L'Atalante* data if

available. If not, cell values were defined by *Rig Seismic* data. If neither *L'Atalante* nor *Rig Seismic* data were available, cell values were assigned from predicted bathymetry.

The regional grid was imported into the software package ArcGIS v8.0. Within Arc, a rectangle feature was defined for each swath with latitude and longitude of vertices defined as determined above. Bathymetry data within the swath was extracted to a separate raster file. Topographic profiles perpendicular to the boundary for each swath were generated from the regional grid and used to define the average seafloor elevation (horizontal datum). These values are reported in Table 3. Using the raster calculator function in the 3-D Analyst extension of ArcGIS, cells above and below the average seafloor depth were extracted from each swath to two separate raster grid files (referred to as above and below). Extracted cell values for the above and below grids were recalculated to reflect the height (in meters) between the horizontal datum and the bathymetric surface using the following equations:

Height above horizontal datum = horizontal datum height – bathymetry value

Height below horizontal datum = horizontal datum height – bathymetry value

The absolute values of these calculated heights is the height in meters (a positive number) between the horizontal datum and the bathymetric surface.

For each of the two raster grids containing cells above and below the horizontal datum, the sum of the recalculated height values was determined. One

single value therefore represented the total recalculated height between the bathymetry surface and horizontal datum of all cells with bathymetry values above (or below) the horizontal datum. This height was multiplied by the cell size. Because the regional grid was in decimal degrees, the area of a cell at different latitudes was calculated using the formula:

Cosine(Latitude)*6371000*p*0.001/180

where 6371000 is the radius of Earth in meters, p is Pi, and 0.001 is the cell size in decimal degrees. By multiplying the total summed heights for cell above and below the horizontal datum by the area (in square m) of a cell at that latitude, the volume above and below the horizontal datum was determined. These values are summed to arrive at the total volume displaced from the horizontal datum.

References

Anderson, H., Webb, T., and Jackson, J., 1993. Focal mechanisms of large earthquakes in the South Island of New Zealand; Implications for the accommodation of Pacific-Australia plate motion. Geophysical Journal International 115 (3): 1032-1054.

Argus, D.F., and Gordon, R.G., 2001. Present tectonic motion across the Coast Ranges and San Andreas fault system in central California. GSA Bulletin 113 (12): 1580-1592.

Barnes, P. M., Mercier de Lepinay, B., Collot, J-Y., Delteil, J., Audru, J-C., 1998. Strain partitioning in the transition area between oblique subduction and continental collision, Hikurangi Margin, New Zealand. Tectonics 17 (4): 534-557.

Bergman, E.A., and Solomon, S.C., 1980. Oceanic intraplate earthquakes; implications for local and regional intraplate stress. Journal of Geophysical Research 85 (B10): 5389-5410.

Bernardel, G., Alcock, M., Petkovic, P., Thomas, S., and Levinson, M., 2000. Seafloor mapping of the South-east Region and adjacent waters – AUSTREA2 cruise report: south-east Tasmania and southern Macquarie Ridge, Australian Geological Survey Organization, Record 2000/46, 25 pp.

Bernardel, G., and Symonds, P.A., 2001. Seafloor mapping of the South-east Region and adjacent waters - AUSTREA final report: southern Macquarie Ridge, Geoscience Australia, Record 2001/46, 78 pp.

Bilham, R., and Williams, P., 1985. Sawtooth segmentation and deformation processes on the southern San Andreas Fault, California. Geophysical Research Letters 12 (9): 557-560.

Bilich, A., Frohlich, C., and Mann, P., 2001. Global seismicity characteristics of subduction-to-strike-slip transitions. Journal of Geophysical Research 106 (9): 19,443-19,452.

Bonatti, E., 1978. Vertical tectonism in oceanic fracture zones. Earth and Planetary Science Letters 37 (3): 369-379.

Bonatti, E., Ligi, M., Gasperini, L., Peyve, A., Raznitsin, Y., and Chen, Y.J., 1994. Transform migration and vertical tectonics at the Romanche fracture zone, Equatorial Atlantic. Journal of Geophysical Research 99 (11): 21,779-21,802.

Bown, J.W., and White, R.S., 1994. Variation with spreading rate of oceanic crustal thickness and geochemistry. Earth and Planetary Science Letters 121 (3-4): 435-449.

Calais, E., Bethoux, N., and Mercier de Lepinay, B., 1992. From transcurrent faulting to frontal subduction: A seismotectonic study of the northern Caribbean plate boundary from Cuba to Puerto Rico. Tectonics 11 (1): 114-123.

Cande, S.C., Raymond, C.A., Stock, J., and Haxby, W.F., 1995. Geophysics of the Pitman fracture zone and Pacific-Antarctic Plate motions during the Cenozoic. Science 270 (5238): 947-953.

Cande, S.C., and Kent, D.V., 1995. Revised calibration of the geomagnetic polarity timescale for the Late Cretaceous and Cenozoic. Journal of Geophysical Research 100 (4): 6093-6095.

Cande, S.C., Stock, J., Muller, R.D., and Ishihara, T., 2000. Cenozoic motion between East and West Antarctica. Nature 404: 145-150.

Cande, S.C., and Stock, J., in review. Pacific-Antarctic-Australia Motion and the Formation of the Macquarie Plate. Geophysical Journal International.

Carbotte, S.M., and Macdonald, K.C., 1994. Comparison of seafloor tectonic fabric at intermediate, fast, and super fast spreading ridges; influence of spreading rate, plate motions, and ridge segmentation on fault patterns, Journal of Geophysical Research 99 (B7): 13,609-13,631.

Chemenda, A., Lallemand, S., and Bokun, A., 2000. Strain partitioning and interplate friction in oblique subduction zones; constraints provided by experimental modeling. Journal of Geophysical Research 105 (3): 5567-5581.

Christeson, G.L., and McNutt, M.K., 1992. Geophysical constraints on the shear stress along the Marquesas fracture zone. Journal of Geophysical Research 97 (4): 4425-4437.

Christoffel, D.A., and Van der Linden, W.J.N., 1972. Macquarie Ridge-New Zealand Alpine Fault transition, In: Hayes, D.E. (Ed.), Antarctic Oceanology II; The Australian-New Zealand Sector, Antarctic Research Series 19: 235-242.

Clague, D.A., and Jarrard, R.D., 1973. Tertiary plate motion deduced from the Hawaiian-Emperor Chain. GSA Bulletin 84 (4): 1135-1154.

Claypool, A.L., Klepeis, K.A., Dockrill, B., Clarke, G.L., Zwingmann, H., and Tulloch, A., 2002. Structure and kinematics of oblique continental convergence in northern Fiordland, New Zealand. Tectonophysics 359 (3-4): 329-358.

Coffin, M.F., Karner, G.D., and Falvey, D.A., 1994. Research cruise yields new details of Macquarie Ridge complex. Eos Trans., AGU 75 (48): 561.

Collot, J-Y., Lamarche, G., Wood, R.A., Delteil, J., Sosson, M., Lebrun, J-F., and Coffin, M.F., 1995. Morphostructure of an incipient subduction zone along a transform plate boundary; Puysegur Ridge and Trench. Geology, 23 (6): 519-522.

Collot, J-Y., Delteil, J., Herzer, R., Wood, R., and Lewis, K.B., 1995. Sonic imaging reveals new plate boundary structures offshore New Zealand: EOS Trans., AGU 76 (1): 1-5.

Daczko, N.R., Wertz, K.L., Mosher, S., and Coffin, M.F., and Meckel, T.A., in review. Extension along the Australian-Pacific transpressional transform plate boundary near Macquarie Island. Geochemistry, Geophysics, Geosystems.

Das, S., 1993. The Macquarie Ridge earthquake of 1989. Geophysical Journal International 115: 778-798.

Davey, E.J., and Smith, E.G.C., 1983. The tectonic setting of the Fiordland region, South-West New Zealand. Geophysical Journal of the Royal Astronomical Society 72 (1): 23-38.

Davies, G.F., 1981. Regional compensation of subducted lithosphere; effects on geoid, gravity and topography from a preliminary model. Earth and Planetary Science Letters 54 (3): 431-441.

De Bremaecker, J-C., 1977. Is the oceanic lithosphere elastic or viscous? Journal of Geophysical Research 82 (14): 2001-2004.

Delteil, J., Collot, J.Y., Wood, R., Herzer, R., Calmant, S., Christoffel, D., Coffin, M.F., Ferriere, J., Lamarche, G., Lebrun, J-F., Mauffret, A., Pontoise, B., Popoff, M., Ruellan, E., Sosson, M., and Sutherland, R., 1996. From strike-slip faulting to oblique subduction: a survey of the Alpine Fault-Puysegur Trench transition, New Zealand, results of cruise Geodynz-Sud leg 2. Marine Geophysical Researches 18: 383-389.

DeMets, C., 1992. Oblique convergence and deformation along the Kuril and Japan trenches. Journal of Geophysical Research 97 (12): 17,615-17,625.

DeMets, C., Gordon, R.G., Argus, D.F., and Stein, S., 1990. Current plate motions. Geophysical Journal International 101 (2): 425-478.

DeMets C., Gordon, R.G., Argus, D.F., and Stein, S., 1994. Effect of recent revisions to the geomagnetic reversal time scale on estimates of current plate motions. Geophysical Research Letters 21 (20): 2191-2194.

DeMets, C., Jansuma, P.E., Mattioli, G.S., Dixon, T.H., Farina, F., Bilham, R., Calais, E., and Mann, P., 2000. GPS geodetic constraints in Caribbean-North America Plate motion. Geophysical Research Letters 27 (3): 437-440.

Deschamps, A.E., Lallemand, S.E., and Collot, J.-Y., 1998. A detailed study of the Gagua ridge; a fracture zone uplifted during a plate reorganisation in the mid-Eocene. Marine Geophysical Researches 20 (5): 403-423.

Dewey, J.F., 1975. Finite plate implications: some implications for the evolution of rock masses at plate margins. American Journal of Science 275-A: 260-284.

Doser, D.I., and Lomas, R., 2000. The transition from strike-slip to oblique subduction in southeastern Alaska from seismological studies. Tectonophysics 316: 45-65.

Duncan, R.A., and Varne, R., 1988. The age and distribution of igneous rocks on Macquarie Island. Papers and Proceedings of the Royal Society of Tasmania 122 (1): 45-50.

Ekstrom, G., Dziewonski, A.M., Salganik, M.P., and Smith, G.P., 1995. The Harvard CMT Project, paper presented at International Union of Geodesy and Geophysics; XXI general assembly, International Union of Geodesy and Geophysics, Boulder, CO, United States, July 2-14, 21, Week B, 331.

Engdahl, E.R., van der Hilst, R., and Buland, R., 1998. Global teleseismic earthquake relocation with improved travel times and procedures for depth determination. Bulletin of the Seismological Society of America 88 (3): 722-743.

Escartin, J., and Cannat, M., 1999. Ultramafic exposures and the gravity signature of the lithosphere near the Fifteen-Twenty fracture zone (Mid-Atlantic Ridge, 14 degrees -16.5 degrees N). Earth and Planetary Science Letters 171 (3): 411-424.

Ewing, M., and Heezen, B., 1956. Some problems of Antarctic submarine geology. Geophysical Monograph, 1 (462): 75-81.

Falconer, R.K.H., 1972. The Indian-Antarctic-Pacific triple junction. Earth and Planetary Science Letters 17 (1): 151-158.

Fitch, T.J., 1972. Plate Convergence, Transcurrent Faults, and Internal Deformation Adjacent to Southeast Asia and the Western Pacific. Journal of Geophysical Research 77 (23): 4432-4460.

Freed, A.M., Lin, J., Shaw, P., and Melosh, H.J., 1995. Long-term survival of the axial valley morphology at abandoned slow-spreading centers. Geology 23 (11): 971-974.

Frohlich, C., Coffin, M.F., Massell, C., Mann, P., Schuur, C.L., Davis, S.D., Jones, T., and Karner, G., 1997. Constraints on Macquarie Ridge tectonics provided by Harvard focal mechanisms and teleseismic earthquake locations. Journal of Geophysical Research 102 (B3): 5029-5041.

Gaina, C., Muller, D.R., Royer, J.-Y., Stock, J., Hardebeck, J., and Symonds, P., 1998. The tectonic history of the Tasman Sea: A puzzle with 13 pieces. Journal of Geophysical Research 103 (B6): 12,413-12,433.

Goff, J.A., 1991. A global and regional stochastic analysis of near-ridge abyssal hill morphology. Journal of Geophysical Research, 96 (B13): 21,713-21,737.

Goff, J.A., 1992. Quantitative characterization of abyssal hill morphology along flow lines in the Atlantic Ocean. Journal of Geophysical Research 97 (B6): 9183-9202.

Goff, J.A., Ma, Y., Cochran, J.R., Shah, A., and Sempere, J.C., 1995. Stochastic analysis of seafloor morphology on the flanks of the Southeast Indian Ridge; the influence of ridge morphology on the formation of abyssal hills. Eos, Transactions, American Geophysical Union 76 (46, Suppl.): 529.

Goscombe, B.D., and Everard, J.L., 2001. Tectonic evolution of Macquarie Island; extensional structures and block rotations in oceanic crust. Journal of Structural Geology 23 (4): 639-673.

Gutscher, M.-A., Malod, J., Rehault, J.-P., Contrucci, I., Klingelhoefer, F., Mendes-Victor, L., and Sprakman, W., 2002. Evidence for active subduction beneath Gibralter. Geology 30 (12): 1071-1074.

Hager, B.H., 1984. Subducted slabs and the geoid; constraints on mantle rheology and flow. Journal of Geophysical Research 89 (B7): 6003-6015.

Hall, C.E., Gurnis, M., and Lavier, L.L., 2002. Initiation of Cenozoic subduction zones of the western Pacific. Eos Trans. AGU 83 (47) Fall Meet. Suppl., Abstract T51D-10.

Hayes, D.E. (Ed.), 1972. Antarctic Oceanology II; The Australian-New Zealand Sector. Antarctic Research Series 19, AGU, 364 pp.

Hayes, D.E., and Talwani, M., 1972. Geophysical investigation of the Macquarie Ridge Complex, in Antarctic Oceanology II; The Australian-New Zealand Sector, Antarctic Research Series 19, AGU, edited by D.E. Hayes, pp. 211-234.

Hilde, T.W.C., Uyeda, S., and Kroenke, L., 1977. Evolution of the western Pacific and its margin. Tectonophysics 38 (1-2): 145-165.

Houtz, R., Ewing, J., and Embley, R., 1971. Profiler data from the Macquarie ridge area, in Antarctic oceanology, I, Antarctic Research Series, AGU, 15: 239-245.

Houtz, R.E., 1972. Eltanin geophysical programs, Cruises 48, 49, 50 and 52, Antarctic Journal of the United States 7 (5): 204.

Jarrard, R.D., 1986a. Relations among subduction parameters. Reviews of Geophysics 24 (2): 217-284.

Jarrard, R.D., 1986b. Terrane motion by strike-slip faulting of forearc slivers. Geology 14 (9): 780-783.

Johansen, B., Vogt, P.R., and Eldholm, O., 1984. Reykjanes Ridge; further analysis of crustal subsidence and time-transgressive basement topography. Earth and Planetary Science Letters 68 (2): 249-258.

Jones, G.M., Hilde, T.W.C., Sharman, G.F., and Agnew, D.C., 1978. Fault patterns in outer trench walls (and their tectonic significance). Journal of the Physics of the Earth 26: S85-S101.

Jones, T.D., and McCue, K.F., 1988. The seismicity and tectonics of the Macquarie Ridge, in Macquarie Island, edited by M.R. Banks and S.J. Smith, Papers and Proceedings of the Royal Society of Tasmania 122 (Part 1): 51-57.

Jones, R.R., and Tanner, P.W., 1995. Strain partitioning in transpression zones. Journal of Structural Geology 17 (6): 793-802.

Kamenetsky, V.S., Everard, J.L., Crawford, A.J., Varne, R., Eggins, S.M., and Lanyon, R., 2000. Enriched end-member of primitive MORB melts; petrology and geochemistry of glasses from Macquarie Island (SW Pacific). Journal of Petrology 41 (3): 411-430.

Kamesh Raju, K.A., Ramprasad, T., Kodagali, V.N., and Nair, R.R., 1993. Multibeam bathymetric, gravity and magnetic studies over 79 degrees E fracture zone, Central Indian Basin. Journal of Geophysical Research 98 (6): 9605-9618.

Kamp, P.J.J., 1986. Late Cretaceous-Cenozoic tectonic development of the southwest Pacific region. Tectonophysics 121: 225-251.

Keller, W.R., 2002. Geophysical Constraints on the Plate Tectonic History of the Emerald Basin and South Tasman Ocean Crust Southwest of New Zealand. AGU abstract, Fall 2002 Meeting, T52A-1185.

Klepis, K.A., and Lawver, L.A., 1996. Tectonics of the Antarctic-Scotia plate boundary near Elephant and Clarence Islands, West Antarctica. Journal of Geophysical Research 101 (B9): 20,211-20,231.

Kobayashi, K., Nakanishi, M., Tamaki, K., and Ogawa, Y., 1998. Outer slope faulting associated with the western Kuril and Japan trenches. Geophysical Journal International 134 (2): 356-372.

Lamarche, G., Collot, J.-Y., Wood, r.A., Sosson, M., Sutherland, R., and Delteil, J., 1997. The Oligocene-Miocene Pacific-Australia plate boundary, south of New Zealand: Evolution from oceanic spreading to strike-slip faulting. Earth and Planetary Science Letters 148: 129-139.

Lamarche, G., and Lebrun, J-F., 2000. Transition from strike-slip faulting to oblique subduction; active tectonics at the Puysegur margin, South New Zealand. Tectonophysics 316 (1-2): 67-89.

Lawver, L.A., Coffin, M.F., Dalziel, I.W.D., Gahagan, L.M., and Campbell, D.A., 2001. The Plates 2001 atlas of plate reconstructions (750 Ma to present day), Plates Progress Report No. 260-0801, UTIG Technical Report No. 189, 83 pp.

Lebrun, J-F., Karner, G.D., and Collot, J-Y., 1998. Fracture zone subduction and reactivation across the Puysegur ridge-trench system, southern New Zealand. Journal of Geophysical Research 103 (4): 7293-7313.

Lebrun, J-F., Lamarche, G., Collot, J-V., and Deltiel, J., 2000. Abrupt strike-slip fault to subduction transition: the Alpine Fault-Puysegur Trench connection, New Zealand. Tectonics 19 (4): 688-706.

Le Pichon, X., 1968. Sea-floor spreading and continental drift. Journal of Geophysical Research 73: 3661-3697.

Lodolo, E., and Coren, F., 1994. The westernmost Pacific-Antarctic plate boundary in the vicinity of the Macquarie triple junction: in Proceedings of the 4th meeting on Earth sciences in Antarctica, prefaced by C.A. Ricci, Terra Antarctica 1 (1): 158-161.

Lodolo, E., Schreider, A.A., and Coren, F., 1996. Sea-floor spreading in the easternmost Indian Ocean reveals cyclicity in ocean crust accretion (0-36 Ma). Marine Geology 134: 249-261.

Lodolo, E., and Coren, F., 1997. A late Miocene plate boundary reorganization along the westernmost Pacific-Antarctic Ridge. Tectonophysics 274 (4): 295-305.

Macario, A., Haxby, W.F., Goff, J.A., Rayan, W.B.F., Cande, S.C., and Raymond, C.A., 1994. Flow line variations in abyssal hill morphology for the Pacific-Antarctic Ridge at 65 degrees S. Journal of Geophysical Research 99 (B9): 17,921-17,934.

Macdonald, K.C., Fox, P.J., Alexander, R.T., Pockalny, R., and Gente, P., 1996. Volcanic growth faults and the origin of Pacific abyssal hills. Nature 380 (6570): 125-129.

Malod, J.A., Karta, K., Beslier, M.O., Zen, M.T. Jr., 1995. From normal to oblique subduction; tectonic relationships between Java and Sumatra. Journal of Southeast Asian Earth Sciences 12 (1-2): 85-93.

Mammerickx, J., Herron, E., and Dorman, L., 1980. Evidence for two fossil spreading ridges in the southeast Pacific. Geological Society of America Bulletin 91: 263-271.

Mammerickx, J., and Sandwell, D., 1986. Rifting of Old Oceanic Lithosphere. Journal of Geophysical Research 91 (B2): 1975-1988.

Marks, K.M., Vogt, P.R., and Hall, S.A., 1990. Residual depth anomalies and the origin of the Australian-Antarctic discordance zone. Journal of Geophysical Research 95 (B11): 17,325-17,337.

Marks, K.M., and Sandwell, D.T., 1991. Analysis of geoid height versus topography for oceanic plateaus and swells using nonbiased linear regression. Journal of Geophysical Research 96 (B5): 8045-8055.

Marks, K.M., and Stock, J.M., 1997. Early Tertiary gravity field reconstructions of the Southwest Pacific. Earth and Planetary Science Letters 152: 267-274.

Massell, C., Coffin, M.F., Mann, P., Mosher, S., Frohlich, C., Duncan, C.S., Karner, G., Ramsay, D., and Lebrun, J.F., 2000. Neotectonics of the Macquarie Ridge Complex, Australia-Pacific plate boundary. Journal of Geophysical Research 105 (6): 13,457-13,480.

Masson, D.G., Fault patterns on outer trench walls. Marine Geophysical Researches 13: 209-225.

McAdoo, D.C., Cladwell, J.G., and Turcotte, D.L., 1978. On the elastic-perfectly plastic bending of the lithosphere under generalized loading with application to the Kuril Trench. Geophysical Journal of the Royal Astronomical Society 54 (1): 11-26.

McAdoo, D.C., 1981. Geoid anomalies in the vicinity of subduction zones. Journal of Geophysical Research 86 (B7): 6073-6090.

McAdoo, D.C., 1982. On the compensation of geoid anomalies due to subducting slabs, Journal of Geophysical Research, 87 (B10): 8684-8692.

McCaffrey, R., 1991. Slip vectors and stretching of the Sumatran fore-arc. Geology 19 (9): 881-884.

McCaffrey, R., 1992. Oblique plate convergence, slip vectors, and forearc deformation. Journal of Geophysical Research 97 (6): 8905-8915.

McCaffrey, R., Global variability in subduction thrust zone-forearc systems, in Special issue; Shallow subduction zones; seismicity, mechanics and seismic potential, Part 2, edited by Dmowska, R., and Ekstrom, G., Pure and Applied Geophysics 142 (1): 173-224.

McCaffrey, R., 1996. Estimates of modern arc-parallel strain rates in fore-arcs. Geology 24 (1): 27-30.

McCaffrey, R., Zwick, P. C., Bock, Y., Prawirodirdjo, L., Genrich, J. F., Stevens, C. W., Puntodewo, S. S. O., and C. Subarya, 2000. Strain partitioning during oblique plate convergent in northern Sumatra; geodetic and seismologic constraints and numerical modeling. Journal of Geophysical Research 105 (B12): 28,363-28,376.

McKenzie, D.P., and Morgan, W.J., 1969. Evolution of triple junctions. Nature 224: 125-133.

Meckel, T.A., Coffin, M.F., Mosher, S., Symonds, P., Bernardel, G., and Mann, P., in review. Underthrusting at the Hjort Trench, Australian-Pacific Plate Boundary: Incipient subduction? Geochemistry, Geophysics, Geosystems.

Melhuish, A., Sutherland, R., Davey, F.J., and Lamarche, G., 1999. Crustal structure and Neotectonics of the Puysegur oblique subduction zone, New Zealand. Tectonophysics 313: 335-362.

Minshull, T.A., Morris, E., and Detrick, R.S., 1995. Gravity anomalies and crustal structure at the Mesozoic Blake Spur fracture zone. Journal of Geophysical Research 100 (9): 17,771-17,779.

Mitchell, N.C., 2001. Transition from circular to stellate forms of submarine volcanoes. Journal of Geophysical Research 106 (B2): 1987-2003.

Molnar, P., Atwater, T., Mammerickx, J., and Smith, S.M., 1975. Magnetic Anomalies, Bathymetry and the Tectonic Evolution of the South Pacific

since the Late Cretaceous. Geophysical Journal of the Royal Astronomical Society 40: 383-420.

Moore, M.A., Anderson, H.J., and Pearson, C., 2000. Seismic and geodetic constraints on plate boundary deformation across the northern Macquarie Ridge and southern South Island of New Zealand. Geophysical Journal International 143: 847-880.

Mortimer, N., 1994. Geological note: igneous and sedimentary rocks dredged from the northern Macquarie Ridge, Southern Ocean. Australian Geological Survey Organization, Journal of Australian Geology and Geophysics 15 (4): 529-537.

Mueller, R. D., and Roest, W.R., 1992. Fracture zones in the North Atlantic from combined Geosat and Seasat data. Journal of Geophysical Research 97 (3): 3337-3350.

Norton, I. O., 2000. Global hotspot reference frames and plate motion, in: The history and dynamics of global plate motions, edited by Richards, M. A., Gordon, R. G., and van der Hilst, R. D., AGU Geophysical Monograph 121, pp. 398.

Parsons, B., and Sclater, J.G., 1977. An analysis of the variation of ocean floor bathymetry and heat flow with age. Journal of Geophysical Research 82 (5): 803-827.

Platt, J.P., Calibrating the bulk rheology of active obliquely convergent thrust belts and forearc wedges from surface profiles and velocity distributions, *Tectonics*, 19 (3), 529-548, 2000.

Polkalny, R.A., 1997. Evidence of transpression along the Clipperton Transform: Implications for processes of plate boundary reorganization. Earth and Planetary Science Letters 146: 449-464.

Royer, J-V., and Gordon, R.G., 1997. The motion and boundary between the Capricorn and Australian plates. Science 277 (5330): 1268-1274.

Ruff, L.J., and Cazenave, A., 1985. SEASAT geoid anomalies and the Macquarie Ridge complex. Physics of the Earth and Planetary Interiors 38 (1): 59-69.

Ruff, L.J., Given J.W., Sanders, C.O., and Sperber, C.M., 1989. Large earthquakes in the Macquarie Ridge Complex: Transitional tectonics and subduction initiation. Pure and Applied Geophysics 129 (1/2): 71-129.

Sandwell, D.T., and Smith, W.H.F., 1997. Marine gravity anomaly from Geosat and ERS 1 satellite altimetry. Journal of Geophysical Research 102 (B5): 10,039-10,054.

Schuur, C.L, Coffin, M.F., Frohlich, C., Massell, C.G., Karner G.D., Ramsay, D., and Caress, D.W., 1998. Sedimentary regimes at the Macquarie Ridge complex; interaction of Southern Ocean circulation and plate boundary bathymetry. Paleooceanography 13 (6): 646-670.

Sclater, J.G., and J. Francheteau, 1970, The implications of terrestrial heat flow observations on current tectonic and geochemical models of the crust and upper mantle of the Earth: Geophysical Journal of the Royal Astronomical Society, V. 20, Issue 5, p. 509-542.

Selkirk, D.R., P.M. Selkirk, and K. Griffen, 1983, Palynological evidence for Holocene environmental change and uplift on Wireless Hill, Macquarie Island: Proceedings of the Linnean Society, New South Wales, V. 107 (1), p. 1-17.

Selkirk, P.M., D.A. Adamson, and M.E. Wilson, 1990, Raised marine terraces on north-west coast of Macquarie Island: Proceedings of the Linnean Society, New South Wales, V. 112 (3), p. 141-152.

Smith, W.H.F., and D.T. Sandwell, 1997, Global seafloor topography from satellite altimetry and ship depth soundings: Science, 277, p.1957-1962.

Stein, C.A., and Stein, S., 1992. A model for the global variation in oceanic depth and heat flow with lithospheric age. Nature 359 (6391): 123-129.

Stern, R. J., and S.H. Bloomer, 1992, Subduction zone infancy: Examples from the Izu-Bonin-Mariana and Jurassic California arcs: GSA Bulletin, V. 104, p. 1621-1636.

Stock, J., and P. Molnar, 1982, Uncertainties in the relative positions of the Australia, Antarctica, Lord Howe, and Pacific plates since the Late Cretaceous**:** Journal of Geophysical Research, Vol. 87, B6, p. 4697-4714.

Summerhayes, C.P., Note on Macquarie ridge and the Tonga-Kermadec complex; are they parts of the mid-ocean ridge system?, *New Zealand Journal of Science,* 10 (3), 808-812, 1967.

Summerhayes, C.P., Marine geology of the New Zealand Subantarctic sea floor, New Zealand Dep. Sci. Ind. Res. Bull., 190, 92 pp., 1969.

Sutherland, R., 1995, The Australia-Pacific boundary and Cenozoic plate motions in the SW Pacific; some constraints from Geosat data: Tectonics, V. 14, Issue 4, p. 819-831.

Talwani, M., Worzel, J. L., and M. G. Landisman, Rapid gravity computations for two-dimensional bodies with application to the Mendocino submarine fracture zone (Pacific Ocean), *Journal of Geophysical Research*, 64 (1), 49-59, 1959.

Teyssier, C., B. Tikoff, and M. Markley, 1995, Oblique plate motion and continental tectonics: Geology, V. 23, No. 5, p. 447-450.

Toth, J., and Gurnis, M., 1998. Dynamics of subduction initiation at preexisting fault zones. Journal of Geophysical Research 103 (B8): 18,053-18,067.

Uyeda, S., and Z. Ben-Avraham, Origin and Development of the Philippine Sea, *Nature*, 240 (104), 176-178, 1972.

Varne, R., R. Gee, Q. Dennis, and G.J. Patrick, 1969, Macquarie island and the cause of oceanic linear magnetic anomalies: Science, V. 166 (3902), p. 230-233.

Varne, R., and M.J. Rubenach, 1972, Geology of Macquarie Island and its relationship to oceanic crust: in Antarctic Oceanology II; The Australian-New Zealand Sector, edited by D.E. Hayes, Antarctic Research Series, V. 19, p. 251-266.

Varne, R., A.V. Brown, and T. Falloon, 2000, Macquarie Island; its geology, structural history, and the timing and tectonic setting of its N-MORB to E-MORB magmatism, in Ophiolites and oceanic crust; new insights from field studies and the Ocean Drilling Program, edited by Y. Dilek, E.M. Moores, D. Elthon, and A. Nicolas, Special Paper - Geological Society of America, V. 349, p. 301-320.

Vlaar, N. J., and M. J. R. Wortel, Lithospheric aging, instability and subduction, *Tectonophysics*, 32 (3-4), 331-351, 1976.

Vogt, P.R., B. Zondek, P.W. Fell, N.Z. Cherkis, and R.K. Perry, Seasat altimetry, the North Atlantic geoid, and evaluation by shipborne subsatellite profiles, *Journal of Geophysical Research*, 89 (B12), 9885-9903, 1984.

Walcott, R.I., 1978. Present tectonics and Late Cenozoic evolution of New Zealand. Geophysical Journal of the Royal Astronomical Society 52: 137-164.

Walcott, R.I.,. 1984. Reconstruction of the New Zealand region for the Neogene, in Collected papers of the Third international meeting on Pacific Neogene stratigraphy, edited by N. de B. Hornibrook, Palaeogeography, Palaeoclimatology, Palaeogeography 46 (1-3): 217-231.

Watts, A.B., and M. Talwani, Gravity Anomalies Seaward of Deep-Sea Trenches and their Tectonic Implications, *The Geophysical Journal of the Royal Astronomical Society*, 36 (1), 57-90, 1974.

Wdowinski, S., Dynamically supported trench topography, *Journal of Geophysical Research*, 97 (B12), p. 17,651-17,656, 1992.

Weissel, J.K., and D.E. Hayes, Magnetic anomalies in the southeast Indian Ocean, In: Hayes, D.E. (Ed.), Antarctic Oceanology II; The Australian-New Zealand Sector, *Antarctic Research Series*, 19, p. 165-196, 1972.

Weissel, J.K., D.E. Hayes, and E.M. Herron, 1977, Plate tectonics synthesis: the displacements between Australia, New Zealand, and Antarctica since the late Cretaceous: Marine Geology, V. 25, p. 231-277.

Wertz, K., J.E. Snow, E. Hellebrand, A. von der Handt, and S. Mosher, 2002, Depleted peridotites of Macquarie Island, an uplifted section of in-situ oceanic crust: Eos Trans. AGU, 83(47),
Fall Meet. Suppl., Abstract V52A-1284.

Wertz, K.L., S. Mosher, N.R. Daczko, and M.F. Coffin, in review. Macquarie Island's Finch-Langdon fault: a ridge-transform inside corner structure: Geology.

Wessel, P., and L. W. Kroenke, The geometric relationship between hot spots and seamounts; implications for Pacific hot spots, *Earth and Planetary Science Letters*, 158 (1-2), 1-18, 1998.

White, R.S., D. McKenzie, and R.K. O'Nions, Oceanic crustal thickness from seismic measurements and rare Earth element inversions, *Journal of Geophysical Research*, 97 (B13), 19,683-19,715, 1992.

Whitmarsh, R.B., 1979, The Owen Basin off the south-east margin of Arabia and the evolution of the Owen Fracture Zone: Geophys. J. R. astr. Soc., V. 38, p. 441-470.

Wiens, D.A., and S. Stein, Age dependence of oceanic intraplate seismicity and implications for lithospheric evolution, *Journal of Geophysical Research*. 88 (B8), 6455-6468, 1983.

Willemann, R.J. and D.A. Storchak, *Data collection at the International Seismological Centre*, Seismological Research Letters, 72, 440-453, 2001.

Wood, R., G. Lamarche, R. Herzer, J. Delteil, and B. Davy, 1996, Paleogene seafloor spreading in the southeast Tasman Sea: Tectonics, V. 15 (5), p. 966-975.

Wortel, M. J. R., and N. J. Vlaar, Age-dependent stubduction of oceanic lithosphere beneath western South America, *Physics of the Earth and Planetary Interiors*, 17 (3), 201-208, 1978.

Yu, G., Wesnousky, S. G., and G. Ekstrom, Slip partitioning along major convergent plate boundaries, in: Dmowska, R., and G. Ekstrom, eds., Shallow subduction zones; seismicity, mechanics and seismic potential; I, Pure and Applied Geophysics, 140 (2), 183-210, 1993.

Vita

Timothy (Tip) Ashworth Meckel was born in Houston, Texas to Lawrence D. (Larry) Meckel and Barbara T. Meckel on September 19, 1972. After graduation from St. John's High School, he attended Colby College in Waterville, Maine. Upon graduating Phi Beta Kappa with a B.A. in Geology, he attended Indiana University's summer geologic field program in Montana where he developed an interest in regional structural and stratigraphic complications. He was asked to return the following summer as an assistant instructor, at which point he was enrolled in the graduate program in the Geology Department at the University of Montana in Missoula. He spent a third summer with Indiana's field school, developing curriculum focusing on the field applications of ground penetrating radar. He incorporated his interest in field geology and geophysics into a MS thesis investigating the applications of GPR for delineating stratigraphic heterogeneity in consolidated sandstone deposits. From Montana, he entered the graduate program at The University of Texas at Austin, where he began a Ph.D. in the Department of Geological Sciences in 1998. While working toward his degree in Austin, he instructed both in the field and in the classroom, went to sea aboard the *R/V Maurice Ewing* offshore western Nicaragua, and was employed as an exploration geologist by ExxonMobil for four months in New Orleans.

Permanent address: 1120 Race St., Denver, Colorado 80206 U.S.A.

This dissertation was typed by the author.